

MTR 06B00000005

MITRE TECHNICAL REPORT

Comparative Performance of Three DSSS/Rake Modems Over Mobile UWB Dense Multipath Channels

June 2005

Phillip A. Bello

Sponsor:
Dept. No.: E530

Contract No.: FA8721-05-C-0001
Project No.: 20AAV530-D1


The views, opinions and/or findings contained in this report are those of The MITRE Corporation and should not be construed as an official Government position, policy, or decision, unless designated by other documentation.

Approved for Public Release; Distribution Unlimited
Case No. 06-0156

©2006 The MITRE Corporation. All Rights Reserved.

MITRE
Center for Air Force C2 Systems
Bedford, Massachusetts

APPROVED BY:

A handwritten signature in black ink, appearing to read 'C. A. Nissen', is written over a horizontal line.

Christopher A. Nissen, Director
D600, Communications and Networking

Abstract

Modems built and analyzed for use on Ultra Wideband (UWB) channels generally use short pulses. Such techniques have been called “impulse radio.” Another suitable class of modems employs Direct Sequence Spread Spectrum (DSSS)/Rake techniques. The latter techniques have the advantage of causing far less time domain interference with other users. This report presents a comparative analysis of the performance of three UWB DSSS/Rake modems used to communicate with mobile platforms over postulated outdoor and indoor dense multipath UWB channel models. The Wide-Sense-Stationary-Uncorrelated-Scattering (WSSUS) channel model has provided a useful tool for modeling random time variant linear channels in the four decades since its introduction. However, with the advent of UWB communications, it is necessary to replace this model which is valid for Narrowband (NB) channels. This paper develops such a replacement. The development is based upon the tapped delay line model of a linear time-variant channel, which is valid for any ratio of bandwidth-to-carrier frequency. For simplicity, the analysis assumes a dense multipath environment such as may be experienced in outdoor and indoor urban environments. The thrust of this study is to derive an UWB channel model for dense multipath that will allow a meaningful comparative modem performance evaluation rather than to develop a new precise characterization of UWB channels. Such a model should be useful in preparation of UWB communication standards.

Rake modems estimate the channel characteristics and carry out an approximate coherent combination of multipath components. The Rake modems analyzed differ in the techniques used to estimate the channel and are called “decision-directed,” “parallel-probe,” and “serial-probe” modems. Three methods of evaluating modem performance are explored: the Signal-to-Noise Ratio (SNR) method, the “Gaussian noise” method, and the “exact” method. The SNR method and the Gaussian noise method provide fast numerical evaluations of performance and accurately predict performance when the large multipath condition $WL_{\text{tot}} \gg 1$ is satisfied, where L_{tot} is the total multipath spread, and W is the bandwidth of the transmitted signal. Numerical results are presented for 2 GHz bandwidth transmitted signals, a 7.5 GHz carrier frequency, and channel Phase Shift Keying (PSK) symbol rates of .15, 1.5, and 15 Megasymbols/sec. The well known rate $\frac{1}{2}$, constraint length 7 convolutional code using 3 bit soft decision Viterbi decoding is assumed. One moving and one stationary platform are postulated, with a velocity of 100 ft/sec for the outdoor channel and 5

ft/sec for the indoor channel. Required values of E_s/N_0 to achieve 10^{-6} decoded error rate are computed as a function of multipath spread.

Acknowledgement

The author gratefully acknowledges the interest and encouragement of Christopher Nissen.

Table of Contents

<u>Section</u>	<u>Page</u>
Abstract	iii
Acknowledgement	v
Table of Contents	vi
List of Figures	vii
1 Introduction	1-1
1.1 Background	1-1
1.2 Executive Summary	1-3
2 System Description	2-1
3 Performance	3-1
3.1 Tapped Delay Line Model Second Order Statistics	3-1
3.1.1 Received Signal	3-2
3.1.2 Canonic Tapped Delay Line Model	3-5
3.1.3 Tap Weight Cross-Correlation Functions and Cross-Power Spectra	3-7
3.1.4 Specialization to Simplified Outdoor and Indoor Dense Multipath Channels	3-11
3.2 Performance Evaluations	3-19
3.2.1 The SNR Method	3-20
3.2.2 The Gaussian Noise Method	3-22
3.2.3 The Exact Method	3-23
3.2.4 Calculations	3-27
3.2.4.1 Comparison of Exact Method and Average Channel Methods	3-28
3.2.4.2 Performance for the Outdoor Dense Large Multipath Channel Model	3-30
3.2.4.3 Calculations for the Indoor Dense Large Multipath Channel Model	3-33
3.2.4.4 Comparison of Decision-Directed, Parallel-Probe and Serial-Probe Modems.	3-36
4 Conclusions	4-1
REFERENCES	RE-1
Appendix A Performance Analysis	A-1
Appendix B Tapped Delay Line Model for the UWB Channel	B-1
Appendix C Tap Gain Correlation Functions for the Band Limited WSSUS Channel	C-1
Appendix D Performance Evaluation of Delay-Compensated Decision-Directed, Parallel Probe, and Serial Probe Rake Modems	D-1

List of Figures

<u>Figure</u>	<u>Page</u>
Figure 1-1. Signal Processing for Rake Combining	1-4
Figure 1-2. Plots of Required E_S/N_0 for 10^{-6} Decoded Error Rate as a Function of Multipath Delay Constant σ . Decision-Directed Modem with and without Delay Compensation. $f_0 = 7.5$ GHz, $W = 2$ GHz, $V = 100$ ft/sec., and Symbol Rates = .15, 1.5, and 15 Mss. Tap Weight Filter Time Constant T_F and Number of Rake Taps R Simultaneously Optimized for Each Point on Curves. Outdoor Dense Large-Multipath Channel.....	1-8
Figure 1-3. Plots of Required E_S/N_0 for 10^{-6} Decoded Error Rate as a Function of Multipath Delay Constant σ with and without Delay Compensation. $f_0 = 7.5$ GHz, $W = 2$ GHz, $V = 5$ ft/sec., and Symbol Rates = .15, 1.5, and 15 Mss. Normalized Tap Weight Filter Time Constant T_F and Number of Rake Taps R Optimized for Each Point on Curves. Indoor Dense Large-Multipath Channel	1-9
Figure 1-4. Comparison of Required E_S/N_0 to Obtain a Decoded Error Rate of 10^{-6} Over the Outdoor Channel for the Decision-Directed, Parallel-Probe, and Serial-Probe Modems at a Symbol Rate of 1.5 Mss. T_F , R , and Probe Parameters g and P Optimized at Each Value of σ . $f_0 = 7.5$ GHz, $W = 2$ GHz, and Relative Terminal Velocity of 100 ft./sec.....	1-11
Figure 1-5. Comparison of Required E_S/N_0 to Obtain a Decoded Error Rate of 10^{-6} Over the Indoor Channel for the Decision-Directed, Parallel-Probe, and Serial-Probe Modems at a Symbol Rate of 1.5 Mss. T_F , R , and Probe Parameters g and P Optimized at Each Value of σ . $f_0 = 7.5$ GHz, $W = 2$ GHz, and a Relative Terminal Velocity of 5 ft./sec.....	1-12
Figure 2-1. System Block Diagram and Canonic Tapped Delay Line Representation.....	2-1
Figure 2-2. High-Level DSSS/Rake Receiver Block Diagram.....	2-5
Figure 2-3 . Signal Processing for Rake Combining	2-5
Figure 2-4. Block Diagram of Decision Directed Rake Channel Measurement Subsystem.....	2-9
Figure 2-5. Illustration of Delay Compensation with Decision-Directed Implementation.....	2-11
Figure 3-1. Normalized Power Spectrum of Tap Weights for Outdoor Dense Multipath Channel Assuming Normalized Bandwidth $r = .1, .5, 1, 1.5$	3-15
Figure 3-2. Normalized Power Spectrum of Tap Weights for Indoor Dense Multipath Channel Assuming Normalized Bandwidth $r = .1, .5, 1, 1.5$	3-15
Figure 3-3. Magnitude of Cross-Spectra vs. Normalized Frequency for $n-m=0, 1, 2, 3$, and 4; $r = 1$; and Outdoor Dense Multipath Channel.....	3-16
Figure 3-4. Magnitude of Cross-Spectra vs. Normalized Frequency for 0, 1, 2, 3, and 4 Tap Separations, $r = 1$, and Indoor Dense Multipath Channel.....	3-16
Figure 3-5. Plot of Magnitude of Normalized Cross-Power Spectrum for Two Adjacent Taps as a Function of Normalized Frequency and Normalized Bandwidth r . Outdoor Dense Multipath Channel.....	3-17

<u>Figure</u>	<u>Page</u>
Figure 3-6. Plot of Magnitude of Normalized Cross-Power Spectrum for Two Adjacent Taps as a Function of Normalized Frequency and Normalized Bandwidth r . Indoor Dense Multipath Channel.	3-17
Figure 3-7. Raw Bit Error Probability as a Function of E_S/N_0 for an Example Outdoor Dense Large Multipath Channel Model with Multipath Delay Constant = 10 ns.	3-29
Figure 3-8. Raw Bit Error Probability as a Function of E_S/N_0 for an Example Outdoor Dense Large Multipath Channel Model with Multipath Delay Constant = 20 ns.	3-29
Figure 3-9. Raw Bit Error Probability as a Function of E_S/N_0 for an Example Outdoor Dense Large Multipath Channel Model with Multipath Delay Constant = 35 ns.	3-30
Figure 3-10. Raw Bit Error Probability as a Function of E_S/N_0 for an Example Outdoor Dense Large Multipath Channel Model with Multipath Delay Constant = 50 ns.	3-30
Figure 3-11. Plots of Required E_S/N_0 for 10^{-6} Decoded Error Rate as a Function of Multipath Delay Constant σ . Decision-Directed Modem with and without Delay Compensation. $f_0 = 7.5$ GHz, $W = 2$ GHz, $V = 100$ ft/sec., and Symbol Rates = .15, 1.5, and 15 Mss. Tap Weight Filter Time Constant T_F and Number of Rake Taps R Simultaneously Optimized for Each Point on Curves. Outdoor Dense Large-Multipath Channel.	3-32
Figure 3-12. Optimal Values of Normalized Tap Weight Measurement Filter Time Constant T_F as a Function of Multipath Delay Constant σ Corresponding to Plots in Figure 3-11.	3-32
Figure 3-13. Optimal Value of the Number of Rake Taps R Corresponding to Plots in Figure 3-11.	3-33
Figure 3-14. Plots of Required E_S/N_0 for 10^{-6} Decoded Error Rate as a Function of Multipath Delay Constant σ with and without Delay Compensation. $f_0 = 7.5$ GHz, $W = 2$ GHz, $V = 5$ ft/sec., and Symbol Rates = .15, 1.5, and 15 Mss. Normalized Tap Weight Filter Time Constant T_F and Number of Rake Taps R Optimized for Each Point on Curves. Indoor Dense Large-Multipath Channel.	3-34
Figure 3-15. Optimal Value of Normalized Tap Weight Measurement Filter Time Constant T_F Corresponding to Plots in Figure 3-14.	3-35
Figure 3-16. Optimal Value of the Number of Rake Taps R Corresponding to Plots in Figure 3-14.	3-35
Figure 3-17. Comparison of Required E_S/N_0 to Obtain a Decoded Error Rate of 10^{-6} Over the Outdoor Channel for the Decision-Directed, Parallel-Probe, and Serial-Probe Modems at a Symbol Rate of 1.5 Mss. T_F , R , and Probe Parameters g and P Optimized at Each Value of σ . $f_0 = 7.5$ GHz, $W = 2$ GHz, and Relative Terminal Velocity of 100 ft/sec.	3-37
Figure 3-18. Comparison of Required E_S/N_0 to Obtain a Decoded Error Rate of 10^{-6} Over the Outdoor Channel for the Decision-Directed, Parallel-Probe, and Serial-Probe Modems at a Symbol Rate of 15 Mss. T_F , R , and Probe Parameters g and P Optimized at Each Value of σ . $f_0 = 7.5$ GHz, $W = 2$ GHz, and Relative Terminal Velocity of 100 ft/sec.	3-38

<u>Figure</u>	<u>Page</u>
Figure 3-19. Comparison of Required E_S/N_0 to Obtain a Decoded Error Rate of 10^{-6} Over the Outdoor Channel for the Decision-Directed, Parallel-Probe, and Serial-Probe Modems at a Symbol Rate of .15 Mss. T_F , R , and Probe Parameters g and P Optimized at Each Value of σ . $f_0 = 7.5$ GHz, $W = 2$ GHz, and Relative Terminal Velocity of 100 ft./sec.....	3-39
Figure 3-20. Comparison of Required E_S/N_0 to Obtain a Decoded Error Rate of 10^{-6} Over the Indoor Channel for the Decision-Directed, Parallel-Probe, and Serial-Probe Modems at a Symbol Rate of 1.5 Mss. T_F , R , and Probe Parameters g and P Optimized at Each Value of σ . $f_0 = 7.5$ GHz, $W = 2$ GHz, and Relative Terminal Velocity of 5 ft./sec.....	3-40
Figure 3-21. Comparison of Required E_S/N_0 to Obtain a Decoded Error Rate of 10^{-6} Over the Indoor Channel for the Decision-Directed, Parallel-Probe, and Serial-Probe Modems at a Symbol Rate of 15 Mss. T_F , R , and Probe Parameters g and P Optimized at Each Value of σ . $f_0 = 7.5$ GHz, $W = 2$ GHz, and Relative Terminal Velocity of 5 ft./sec.....	3-41
Figure 3-22. Comparison of Required E_S/N_0 to Obtain a Decoded Error Rate of 10^{-6} Over the Indoor Channel for the Decision-Directed, Parallel-Probe, and Serial-Probe Modems at a Symbol Rate of 1.5 Mss. T_F , R , and Probe Parameters g and P Optimized at Each Value of σ . $f_0 = 7.5$ GHz, $W = 2$ GHz, and Relative Terminal Velocity of 5 ft./sec.....	3-42

List of Tables

<u>Table</u>	<u>Page</u>
Table A-1 Input Signal to Noise Ratio (dB) in the Bandwidth W	A-42

1 Introduction

1.1 Background

Modems built and analyzed for use on UWB¹ channels generally use short pulses. Such techniques have been called “impulse radio” [1,2,3]. Another suitable class of modems employs DSSS Rake [4] techniques. An advantage of the DSSS modem is that the peak transmitted power is very much less than that of the impulse radio modem for the same average transmitted power. Thus, assuming comparable efficiencies for the modem types, the use of DSSS should provide substantially less time-domain interference to other users than the impulse radio modems.² Comparable efficiencies can only be achieved if the impulse radio modem employs coherent combining of multipath components as is done by the DSSS/Rake modem. With terminal motion, techniques employed for coherent combining in these modems can be degraded due to time selective fading, resulting in increased SNR requirements to achieve a desired performance. In this report, we analyze the performance of DSSS/Rake modems when used to communicate over an UWB channel in which there is terminal motion and a dense (e.g., urban) multipath environment. Considering that Gigahertz (GHz) bandwidths may be involved, there are clearly implementation challenges for digitally implemented DSSS/Rake modems (e.g., analog to digital (A/D) converters for digital processing of signals of these bandwidths). However, these hardware issues will be resolved as the technology advances. In this report, we assume that the technology is or will be available to implement the necessary signal processing for the types of Rake combining discussed.

In order to carry out the performance evaluation, it is necessary to use a channel model which does not presuppose the NB assumption

¹ The FCC allocated band for UWB communications is from 3.1 to 10.6 GHz.

² If all the potential users are separated by dense multipath channels, the large peak to average power ratio of the impulse radio received signal will be reduced significantly by the “smearing” of the channel. However in a dynamic mobile situation such a fortuitous condition cannot be guaranteed.

$$r = W/f_0 \ll 1 \quad (1-1)$$

where W is the transmitted signal bandwidth, f_0 is the “center” frequency, and r is the bandwidth normalized to the center frequency. In this connection, one may regard a low-pass transmission band with highest frequency W Hz as a bandpass transmission with center frequency $=W/2$. This will result in the maximum value of $r = 2$. It is customary to define the UWB channel by the inequality $r \geq .25$. From a channel modeling and performance evaluation point of view, it is more meaningful to define the WB (wide band) channel model where the parameter r can cover the range of possible values. The model reduces to the NB channel when $r \ll 1$ and becomes an UWB channel when, say, $r \geq .25$.

The Wide-Sense-Stationary-Unrelated-Scattering (WSSUS) channel model [5] has been used extensively for the purpose of modem performance evaluation over wireless channels. Stochastic performance evaluation requires some degree of statistical regularity, so one may regard the Wide-Sense Stationary (WSS) property as necessary for such evaluation. On the other hand, the US (uncorrelated scattering) property is not necessary for analytical evaluations. The WSSUS model, in effect, is a “microscopic” representation of the channel as a continuum of statistically independent non-moving wide-sense-stationary scintillating elemental scatterers. Thus, the question arises as to the WSSUS model applicability for moving terminals and moving reflecting objects. In [6], this question was taken up in regard to modeling the orbital dipole channel, an artificial scatter channel proposed for military communications [7]. It was found that r needed to be sufficiently small³ before the WSSUS model could be justified.

For this reason, we found it necessary to start the analysis at a more fundamental level than the WSSUS channel: the tapped delay line model of a linear time-variant channel [5][8]. Such a model, which is valid for any r , is developed in Appendix B for the UWB channel. As it turns out, using this formulation, Section B.4.1 derives a condition for

³ cf. the equation at the end of Section I in [6].

validity of the WSSUS model, essentially identical to that derived in [6], although, in the present case, the terminals are moving and the reflectors are assumed stationary. The bottom line is that, strictly speaking, the WSSUS channel is appropriate only for NB channels and, thus, the US hypothesis is invalid for WB channels and for the UWB channel in particular. The correct stochastic model for evaluating the performance of modems over the WB channel is to use the WSS channel model [5].

The DSSS/Rake modems proposed here have already been analyzed [9] for wideband high frequency (WBHF) communications and demonstrated experimentally by The MITRE Corporation for the decision-directed Rake approach. It is important to note that the presence of UWB antenna frequency selective distortion and antenna transfer functions, which change with the direction of propagation, pose no limitations to this type of modem. Transmission masks can be inserted to avoid interference with various NB users. The proposed coherent rake processors automatically compensate for the linear distortions caused by transmission filters, antennas, multipath, and receiver filters, including noise-whitening filters. It is essential that an appropriate noise-whitening filter or interference excisor precede the DSSS/Rake modem in order to effectively excise NB interference. This report does not take up the design and performance of noise-whitening filters. For analysis purposes, we assume that the noise at the input to the modem is white and bandlimited to W Hz.

1.2 Executive Summary

The theoretical foundation for operation of the DSSS/Rake modem is based upon a representation of the channel as a uniformly tapped delay line with complex time-variant weights and tap delay separation equal to the reciprocal of the transmitted signal bandwidth W . Figure 1-1 presents a block diagram of the signal correlation and combining portion of the Rake modem. Section 2 presents a more complete set of block diagrams. A local pseudo noise (PN) sequence generator clocked at W Hz feeds a shift register. Uniformly delayed versions of the PN sequence are correlated over successive data symbols with the noise-

uncorrelated direct sequence PN modulation is used with the probe signal. Since both DSSS signals are being transmitted over the same band occupancy, they are acted upon by the same time-variant channel. Thus, channel measurements employing the probe DSSS received signal can be used to complex weight the correlator outputs of the data DSSS subsystem. The serial-probe technique involves inserting a known data subsequence serially in the data stream at periodic symbol times. At the receiver, only the known data symbols are used for the channel measurement by feeding them to a channel measurement filter. As in the parallel probe case, the channel measurements from the serial probe subsystem are used to complex weight the correlator outputs of the data DSSS subsystem. The decision-directed approach uses no dedicated probing signals. Instead, it creates the effect of a dedicated probing signal through multiplication of the output data decisions by appropriately delayed correlator outputs, ideally canceling out the data modulation.

Section 3 presents performance results for two hypothetical multipath channels: The outdoor base station to urban mobile channel and the indoor fixed terminal to mobile terminal. To simplify the performance analysis, we have confined our attention to a *dense large-multipath* environment. The term dense multipath means that each tap weight in the tapped delay line model is composed of a large number of physical 3D multipath contributions, none of which dominates in strength. The term large multipath means that $WL_{\text{tot}} \gg 1$, where L_{tot} is the total multipath spread. For brevity, sometime we will call the *outdoor dense large multipath* and the *indoor dense large multipath* channels the *outdoor* and *indoor* channel models, respectively. Section 3.1 presents an overview of the WB channel modeling effort. Appendix B presents the detailed WB channel model derivation. Section 3.2 presents both coded and uncoded error rate performance evaluations for both the indoor and outdoor channel models. The detailed analyses may be found in Appendices A and D.

There are two noteworthy consequences to WB as opposed to NB channel modeling. One consequence is that antenna distortions will generally show dependence upon the direction of transmission and arrival of a signal. However, any distortion caused by the

antenna will pale in insignificance by comparison with the distortion caused by the dense multipath channel models assumed in the performance analysis. Transmission and reception angular dependence of distortion will not alter this fact. For this reason, to simplify the analysis, we do not include this dependence in our simplified models used for performance computation.

The other consequence of WB transmission is the need to properly include the effects of time-scale change in the channel model. The NB simplification of representing the effect of time-scale changes caused by motion via constant Doppler shifts across the band is no longer possible. There is no way to design out the effects of time-scale changes upon the channel model. Consequently, the effect of time-scale change is included in our analysis at the outset. The channel model used allows the modem to be exercised over a range of multipath spreads and terminal velocities to be expected in practice and for a selectable normalized bandwidth r ($0 < r < 2$). *The thrust of this study is to validate the DSSS/Rake modem performance over a meaningful UWB channel model rather than to develop a new precise characterization of UWB channels.*

In the numerical performance evaluations, we have assumed a tapped delay line channel model with an exponentially decreasing average tap weight as the tap delay increases. σ , the multipath delay constant, is defined as the value of delay at which the tap weight drops by $\frac{1}{e}$. Values of σ in the range $10 < \sigma < 300$ ns are used in performance calculations. The transmitted signal bandwidth and center frequency assumed in the calculations are 2 GHz and 7.5 GHz, respectively. Performance is computed for channel symbol rates of .15, 1.5, and 15 Megasymbols/sec (Mss). The well known rate $\frac{1}{2}$, constraint length 7 convolutional code using 3 bit soft decision, Viterbi decoding was assumed. For the outdoor channel, the velocity of the moving terminal, V , is assumed to be 100 ft/sec, while for the indoor channel, V is assumed to be 5 ft/sec.

For the outdoor channel, Figure 1-2 presents plots of required E_s / N_0 (the ratio of energy/bit to noise power density⁴) to achieve 10^{-6} decoder output error rate for the decision-directed modem. As indicated, performance is presented with and without the use of a technique called “delay compensation” [30] which reduces the degradation due to time-selective fading. The process of channel measurement for the three modems involves a tap-weight-measurement filter. Degradation in performance results from the decorrelation between the estimated tap weight fluctuations and the tap weight fluctuations actually present at the Rake correlator output. Part of this decorrelation is caused by the delay of the tap weight measurement subsystem. The degradation due to time selectivity can be reduced by introducing a compensating delay in the signal path.

In these calculations, the parameters R (the number of Rake correlators) and T_F (the time constant of the channel measurement filter) are selected at each value of E_s / N_0 to maximize the output SNR. Plots of these optimal values of R and T_F are presented in Section 3.2. We see from Figure 1-2 that as the data rate increases, the modem becomes more efficient, that is to say, at the same value of σ the required value of E_s / N_0 for 10^{-6} error rate decreases. The minimum value of E_s / N_0 is 2 dB corresponding to perfect channel measurement. As the symbol rate increases, the number of symbols averaged per unit time in the tap weight filter increases. The tap weights are thus less noisy for the same averaging time as the data rate increases. There are two consequences to this phenomenon. First, a larger number of taps, R , can be used for combining with increasing data rate because the tap weights are less noisy. Second, a shorter averaging time can be used with the higher data rate which leads to less time selective fading degradation.

⁴ E_s/N_0 is also the ratio of the received signal power to the noise power in a bandwidth equal to the channel symbol rate.

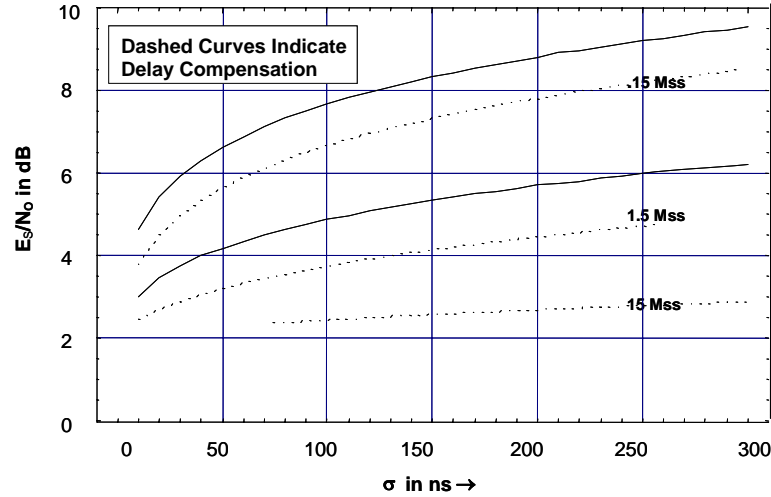


Figure 1-2. Plots of Required E_s/N_0 for 10^{-6} Decoded Error Rate as a Function of Multipath Delay Constant σ . Decision-Directed Modem with and without Delay Compensation. $f_0 = 7.5$ GHz, $W = 2$ GHz, $V = 100$ ft/sec., and Symbol Rates = .15, 1.5, and 15 Mss. Tap Weight Filter Time Constant T_F and Number of Rake Taps R Simultaneously Optimized for Each Point on Curves. Outdoor Dense Large-Multipath Channel.

Delay compensation improves performance particularly at the lower data rates where improvements in excess of 1 dB are indicated. With delay compensation, it is possible to use a larger value of TF at the same data rate for the same degree of time selective distortion. The resulting improved channel measurement allows use of larger values of R. That is to say, the optimal values of TF and R increase, which results in a lower value of required E_s/N_0 to achieve 10^{-6} error rate.

The increasing degradation, due to fast fading as the data rate decreases, is clearly evident in Figure 1-2. Assuming delay compensation at $\sigma = 300$ ns, there is around 5.5 dB larger E_s/N_0 required at a symbol rate of .15 Mss than at 15 Mss to obtain an error rate of 10^{-6} . At $\sigma=50$ ns, this drops to around 3.3 dB larger E_s/N_0 . Figure 1-3 presents an analogous set of curves for the indoor channel. Due to the lower terminal velocity (5 ft/sec as opposed to 100 ft/sec), the degradation due to time selective fading is reduced.

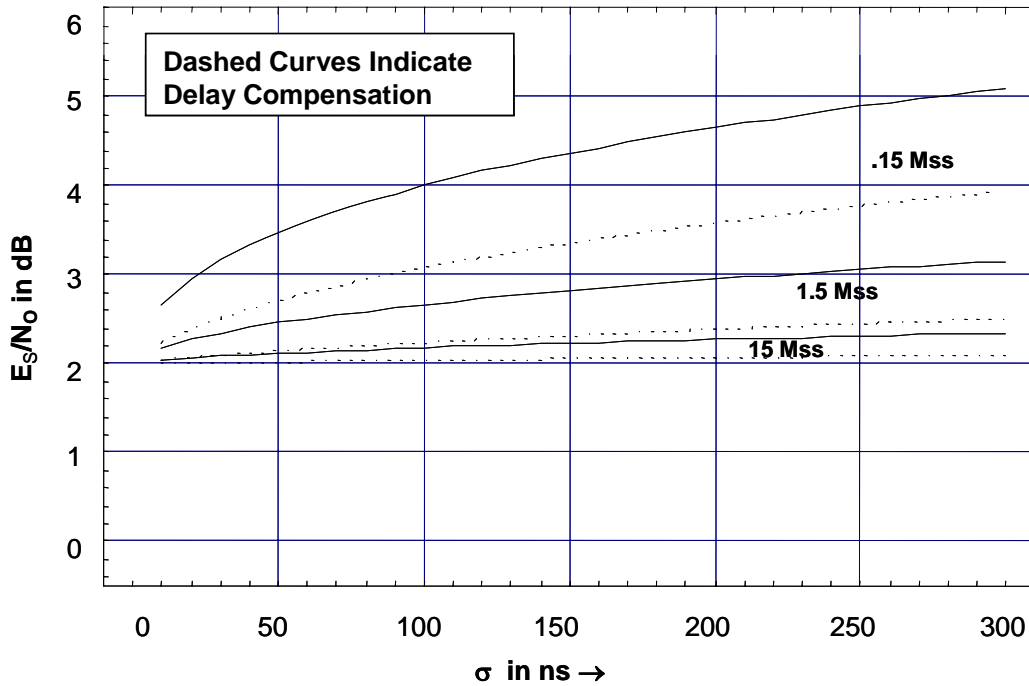


Figure 1-3. Plots of Required E_s/N_0 for 10^{-6} Decoded Error Rate as a Function of Multipath Delay Constant σ with and without Delay Compensation. $f_0 = 7.5$ GHz, $W = 2$ GHz, $V = 5$ ft/sec., and Symbol Rates = .15, 1.5, and 15 Mss. Normalized Tap Weight Filter Time Constant T_F and Number of Rake Taps R Optimized for Each Point on Curves. Indoor Dense Large-Multipath Channel.

The parallel probe and serial probe Rake modems are analyzed in Appendix D. Section 3.2.4.4 compares the performances of the decision-directed, parallel-probe, and serial-probe modems assuming delay compensation for data rates of .15, 1.5, and 15 Mss. For each figure, the required value of E_s / N_0 to obtain a decoded error rate of 10^{-6} is plotted vs. the multipath constant σ . In addition, the optimal values of normalized parallel-probe transmitted signal strength g and serial-probe modem probe period P (in units of data symbols) are plotted vs. σ . The time constant of the tap weight filter, T_F , and the number of Rake taps, R , are optimized for each value of σ .

It is found that the performances of the optimized parallel-probe and serial-probe modems are virtually identical. In addition, the decision-directed modem is always better, with increasing improvement as σ increases. The larger the impact of time-selective fading, as when lower data rates are used or the terminal velocity is higher, the greater the

improvement of the decision-directed modem over the probe modems. Reduced requirements on E_s / N_0 for the decision-directed modem range from a fraction of a dB to well over 2 dB. Although the performance of the decision-directed modem does not include degradation due to errors in decision-directed operation, this degradation is estimated to be a small fraction of a dB at the output SNR required to achieve a decoded bit error probability of 10^{-6} . Figures 1-4 and 1-5 present performance plots for the outdoor and indoor channels, respectively, for the 1.5 Mss symbol rate.

At sufficiently high data rates, it is necessary to consider performance limitations caused by “self-noise.” Self-noise is the residual signal appearing at a Rake correlator output due to all the other tap weight signals in the tapped delay line channel model⁵. A sufficient condition for neglecting the contribution of self-noise is that the received SNR in the bandwidth W , ρ_i , be much less than a threshold Γ , dependent upon the terminal equipment composite impulse response. With the assumed Gaussian shaped terminal equipment impulse response used, it is shown that $\Gamma = -7.35$ dB. For the numerical results obtained in this report, the input SNR is much less than -7.35 dB, indicating that the impact of self-noise will be small or negligible for these cases. However, these calculations apply to the case of no-noise excision. With an increasing percentage of the band excised, the threshold Γ decreases; for sufficiently high levels of excision, self-noise will have to be considered in the performance analysis.

⁵ The term self-noise was coined by R.Price in his analysis of a Rake modem performance [31]

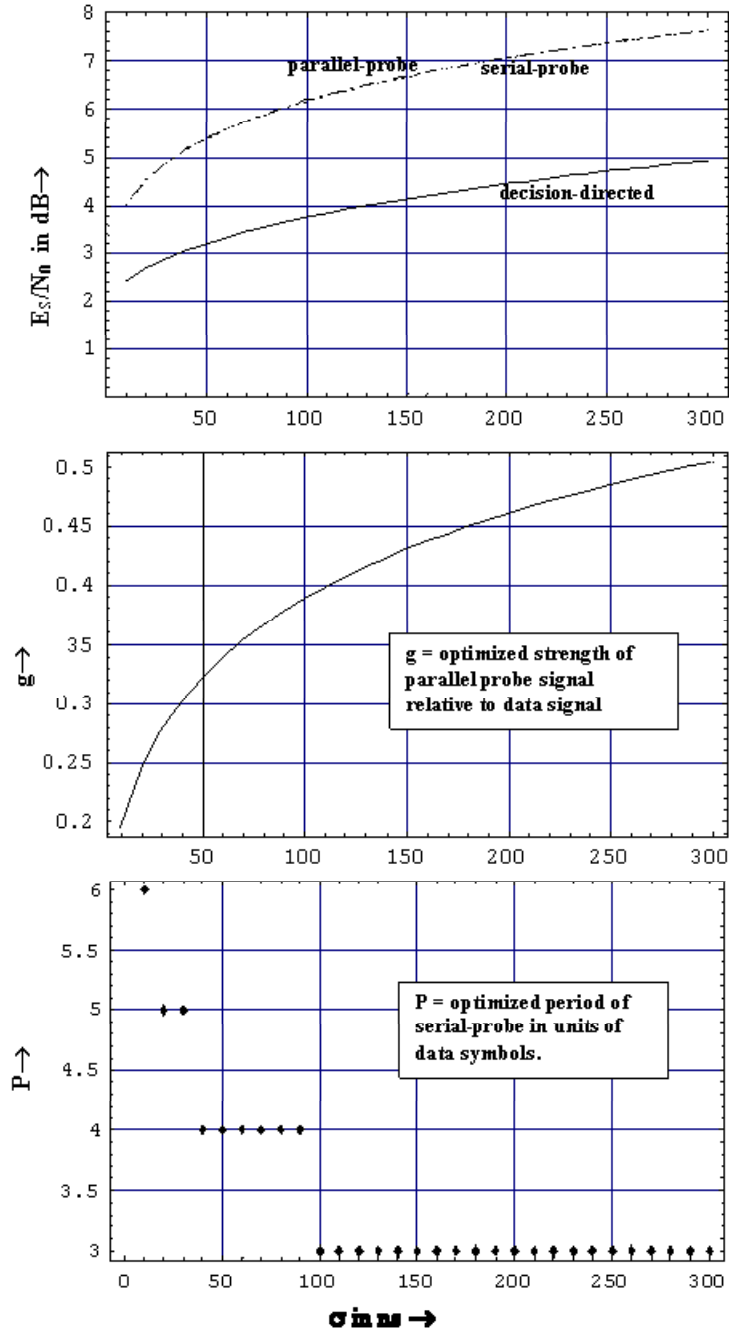


Figure 1-4. Comparison of Required E_s/N_0 to Obtain a Decoded Error Rate of 10^{-6} Over the Outdoor Channel for the Decision-Directed, Parallel-Probe, and Serial-Probe Modems at a Symbol Rate of 1.5 Mss. T_F , R , and Probe Parameters g and P Optimized at Each Value of σ . $f_0 = 7.5$ GHz, $W = 2$ GHz, and Relative Terminal Velocity of 100 ft./sec.

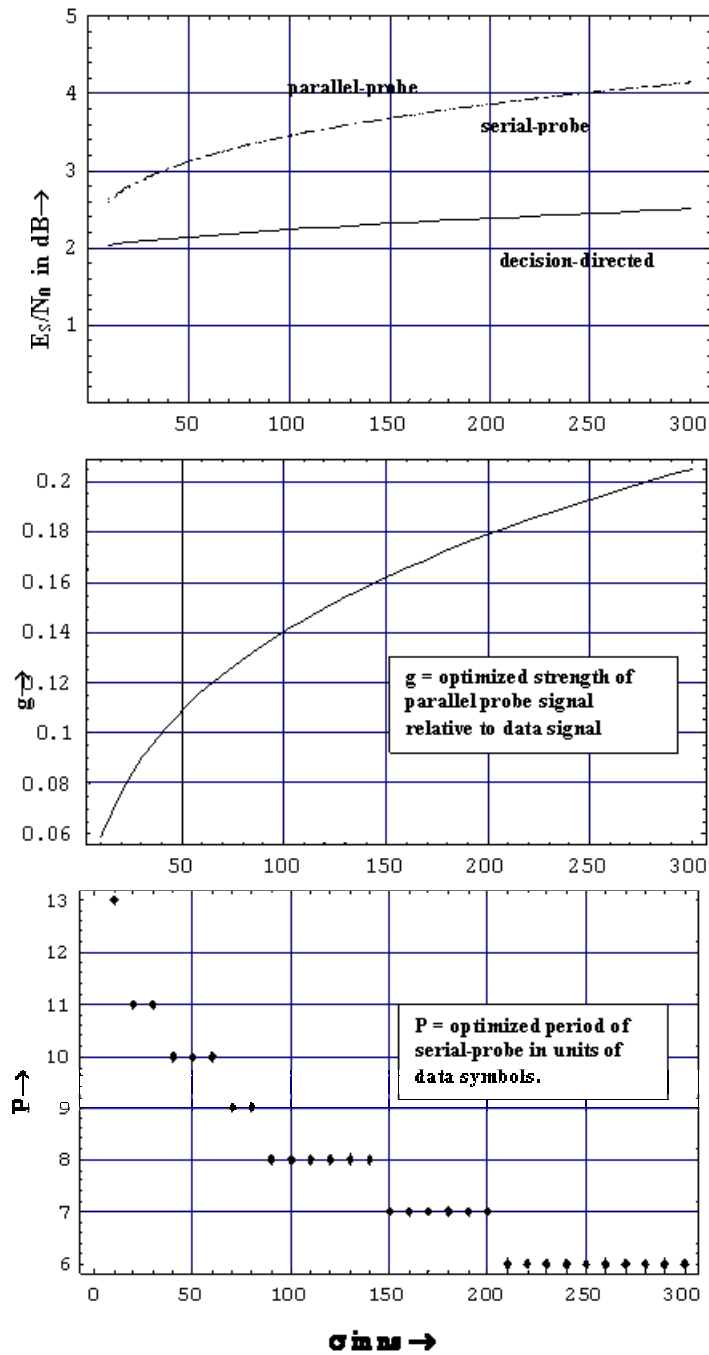


Figure 1-5. Comparison of Required E_s/N_0 to Obtain a Decoded Error Rate of 10^{-6} Over the Indoor Channel for the Decision-Directed, Parallel-Probe, and Serial-Probe Modems at a Symbol Rate of 1.5 Mss. T_F , R , and Probe Parameters g and P Optimized at Each Value of σ . $f_0 = 7.5$ GHz, $W = 2$ GHz, and a Relative Terminal Velocity of 5 ft./sec.

2 System Description

A high-level block diagram of the system to be analyzed is shown in Figure 2-1. Although not explicitly indicated in this diagram, it is assumed that an appropriate coder and decoder are part of the system. A baseband DSSS BPSK signal is up-converted to an appropriate intermediate frequency and then transmitted via an appropriate antenna subsystem. The antenna radiates signals in directions allowed by the antenna pattern and with distortions generally dependent upon the direction of transmission. It is assumed that a large number of reflecting/scattering objects with different reflecting /scattering coefficients intercept the radiated signal at different angles and reflect or reradiate the signals toward the receiving antenna and other reflectors/scatterers.

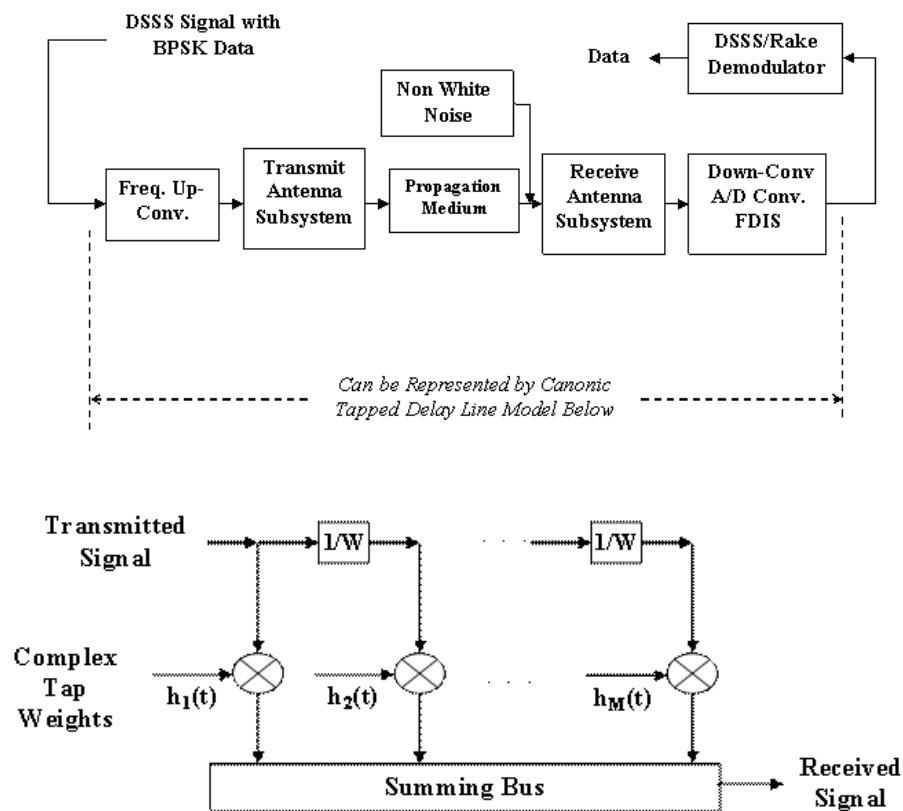


Figure 2-1. System Block Diagram and Canonic Tapped Delay Line Representation.

The receiving antenna also generally has a frequency selective antenna pattern, i.e., a transfer function which depends upon angle of arrival. Then the received radio frequency (RF) signal is the sum of these arriving multipath components plus a possible direct path and non-white noise. After filtering and complex down-conversion, the signal is fed to a noise whitener before being fed to the DSSS/Rake modem. Noise whiteners have various implementations. In the diagram, it is shown as a frequency domain interference suppressor (FDIS), indicating a Fast Fourier Transformation (FFT)-based interference excision implementation. Although not shown in the system diagram, transmitter and receiver antenna platforms may be moving. In addition, some scatterers and reflectors may be moving. These motions result in time-scale changes on the direct path received signal and on each multipath signal, with the change related to the rate of change of the corresponding travel path length. Time-scale change results in Doppler shifts, which vary across the transmitted signal bandwidth, and are proportional to frequency and the rate of change of path length. Only for the NB channel can the approximation be made that the whole band is subjected to the same Doppler shift.

Notwithstanding the complexity of the foregoing “microscopic” channel representation, if we assume the channel is linear and transmission band limited, it is represented rigorously as a canonical uniformly tapped delay line with real or complex ^[5,8] time varying weights, depending upon whether real low-pass or complex low-pass signal representations are used. The tap spacing must be equal to or smaller than $1/W$ where W is the transmitted signal bandpass bandwidth or $1/2W$ in the case of a low-pass signal bandwidth of W . The number of tap weights depends upon the delay spread of the multipath components and the sharpness of the skirts of the transmitter band-limiting filter. We assume there is a finite number of taps with tap weights having significant strength. Figure 2-1 shows the complex low-pass tapped delay line representation for a bandpass transmitted signal with complex time-variant tap weights. Note that M taps are shown, so that the total multipath spread modeled by this tapped delay line is

$$L_{\text{tot}} = (M - 1) / W \quad (2-1)$$

For simplicity of notation, we assume that the receiver synchronization process sets the earliest tap gain of significant strength at the first tap of the tapped delay line model. This representation we call the “excess-delay” tapped delay line model⁶.

The tapped delay line model is a “macroscopic” representation with a system function determined entirely by the joint statistics of the tap weights. As indicated in Figure 2-1, we use this model to replace the contents of the system block diagram situated between the vertical dashed lines. In order to carry out performance analyses, we will assume there is sufficient regularity in the dense multipath environment that the tap weights are wide-sense-stationary. We will make other assumptions necessary to carry out performance evaluations, however, always retaining the WB character of the channel, wherein performance is dependent on the parameter r . Appendix B analyzes the statistical behavior of the tap weights and provides the information needed in Appendices A and D to evaluate the performance of the DSSS/Rake modems.

Figure 2-2 presents a possible high-level block diagram of the signal processing in the receiver. The received signal is complex down-converted to 0 frequency with a locally generated estimate of the center frequency obtained from the frequency tracking loop. After complex A/D conversion (which includes an appropriate anti-alias filter) the signal is noise-whitened (in this case with an FDIS) and fed to the Rake processor. As will be discussed in detail, the front-end Rake processing involves the correlation of the input signal with delayed, locally generated, versions of the non-data-modulated transmitted PN sequence. The local PN sequence generator timing is obtained with the aid of a code tracking loop. Note that the two tracking loops have the same general structure in which the discriminator output is fed in cascade to a loop filter, a numerically controlled oscillator (NCO), and a frequency synthesizer. Both the frequency discriminator and the time discriminator are based upon the channel measurement outputs of the Rake processor. As will be shown, the Rake

⁶ The excess-delay tapped delay line channel model is discussed in Section B.3 of Appendix B.

processor provides measurements of the instantaneous complex weights⁷ in the tapped delay line model of the channel shown in Figure 2-1. Such measurements provide the fundamental information needed to construct effective time and frequency discriminators and a variety of implementations are possible. The implementation of such discriminators is not discussed in this report.

Figure 2-3 presents a block diagram of the signal correlation and combining portion of the Rake. For the system design chosen here, the direct sequence chip rate equals the bandwidth W of the transmitted signal. This choice simplifies the analysis and is also a reasonable practical choice. It means that if rectangular pulses of duration

$$\Delta = 1/W \quad (2-2)$$

were used, they would be distorted and overlapping in the transmitted signal. This would increase the peak-to-average power ratio above unity and require the use of linear power amplifiers. Since the UWB signal will be transmitting at low power, there is no difficulty in obtaining sufficient average power for reliable communications with linear amplifiers. The data symbol duration is assumed very much larger than Δ , i.e.,

$$T/\Delta = N = TW \gg 1 \quad (2-3)$$

where N is the number of chips in a symbol. It may be shown that any intersymbol interference has little effect on output SNR because it gets suppressed by the processing

⁷ Actual time sampled estimates of the tap weights are provided at the data symbol rate $1/T$, where T is the symbol duration.

Returning to Figure 2-3, we note that the direct sequence PN generator is clocked at a nominal rate of W cycles/sec and is fed to a shift register clocked at that same rate. The actual clocking rate is determined by the code tracking loop. Since the epochs of the symbol sequence are tied in a known way to the PN sequence epochs, the epochs of a received data signal are known once the PN sequence epochs are specified. Each delayed PN sequence from the shift register is correlated with the received signal from the FDIS. Specifically, after multiplication, the resulting stream is repeatedly integrated and dumped (I&D) from start time to stop time for successive symbols as determined by the timing of the locally generated code sequence. Thus, the correlator outputs are sequences clocked at the symbol rate $1/T$.

As shown in Appendix A, the p^{th} correlator output for the k^{th} I&D period, can be expressed as the sum of three terms: a signal term, a noise term, and a “self-noise” term. In Appendix A, it is shown that the signal term is given by the product $d_k W \tilde{h}_p \left(kT + \frac{T}{2} + \frac{p}{W} \right)$, where d_k is the data modulation for the k^{th} symbol (assumed ± 1) and $\tilde{h}_p(t)$ is a filtered version of the tap weight $h_p(t)$. The noise term is due to the result of correlating the (p/W -delayed) PN sequence with the input white noise. Self-noise is the residual signal appearing at the p^{th} correlator output due to all the other tap weight signals in the tapped delay line model. Ideally, the correlation operation suppresses these signals so that its affect on modem performance is negligible. As discussed in Section A.5, using results from [9], a sufficient condition for neglecting the contribution of self-noise to the combiner output is that the received SNR in the bandwidth W , ρ_i , be much less than a threshold Γ dependent upon the terminal equipment composite impulse response. For the assumed Gaussian-shaped terminal equipment impulse response used, it is shown that $\Gamma = -7.35$ dB. To summarize, the p^{th} correlator output for the k^{th} symbol may be expressed as

$$y_{pk} = d_k W \tilde{h}_p \left(kT + \frac{T}{2} + \frac{p}{W} \right) + n_{pk} + x_{pk} \quad (2-4)$$

where n_{pk} and x_{pk} are the p^{th} correlator output noise and self noise, respectively.

The tap weight estimation subsystem generates estimates of the tapped delay line model tap weights, sampled at $t = kT$. These estimates are denoted by $\{g_{pk}; p=1,2, \dots,R\}$. As shown in Figure 2-3, the I&D outputs are complex multiplied by the conjugate of the tap weight estimates and then summed to form the Rake output. Thus, the real part of the Rake combiner output for the k^{th} symbol is given by

$$C_k = \text{Re} \left\{ \sum_{p=0}^{R-1} g_{pk}^* y_{pk} \right\} = \text{Re} \left\{ d_k \sum_{p=0}^{R-1} W g_{pk}^* \tilde{h}_p \left(kT + \frac{T}{2} + \frac{p}{W} \right) + \eta_k \right\} \quad (2-5)$$

where η_k is the sum of the noise and self-noise contributions at the combiner output. For slow fading

$$\tilde{h}_p \left(kT + \frac{T}{2} + \frac{p}{W} \right) \rightarrow h_p \left(kT + \frac{T}{2} + \frac{p}{W} \right), \quad (2-6)$$

For fading slow enough and adequate SNR, sufficiently long averaging times can be employed in the channel measurement circuits to essentially remove the tap weight noise.

Then,

$$g_{pk} \rightarrow h_p \left(kT + \frac{T}{2} + \frac{p}{W} \right) \quad (2-7)$$

With such ideal conditions

$$C_k = d_k \sum_{p=0}^{R-1} W \left| h_p \left(kT + \frac{T}{2} + \frac{p}{W} \right) \right|^2 + \text{Re} \{ \eta_k \} \quad (2-8)$$

For binary PSK data, the real part of the summer output is fed to the decoder. Note that R Rake correlator taps or “fingers,” as they are sometimes called, are shown in Figure 2-3, while the tapped delay line model is shown as having M taps. The multipath spread of the channel is not known a priori, so that if the cost is not prohibitive, R can be selected for the reasonable worst multipath scenario. Then, when in fact it turns out that $M < R$, those tap weight estimates will ideally be negligible where the corresponding tap weights of the tapped delay line model are negligible. Such fingers will then contribute little to the Rake combiner output. In actual practice, a large number of such taps can contribute significant noise to the

combiner output unless the channel measurement is very good. The performance analyses to be presented include the performance degradation due both to noisy tap weights and to time selective fading distortion in the tap weight estimates.

We consider now the channel measurement subsystem. In [9], four channel measurement subsystems are defined for Rake combining. We will consider only three which are relevant here: decision-directed, parallel probe⁸, and serial probe channel measurement. Figure 2-4 presents a block diagram showing within dashed lines the decision-directed channel measurement subsystem portion for the p^{th} Rake finger. The same procedure is used for all R fingers. As mentioned, assuming binary PSK data is transmitted, the real part of the Rake combiner output is fed to the decoding subsystem. A hard binary (± 1) decision is made on the real part. These decisions are multiplied by the p^{th} correlator output to cancel out the data modulation. To simplify the discussion, we assumed that this decision takes infinitesimally greater than T seconds. Referring to (2-4) we see that this decision, if correct, will be given by d_{k-1} at the start of the k^{th} symbol.

Thus, to cancel out the data modulation, we must delay the output of the p^{th} correlator by one symbol clock time. The multiplier output is fed to a digital filter clocked at the symbol rate $1/T$. With fading slow compared to the symbol rate, it is possible to average over many symbols and thus improve the SNR at the measurement filter output relative to the SNR at the correlator output. There is an optimum filter time constant because if too long an averaging time is selected, the fading will cause distortion of the desired tap weight function being measured, while too short an averaging time will result in needless loss in output SNR. It may be seen that there is also an optimal number R of Rake

⁸ A parallel probe Rake modem was proposed and analyzed by Bello and Raemer in 1962 [12][13] assuming a WSSUS model of the Orbital Dipole channel. In this modem the information was conveyed by either digital or analog signals.

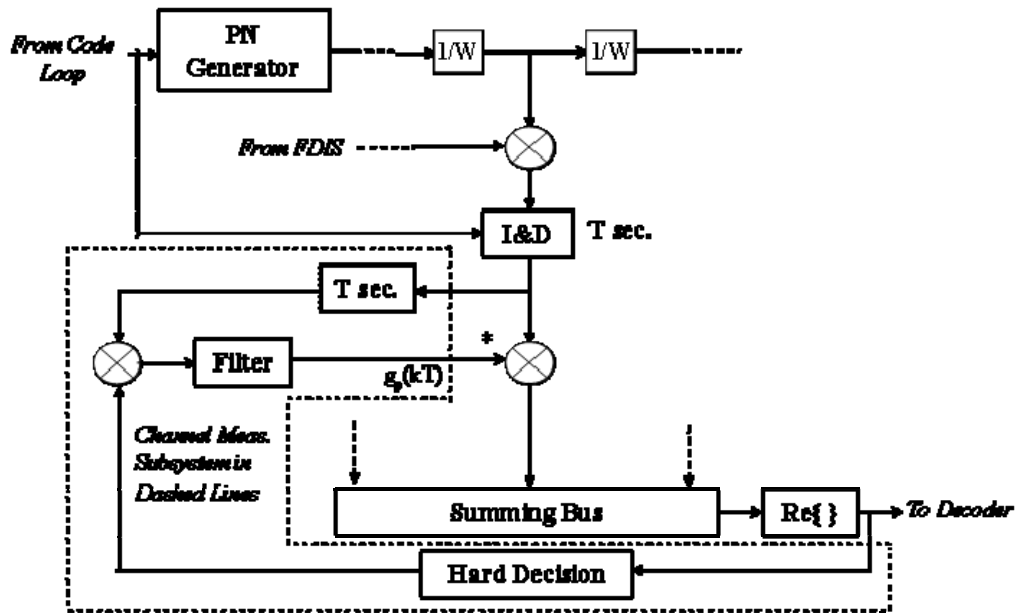


Figure 2-4. Block Diagram of Decision Directed Rake Channel Measurement Subsystem.

correlators since too small a value of R will fail to extract the energy in some tapped delay line model tap weights while too large a value of R will cause an increase in noise output due to tapped delay line model tap weights having little signal.

The SNR degradation of the decision-directed modem performance due to decision errors is not amenable to exact analysis. An approximate analysis of the impact of decision directed errors on a DSSS/Rake WBHF modem was carried out in [9]. Also, decision-directed operation with a DPSK modem was examined by Proakis et al [10] using simulation. A central conclusion of this study was that detection using a phase reference obtained through the decision-directed technique outlined herein results in system error rates which are generally lower, at all SNRs, than error rates of corresponding non-decision-directed phase measurement schemes. The decision-directed measurement technique has also been implemented for use with the WBHF DSSS/Rake modem developed at MITRE and, its effective operation supports these conclusions. For decision errors (i.e. raw bit error rates) of the order of .01 or less, it appears that negligible degradation in performance occurs. The

performance analysis presented in Appendix A ignores the effect of decision-directed errors⁹. Appendix D modifies the decision-directed performance analysis results to generate analytical results for the parallel and serial probe measurement subsystems.

The parallel probe measurement subsystem employs a separate non-data-modulated DSSS signal transmitted simultaneously with the data modulated DSSS signal. A separate uncorrelated direct sequence, PN modulation is used with the probe signal. Since both DSSS signals are being transmitted over the same band-occupancy, they are acted upon by the same time variant channel. Thus, channel measurements employing the probe DSSS received signal can be used to weigh the receiver data DSSS correlator outputs. Channel measurement with the received probing signal is a simplified version of that shown in Figure 2-4, in which the decision directed operation is removed and the correlator output is fed directly to the tap weight measurement filter. It is clear that this technique requires more hardware than the decision-directed approach. Also, power is needed for the probe which reduces the power available for data transmission.

The serial probe technique involves inserting a known data subsequence in the data stream at known symbol times. At the receiver only, the known data symbols are used for the channel measurement by feeding them to a channel measurement filter. Very little additional hardware is needed. However, the power spent on the known subsequence is not available for actual data symbols. In addition, the symbol rate has to be increased to maintain the same information throughput.

As discussed, the process of channel measurement for the three modems involves a tap-weight measurement filter. Degradation in performance results from the decorrelation between the estimated tap weight fluctuations and the tap weight fluctuations actually present at the Rake correlator output. Part of this decorrelation is caused by the delay of the tap-

⁹ Signal acquisition with decision-directed operation may result in a 180 degree ambiguity in the output raw data signal. This is not a unique problem of the DSSS/Rake modem. Clark and Cain ([11], Section 6.6.1) discuss the resolution of the problem for channels using PSK modulation and convolutional codes. One way this problem may be handled is by differential encoding/decoding around a transparent code. With this solution a doubling of the error rate results due to the differential encoding/decoding. Other approaches result in no performance loss.

weight measurement subsystem. For a “boxcar” tap-weight measurement filter, which averages over N_F I&D cycles, there is an average delay of $T(N_F+1)/2$ including the delay of T introduced to correct for the decision delay of the decision-directed modem as shown in Figure 2-4. The degradation due to time selectivity can be reduced by introducing a compensating delay in the signal path. The use of a compensating delay was discussed in [9]. Introduction of this compensating delay is simple with the parallel and serial probes since the measurement subsystem is separate from the data stream. However, delay compensation can still be introduced in the decision directed system as shown in Figure 2-5. This is done by introducing a parallel data path after each correlator containing the compensating delay. The decision-directed derived tap weight is also used to conjugate multiply the delayed correlator output. A separate adder is used to combine the delayed weighted correlator outputs to be sent to the decoder.

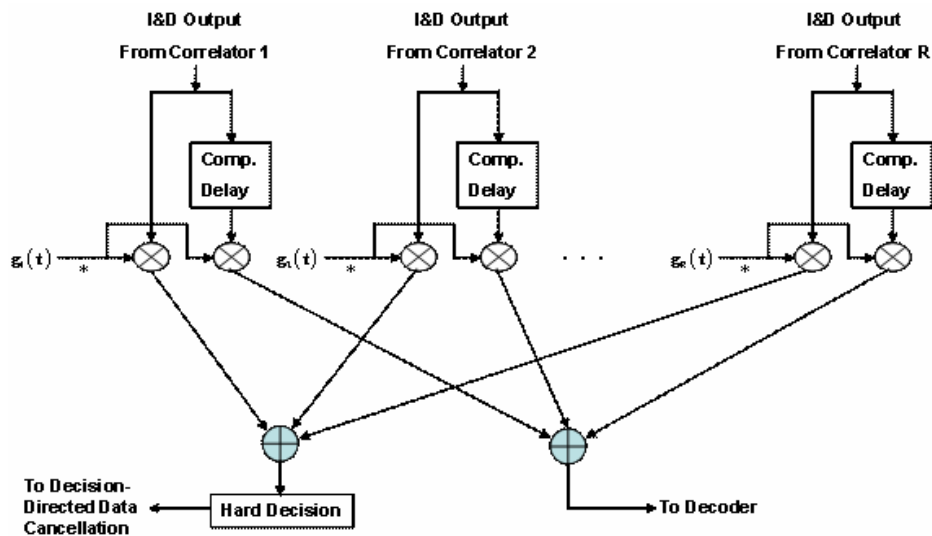


Figure 2-5. Illustration of Delay Compensation with Decision-Directed Implementation.

3 Performance

In this section, we present performance results for two hypothetical multipath channels: the outdoor base-station to urban mobile channel and the indoor fixed terminal to mobile terminal. To simplify the performance analysis, we assume a *dense multipath* environment. In simple terms, this definition means that each tap weight in the tapped delay line model is composed of a large number of multipath contributions, none of which dominates in strength. For brevity, we will call the idealized multipath channels used to evaluate the DSSS/Rake modem, the *outdoor dense multipath* and the *indoor dense multipath* channels. The most important consequence of the dense multipath assumption is that the tap weights in the complex low-pass-model approach complex Gaussian processes due to the Central Limit Theorem. If one assumes this limit has been approached close enough, and the cross-correlation functions of the tap weights can be determined, a complete statistical description of the tap weights is available, and an analytical approach to error rate evaluation is possible using results of Turin [14].

In Section 3.1, we present an overview of the channel modeling effort and the theoretical expressions arrived at for the cross-correlation functions and cross-power spectra for the tap weights. We also outline the assumptions and rationale for the derivations. Appendix B presents the detailed tapped delay line channel model analysis. In Section 3.2, we present both coded and uncoded error rate performance evaluations for both the indoor and outdoor dense multipath channels. The detailed analyses may be found in Appendices A and D.

3.1 Tapped Delay Line Model Second Order Statistics

Section 3.1.1 formulates an expression for the received signal and the time variant impulse response of the WB channel that serves as the basis for representing the tap weights in the tapped delay line channel model in Appendix B. Section 3.1.2 relates the complex weights in the tapped delay line model of the channel to the time variant impulse response derived in Section 3.1.1. Section 3.1.3 presents theoretical tap weight cross-correlation functions and cross- power spectra. Section 3.1.4 applies these results to specific outdoor

and indoor dense multipath channels. Detailed derivations of these results are presented in Appendix B.

3.1.1 Received Signal

There are two noteworthy consequences to WB as opposed to NB channel modeling. One consequence is that antenna distortions will generally show dependence upon the direction of transmission and arrival of a signal. However, any distortion caused by the antenna will pale in insignificance by comparison with the distortion caused by the dense multipath channel models assumed in the performance analysis. For this reason, to simplify the analysis, we do not include antenna distortion in our simplified models used for performance computation. The other consequence of WB transmission is the need to properly include the effects of time scale change in the channel model. The NB simplification of representing the effect of time scale changes caused by motion via constant Doppler shifts across the band is no longer possible. There is no way to design out the effects of time-scale changes upon the channel model. Consequently, the effect of time-scale change is included in our analysis at the outset.

We will use complex envelopes for band-pass waveform representations. Thus, the real transmitted signal $x(t)$ and real received signal of the channel are represented in the form

$$x(t) = \text{Re}\{z(t)e^{j2\pi f_0 t}\} \quad (3-1)$$

$$y(t) = \text{Re}\{w(t)e^{j2\pi f_0 t}\} \quad (3-2)$$

where $z(t)$ and $w(t)$ are the complex envelopes of the input and output signals, respectively, and f_0 is the carrier or center frequency. We assume that the real transmitted signal is bandlimited to $(f_0 - W/2 \leq f \leq f_0 + W/2)$ Hz. In this case $z(t)$ is bandlimited to the frequency band $|f| \leq W/2$. A proper representation of time-variable delays with the complex envelope formulation is fundamental to modeling the complex WB channel. Thus, consider that the transmitted signal $x(t)$ is subjected to a time variable delay $\tau(t)$. Then the received signal is given by

$$y(t) = x(t - \tau(t)) \quad (3-3)$$

It follows from (3-1) and (3-2) that the complex envelope of the received signal is given by

$$w(t) = z(t - \tau(t))e^{-j2\pi f_0 \tau(t)} \quad (3-4)$$

Thus, in addition to the expected time variable delay imposed on the transmitted complex envelope, there is an exponential factor producing a time variable phase modulation. If we expand $\tau(t)$ in a power series in t and retain only the first two terms, it is seen that the effect of the time variable delay on the exponential is to produce a phase shift and a Doppler shift. The effect on the received complex envelope term $z(t - \tau(t))$ is to produce a time-scale change and a delay.

We consider first the most elementary WB channel, consisting of transmit and receive antennas, a direct path between transmitter and receiver, and no multipath. The direct-path distortion is caused by the filtering operations of the transmitter and receiver terminal equipment including the antennas. Let $g_0(\xi)$ be defined as the direct path reference impulse response¹⁰ complex envelope, i.e., the response with transmit and receive antennas separated by a reference distance¹¹ and with the direct path delay removed. Thus, if a signal with complex envelope $z(t)$ is transmitted over this reference channel, the received signal has the complex envelope $w_0(t)$, given by

$$w_0(t) = \int z(t - \xi)g_0(\xi)d\xi \quad (3-5)$$

We call $w_0(t)$ the direct-path reference received signal. With antennas separated at normal operating ranges and mobile platforms, the direct path impulse response becomes time-variant. If $h(t, \xi)$ is the time variant complex envelope impulse response¹² of a channel,

¹⁰ This impulse response includes all filtering due to the transmitter and receiver and is sometimes called the terminal equipment impulse response.

¹¹ \geq the minimum needed to achieve far-zone antenna patterns.

¹² There are many ways to represent the input/output relationship for a time variant random channel [5]. To distinguish $h(t, \xi)$ from other possible relationships, in [5] $h(t, \xi)$ is called the Input Delay Spread function.

then the output complex envelope $w(t)$ is related to the input complex envelope $z(t)$ by the convolution integral

$$w(t) = \int z(t - \xi) h(t, \xi) d\xi \quad (3-6)$$

With mobile platforms, the direct path impulse response becomes

$$h(t, \xi) = a_0(t) g_0(\xi - \xi_0(t)) e^{-j2\pi f_0 \xi_0(t)} \quad (3-7)$$

The direct path delay is given by $\xi_0(t)$, and $a_0(t)$ is an amplitude factor accounting for path-loss changes including the effect of antenna pattern and “R²” losses.

Using (3-5) and (3-7), in (3-6) it is found that the direct path channel response for moving terminals is given by

$$w(t) = a_0(t) w_0(t - \xi_0(t)) e^{-j2\pi f_0 \xi_0(t)} \quad (3-8)$$

Consider next a direct path plus a single “reflected” path. A multipath component may be created by single or multiple reflections, scattering, or diffractions. However, for simplicity, we use the single term "reflected" to represent the process of multipath formation. The impulse response of this channel can be represented as

$$h(t, \xi) = a_0(t) e^{-j2\pi f_0 \xi_0(t)} g_0(\xi - \xi_0(t)) + a_1(t) e^{j\phi_1(t)} e^{-j2\pi f_0 \xi_1(t)} g_0(\xi - \xi_1(t)) \quad (3-9)$$

The 1 subscript has been used to denote the reflected path complex weight and path delay. Note that $a_1(t)$ includes the effect of reflection loss in addition to path loss. A phase shift $\phi_1(t)$, due to the reflection process, has also been included. Even with multiple reflections, the received signal can be regarded as coming from a mirror image transmit antenna along a virtual line-of-sight path producing a net delay of $\xi_1(t)$. It follows that the received signal is now given by

$$w(t) = a_0(t) e^{-j2\pi f_0 \xi_0(t)} w_0(t - \xi_0(t)) + a_1(t) e^{j\phi_1(t)} e^{-j2\pi f_0 \xi_1(t)} w_0(t - \xi_1(t)) \quad (3-10)$$

It is the sum of two differently weighted, time-scaled, and delayed replicas of the reference received signal.

Generalizing to the multiple-path case with K paths in addition to the direct path, the impulse response for the WB channel is given by

$$h(t, \xi) = \sum_{k=0}^K a_k(t) e^{j\phi_k(t)} e^{-j2\pi f_0 \xi_k(t)} g_0(\xi - \xi_k(t)) \quad (3-11)$$

where a_k , ϕ_k ¹³, and ξ_k , $k > 1$, are the path loss, reflector phase shift, and delay for the k th multipath component¹⁴. The corresponding received signal is represented by

$$w(t) = \sum_{k=0}^K a_k(t) e^{j\phi_k(t)} e^{-j2\pi f_0 \xi_k(t)} w_0(t - \xi_k(t)) \quad (3-12)$$

Note that we have not included frequency dependence of reflection coefficients.

However this frequency dependence is a second order effect as it is swamped by the time variant frequency selective distortion produced by the multipath spread of the multiple paths per se. The inclusion of such distortion would complicate the model considerably but is not likely to have a significant impact on the comparative evaluation of modem performance.

3.1.2 Canonic Tapped Delay Line Model

It is assumed that the time-variant channel is band limited¹⁵ with a center frequency f_0 . As a consequence, via the Sampling Theorem, the complex envelope of the time variant impulse response of the channel, $h(t, \xi)$, may be represented in the form

¹³ $\phi_0 = 0$.

¹⁴ If one wishes to include the effect of transmission and arrival angle dependence upon antenna distortion, then (3-11) must be changed to

$$h(t, \xi) = \sum_{k=0}^K a_k(t) e^{j\phi_k(t)} e^{-j2\pi f_0 \xi_k(t)} g_k(\xi - \xi_k(t))$$

which allows for a different reference impulse response for every multipath component.

$$h(t, \xi) = \sum_n h\left(t, \frac{n}{W}\right) \text{sinc}\left(W\left(\xi - \frac{n}{W}\right)\right) \quad (3-13)$$

where W is equal to or greater than the actual (two-sided) bandwidth of the channel. Using (3-13) and assuming the input signal bandwidth is equal to or less than W Hz, we obtain the tapped delay line input/output representation, where $z(t)$ is the input and $w(t)$ is the output,

$$w(t) = \sum_n h_n(t) z\left(t - \frac{n}{W}\right) \quad (3-14)$$

and

$$h_n(t) = \frac{1}{W} h\left(t, \frac{n}{W}\right) \quad (3-15)$$

$h_n(t)$ is the time-variant weight associated with the tap delay n/W .

Using (3-13) in (3-15) we find the n^{th} tap weight for the WB channel is given by

$$h_n(t) = \frac{1}{W} \sum_{k=0}^K a_k e^{j\phi_k} e^{-j2\pi f_0 \xi_k(t)} g_0\left(\frac{n}{W} - \xi_k(t)\right) \quad (3-16)$$

There are three sources of time variation in $h_n(t)$, the path weight a_k , the phase shift ϕ_k , and the path delay $\xi_k(t)$. We have not explicitly indicated the time variations of a_k and ϕ_k because these variations are usually much slower than the variations introduced by $\xi_k(t)$. The contribution to the n^{th} tap weight due to a multipath component with an increasing or decreasing delay $\xi_k(t)$ not only produces an increasing or decreasing phase shift $2\pi f_0 \xi_k(t)$ but also, as discussed in detail below, produces a pulse $g_0\left(\frac{n}{W} - \xi_k(t)\right)$. As a result, in a dense multipath environment, each tap weight consists of a sum of randomly arriving overlapping random pulses. The spectral spread of the tap weight process is due primarily to the combined variation in phase of $e^{-j2\pi f_0 \xi_k(t)}$ and to the spectral spread of the individual pulses $\left\{g_0\left(\frac{n}{W} - \xi_k(t)\right)\right\}$. The character of the individual pulses is made evident by using two terms

¹⁵ To be more precise, it is assumed that the time-variant transfer function of the complex low-pass channel, $T(f, t)$, defined as the Fourier Transform of $h(t, \xi)$ with respect to the delay variable ξ , is zero for $|f| \leq W/2$. This will occur if, as assumed here, the real band pass transmitter filter is band-limited to $|f - f_0| \leq W/2$.

in a power series expansion in t of the time variant delay and assuming that this linear variation in $\xi_k(t)$ is a good approximation over an interval of time equal to the duration of the pulse $g_0(\frac{n}{W} - \xi_k(t))$. Such pulses are then scaled and time shifted replicas of the reference pulse $g_0(t)$. Using the power series approximation

$$\xi_k(t) \approx \tau_k + \frac{v_k}{f_0} t$$

we obtain the following representation of the n^{th} tap weight

$$h_n(t) = \frac{1}{W} \sum_{k=0}^K a_k e^{j\phi_k} e^{-j2\pi v_k t} g_0\left(-\frac{v_k}{f_0} t - \tau_k + \frac{n}{W}\right) \quad (3-17)$$

where

$$v_k = \frac{f_0}{c} v_k \quad (3-18)$$

is the Doppler shift that would be produced at the frequency f_0 by a path velocity v_k equal to the rate of change of the k^{th} multipath component path length. c is the velocity of light. For simplicity, we have absorbed a phase shift $-2\pi f_0 \tau_k$ in the phase term ϕ_k . Examination of (3-17) shows that the n^{th} tap weight is the sum of randomly delayed, stretched, and frequency-shifted versions of the reference impulse response.

3.1.3 Tap Weight Cross-Correlation Functions and Cross-Power Spectra

In the derivation of the tap weight correlation functions and power spectra, the following assumptions are made for the multipath components of the excess delay channel¹⁶:

1. The arrival times $\{\tau_k\}$ follow a Poisson distribution with an average arrival rate of $\beta(n/W)$ per second for $k \in \alpha(n/W)$ ¹⁷.
2. The phases $\{\phi_k\}$ are independent of other parameters and independent and identically distributed (i.i.d.) with uniform probability density function (PDF) over $(0, 2\pi)$.

¹⁶ For a detailed discussion of these parameters, the reader is referred to Appendix B.

¹⁷ The set $\alpha(n/W)$ is defined at the end of Section B.2. It is the set of multipath components contributing to the n^{th} tap weight.

3. The path-amplitude a_k and Doppler shift v_k of the k^{th} multipath component are assumed to have a joint PDF $W(a, v, n/W)$ for $k \in \alpha(n/W)$ and are assumed i.i.d over k .
4. Small variations in tap weight statistics occur with small changes in tap delay position (n/W) . This is called the *smooth* assumption.

Using these assumptions, it is shown in Appendix B that the cross-correlation functions between the m^{th} and n^{th} tap weights is given by the following integral (see (B.51)),

$$\overline{h_n^*(t)h_m(t+\tau)} \triangleq R_{nm}(\tau) = \frac{1}{W} Q\left(\frac{m+n}{2W}\right) \int F\left(v, \frac{m+n}{2W}\right) e^{-j2\pi v\tau} C(-rv\tau + m-n) dv \quad (3-19)$$

and the cross-power density spectrum for tap weights m and n by (see (B.54)),

$$P_{nm}(f) = \int R_{nm}(\tau) e^{-j2\pi f\tau} d\tau = \frac{1}{W} \hat{Q}\left(\frac{m+n}{2W}\right) \int F\left(v, \frac{m+n}{2W}\right) \frac{1}{|v|r} E\left(-\frac{f+v}{vr}\right) e^{-j2\pi(m-n)\left(\frac{f+v}{vr}\right)} dv \quad (3-20)$$

where r is the normalized bandwidth given by (1),

$$F\left(v, \frac{n}{W}\right) = \frac{\int a^2 W\left(v, a, \frac{n}{W}\right) da}{\iint a^2 W\left(v, a, \frac{n}{W}\right) da dv} \quad (3-21)$$

is an amplitude-weighted Doppler PDF and

$$\hat{Q}\left(\frac{n}{W}\right) = \beta\left(\frac{n}{W}\right) \iint a^2 W\left(v, a, \frac{n}{W}\right) da dv \quad (3-22)$$

is the *power delay profile*¹⁸.

The function

$$C(\tau) = \int g^*(\xi)g(\xi + \tau) d\xi \quad (3-23)$$

¹⁸ We have adopted popular terminology to describe the tap weight average power as a function of tap delay.

is the aperiodic auto-correlation function of $g(t)$, the normalized direct path reference impulse response of the system in the absence of multipath. As noted previously, this impulse response models the effect of the filtering in the terminals. $g(t)$ is normalized to unit bandwidth ($W = 1$) and unit “energy.”¹⁹ $E(f)$ is the energy density spectrum corresponding to $C(\tau)$,

$$E(f) = \int C(\tau) e^{-j2\pi f\tau} d\tau \quad (3-24)$$

The strength of the n^{th} tap weight is given by

$$|\overline{h_n(t)}|^2 = R_{nn}(0) = \frac{1}{W} \widehat{Q}\left(\frac{n}{W}\right) \quad (3-25)$$

It is instructive to compare the tap gain correlation functions and spectra for the WB channel as summarized above with corresponding ones for a channel consisting of a filter with the same band limited normalized direct-path reference impulse response $g(t)$, in cascade with a hypothetical WSSUS²⁰ channel [5]. In this comparison, we make use of the *smooth* assumption defined previously which implies that the delay-Doppler scattering function $S(\xi, \nu)$ changes little over a delay (ξ) interval comparable to the duration of $g(t)$.

Equations (C-8) and (C-10), respectively, repeated below, present the tap gain cross-correlation functions for the band limited WSSUS channel using the smooth assumption

$$R_{nm}(\tau) = C(m-n) \frac{1}{W} Q\left(\tau, \frac{m+n}{2W}\right) \quad (3-26)$$

$$P_{nm}(f) = C(m-n) \frac{1}{W} S\left(\frac{n}{W}, f\right) \quad (3-27)$$

¹⁹ The energy of the corresponding real waveform would be 2.

²⁰ The WSSUS channel can be represented as a continuum of fixed statistically independent scatterers which cause statistically stationary scintillation. The power spectrum and auto-correlation function for scatterers causing delays in the interval $(\xi, \xi + d\xi)$ is given by $S(\xi, f)d\xi$ and $Q(\tau, \xi)d\xi$, respectively, where $S(\xi, f)$ is called the scattering function [5]. We call $Q(\tau, \xi)$ the tap gain correlation function (an alternate terminology was used by the author in [5] but the present terminology has a more intuitive appeal).

Consider now (3-19) and the form that the tap weight cross-correlation function takes as r approaches 0 for the WB channel,

$$\begin{aligned}\lim_{r \rightarrow 0} R_{nm}(\tau) &= C(m-n) \frac{\widehat{Q}\left(\frac{m+n}{2W}\right)}{W} \int F\left(v, \frac{m+n}{2W}\right) e^{-j2\pi v\tau} dv \\ &= C(m-n) \frac{\widehat{Q}\left(\frac{m+n}{2W}\right)}{W} D\left(-\tau, \frac{m+n}{2W}\right)\end{aligned}\quad (3-28)$$

where

$$D\left(\tau, \frac{m+n}{2W}\right) = \int F\left(v, \frac{m+n}{2W}\right) e^{-j2\pi v\tau} dv \quad (3-29)$$

is the characteristic function of the loss-weighted Doppler PDF. Fourier transforming the limit (3-28) we find that as r approaches 0, the tap weight cross-power spectrum approaches a limiting form

$$\lim_{r \rightarrow 0} P_{nm}(f) = C(m-n) \frac{1}{W} \widehat{Q}\left(\frac{m+n}{2W}\right) F\left(-f, \frac{m+n}{2W}\right) \quad (3-30)$$

Comparing the expressions for the WSSUS channel with those for the channel modeled here in the limit as r approaches 0, we can make the following identifications

$$Q(\tau, \xi) = \widehat{Q}(\xi) D(-\tau, \xi) \quad (3-31)$$

$$S(\xi, f) = \widehat{Q}(\xi) F(-f, \xi) \quad (3-32)$$

Thus, with the smooth assumption, we have shown that the NB channel (i.e., the WB channel for $r \rightarrow 0$) can be represented as the cascade of the direct path reference filter with a WSSUS channel having the scattering and tap gain correlation functions given by equations (3-32) and (3-31), respectively, since $D(0, \xi) = 1$, $\widehat{Q}(\xi) = Q(0, \xi) \equiv Q(\xi)$, which is identical to the delay power spectrum of the WSSUS model.

3.1.4 Specialization to Simplified Outdoor and Indoor Dense Multipath Channels

To carry the evaluations further, it is necessary to specify the amplitude-weighted Doppler PDF $F(v, n/W)$, the power delay profile $\widehat{Q}(\xi)$, and the auto-correlation function of the normalized terminal equipment impulse response, $C(\tau)$. In this section we summarize from Appendix B, the evaluation of tap weight correlation functions and spectra for two simplified but non-trivial WB examples: the outdoor base-station to urban mobile channel and the indoor fixed terminal to mobile terminal channel. In addition to the dense multipath assumption, in both cases we make four simplifying assumptions which are discussed in Appendix B:

1. Hypothetical isotropic antenna patterns at transmitter and receiver.
2. The multipath path-loss $(a_k)^2$ and Doppler shift v_k are statistically independent for $k \in \alpha_n$.
3. The Doppler PDF is independent of tap weight.
4. The power delay profile is exponentially decreasing.

With assumption (4), the power delay profile takes the exponential form

$$\widehat{Q}(\xi) = \frac{1}{\sigma} e^{-\frac{\xi}{\sigma}}; \sigma \geq 0 \quad (3-33)$$

where σ is the delay at which the power delay profile decreases by the factor e . Thus,

$$\frac{1}{W} \widehat{Q}\left(\frac{n}{W}\right) = \frac{1}{\sigma W} e^{-\frac{n}{\sigma W}} \quad (3-34)$$

Note, we have normalized $\widehat{Q}(\xi)$ to unit area.

In keeping with the smooth assumption used throughout, we assume that the delay constant

$$\sigma \gg 1/W \quad (3-35)$$

With assumptions (2) and (3) the joint PDF $W(\nu, \mathbf{a}, n/W)$ factors into the product $W(\mathbf{a}, n/W)W(\nu)$ where $W(\nu)$ is the common Doppler PDF for the tap weights. As discussed in Section B.5, the Doppler PDF for the outdoor channel is selected as

$$W(\nu) = \begin{cases} \frac{1}{\pi v_{\max} \sqrt{1 - \frac{\nu^2}{v_{\max}^2}}}; & |\nu| \leq v_{\max} \\ 0 & ; |\nu| > v_{\max} \end{cases} \quad (3-36)$$

and for the indoor channel as

$$W(\nu) = \begin{cases} \frac{1}{2v_{\max}}; & |\nu| \leq v_{\max} \\ 0 & ; |\nu| > v_{\max} \end{cases} \quad (3-37)$$

where

$$v_{\max} = \frac{v_R}{c} f_0 \quad (3-38)$$

is the maximum Doppler shift, c is the velocity of light, f_0 is the carrier frequency, and v_R is the speed of the mobile.

It is interesting to note from (3-32) that the above assumptions lead to the following factorable delay-Doppler scattering function for the approximating WSSUS channel when $\tau \rightarrow 0$,

$$S(\xi, f) = \hat{Q}(\xi)W(-f) \quad (3-39)$$

In the numerical evaluations, it is convenient to use normalized Doppler PDFs where the maximum Doppler shift is normalized to unity. The normalized Doppler PDFs corresponding to (3-36) and (3-37) are given, respectively, by

$$U(x) = \begin{cases} \frac{1}{\pi \sqrt{1 - x^2}}; & |x| \leq 1 \\ 0 & ; |x| > 1 \end{cases} \quad (3-40)$$

$$U(x) = \begin{cases} \frac{1}{2}; & |x| \leq 1 \\ 0; & |x| > 1 \end{cases} \quad (3-41)$$

For illustrative purposes, we assume that the energy density spectrum of the reference direct path impulse response equals the energy density spectrum of a Gaussian shaped pulse truncated to a bandwidth which encompasses 99.9 percent of the energy. This leads to the following expressions for the normalized energy density spectrum, $E(f)$, and aperiodic auto-correlation function, $C(\tau)$ ²¹,

$$E(f) = 2.628e^{-21.655f^2}; |f| \leq \frac{1}{2} \quad (3-42)$$

$$C(\tau) \approx e^{-.4558\tau^2} \quad (3-43)$$

With the above definitions and assumptions, the common normalized tap weight cross-correlation function as a function of the normalized delay $t = \tau v_{\max}$, is found to be given by the integral

$$c(t, r, m - n) = \frac{R_{nm}(t/v_{\max})}{\hat{Q}\left(\frac{m+n}{2W}\right)/W} = \int_{-1}^1 U(x) e^{-j2\pi x t} e^{-.4558(-rxt+m-n)^2} dx \quad (3-44)$$

and the normalized auto-correlation function by

$$c(t, r) = \int_{-1}^1 U(x) e^{-j2\pi x t} e^{-.4558(rxt)^2} dx \quad (3-45)$$

where r is the normalized bandwidth.

In terms of the normalized frequency variable $g = f/v_{\max}$, the normalized cross-power spectra is given by

²¹ We are neglecting the small perturbation caused by the truncation of the Gaussian shaped energy density spectrum.

$$p(g, r, m - n) = \frac{v_{\max} P_{nm}(g v_{\max})}{\hat{Q}\left(\frac{m+n}{2W}\right)/W} = \int U(y) \frac{1}{|y|r} E\left(-\frac{g+y}{yr}\right) e^{-j2\pi(m-n)\left(\frac{g+y}{yr}\right)} dy \quad (3-46)$$

and the normalized power spectrum of the n^{th} tap weight by

$$p(g, r) = \int U(y) \frac{1}{|y|r} E\left(-\frac{g+y}{yr}\right) dy \quad (3-47)$$

Note that the normalized tap weight auto-correlation function and power spectrum are independent of tap number while the corresponding normalized cross averages are dependent only on the difference of the tap numbers. Since, by hypothesis, $E(f)$ is zero outside the band $-1/2 < f < 1/2$, and $U(y)$ is zero outside the interval $-1 < f < 1$, the limits on the integrals in (3-38) and (3-39) are given by $\{\text{Max}[-1, -g/(1-r/2)], -g/(1+r/2)\}$ for $g > 0$ and by $\{-g/(1+r/2), \text{Min}[1, -g/(1-r/2)]\}$ for $g < 0$. When $|g| > (1+r/2)$, the integration intervals vanish and the integral is zero. Figures 3-1 and 3-2 present plots of the normalized tap gain power spectrum $p(g, r)$ vs. g with r as a family parameter, for the outdoor and indoor dense multipath cases, respectively. For both cases, as $r \rightarrow 0$, the normalized power spectrum of the n^{th} tap weight approaches the assumed normalized Doppler PDF. Figures 3-3 and 3-4 present plots of the magnitude of the cross-power spectra for the outdoor and indoor dense multipath cases, respectively, assuming tap number separations $n-m = 0, 1, 2, 3, 4$ and $r = 1$. Figures 3-5 and 3-6 provide 3D plots of the magnitude of the cross-power spectrum for two adjacent taps as a function of the normalized frequency and the normalized bandwidth for the outdoor and indoor dense multipath cases, respectively.

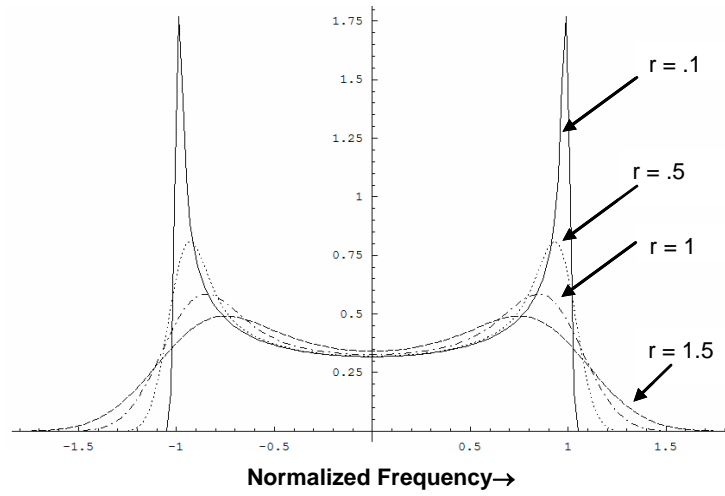


Figure 3-1. Normalized Power Spectrum of Tap Weights for Outdoor Dense Multipath Channel Assuming Normalized Bandwidth $r = .1, .5, 1, 1.5$.

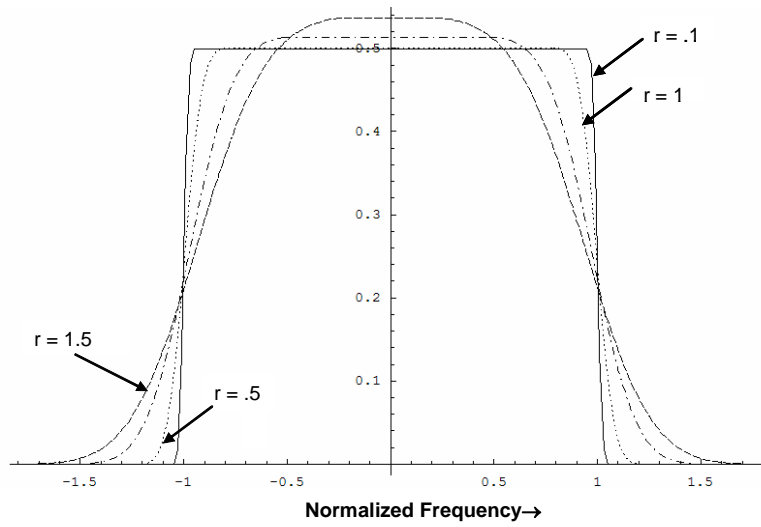


Figure 3-2. Normalized Power Spectrum of Tap Weights for Indoor Dense Multipath Channel Assuming Normalized Bandwidth $r = .1, .5, 1, 1.5$.

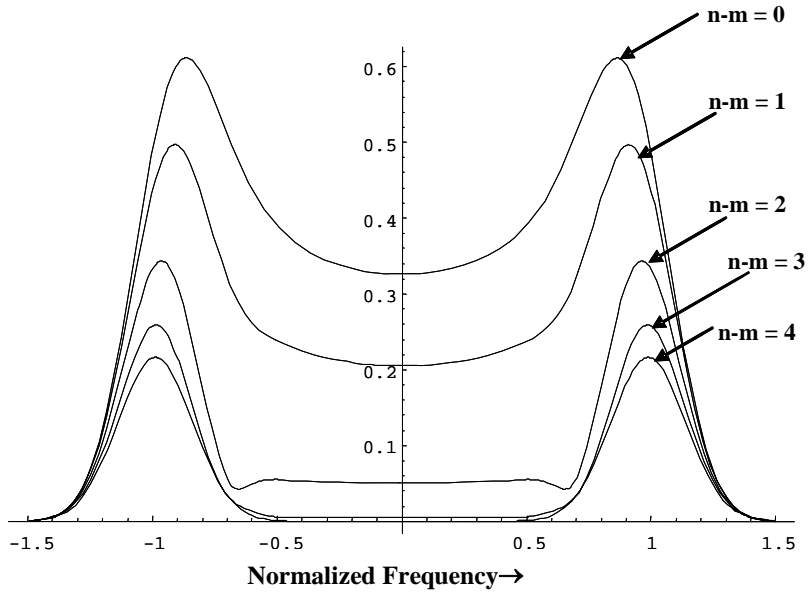


Figure 3-3. Magnitude of Cross-Spectra vs. Normalized Frequency for $n-m=0, 1, 2, 3,$ and 4 ; $r = 1$; and Outdoor Dense Multipath Channel.

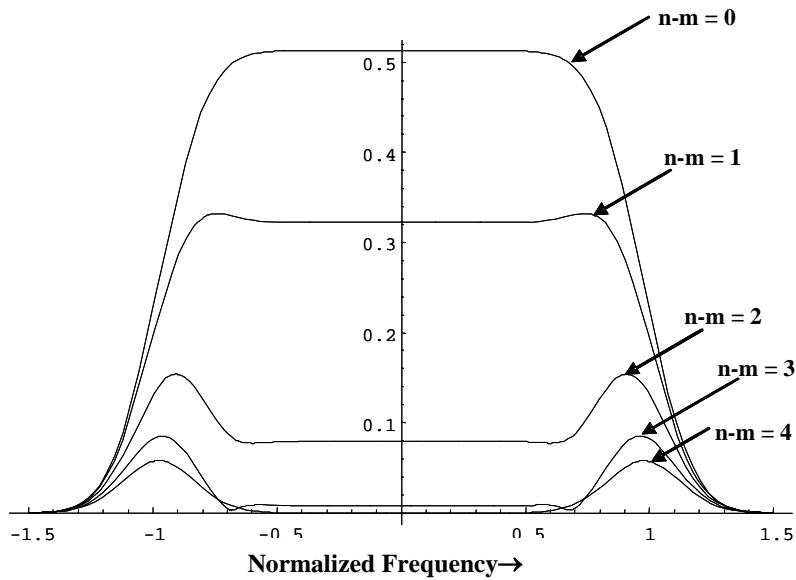


Figure 3-4. Magnitude of Cross-Spectra vs. Normalized Frequency for $0, 1, 2, 3,$ and 4 Tap Separations, $r = 1$, and Indoor Dense Multipath Channel.

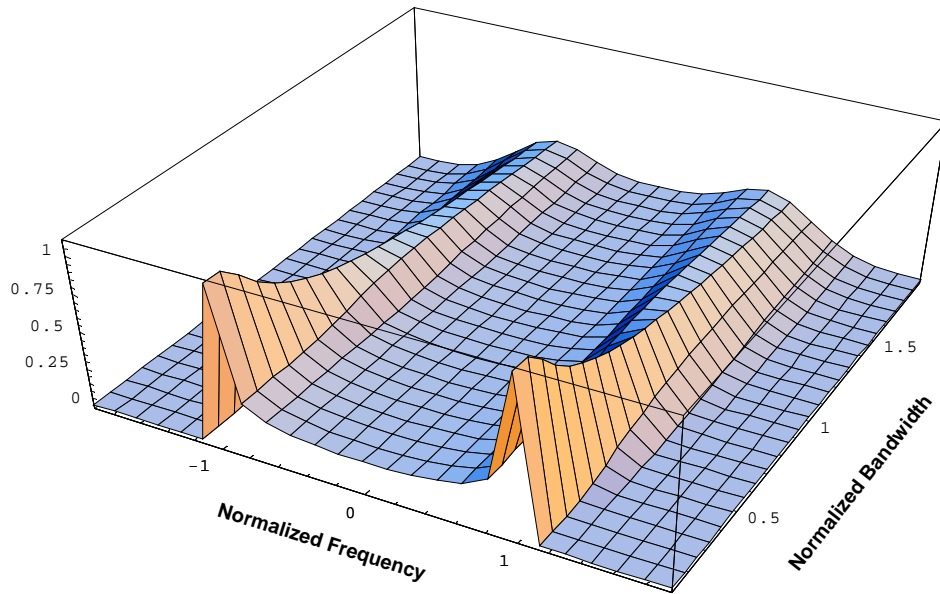


Figure 3-5. Plot of Magnitude of Normalized Cross-Power Spectrum for Two Adjacent Taps as a Function of Normalized Frequency and Normalized Bandwidth r . Outdoor Dense Multipath Channel.

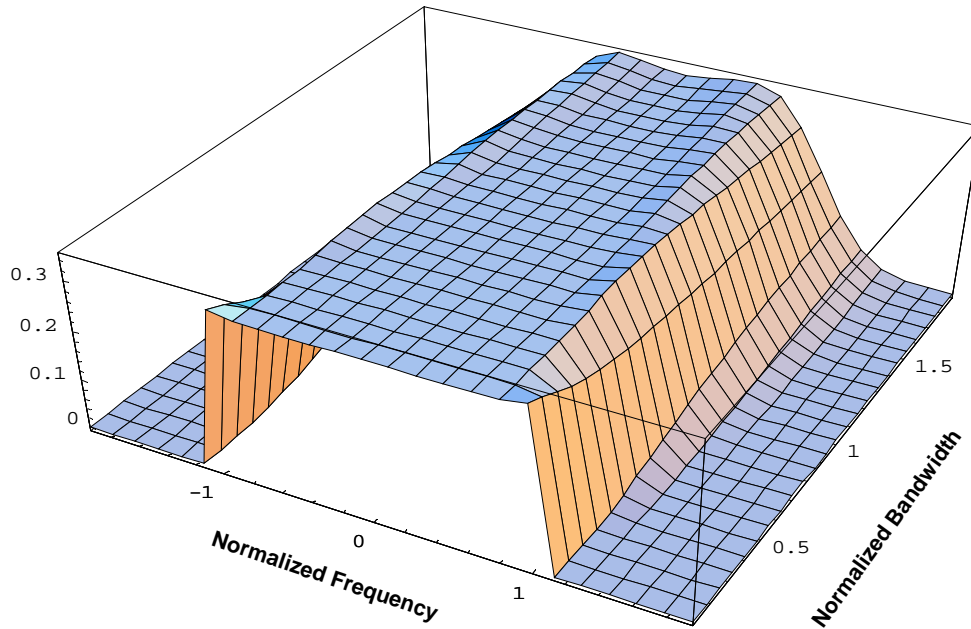


Figure 3-6. Plot of Magnitude of Normalized Cross-Power Spectrum for Two Adjacent Taps as a Function of Normalized Frequency and Normalized Bandwidth r . Indoor Dense Multipath Channel.

3.1.5 Relation of Channel Model to Standards

The IEEE 802.15 standards task group has established standard UWB channel models to be used for the evaluation of personal area network physical layer proposals [32]. This work emphasizes modeling stationary paths via statistics of the Power Delay Profile (PDP) and path loss. While many useful channel measurements have been taken and corresponding papers published (e.g., see [34]-[40] selected from [33]) since the publication of the standards paper in December 2003, the modeling focus has not materially changed from stationary terminals.

The need for a change was clearly indicated in [32]. We quote²² “The 802.15 standard model assumes that the channel stays either completely static, or changes completely from one data burst (about 100 μ s) to the next. While this covers extreme cases, some important aspects, like adaptive channel estimation and interleaving, cannot be simulated realistically. Because of this, the standard recommends the use of a more detailed model when time variance is of importance.” The study presented here is a step in that direction, developing a mobile UWB channel model for dense multipath which is characteristic of shadowed non-LOS channels. The analysis can be readily extended to the LOS case. In the same spirit as suggested in [32] for use of the standard model, the model proposed here is recommended for the comparative evaluation of mobile UWB modems rather than the absolute prediction of modem performance.

The proposed model is generic so that measurement campaigns will be needed to parameterize the model. However, since the PDP arises naturally in the development of the model presented here, it is suggested that PDP measurements be used in the absence of further measurement campaigns. For illustration purposes only numerical results describing the model

²² This is from the second paper in [32].

characteristics have been presented using the familiar exponentially decaying PDP (e.g. see [33]).

3.2 Performance Evaluations

Assuming complex Gaussian tap weights, the raw error probability equates to the probability that a quadratic form in complex Gaussian random variables is negative. This problem was evaluated first by Turin [14]. We call this method of evaluation, the “exact” method. In addition, two approximations to the error probability are presented that do not assume complex Gaussian tap weights. These are called *average channel* approximations and are termed the *SNR method* and the *Gaussian noise method*. Appendix A provides detailed derivations of the performance evaluations.

The SNR method is simplest. In effect, it is assumed that the time variant channel combined with the Rake processing can be represented by a time-discrete, time-invariant Gaussian channel. For this representation to be useful, certain quadratic forms in filtered tapped delay line model weights must be well approximated by their averages and the combiner output noise must be approximated by Gaussian noise. Each of these approximations are valid asymptotically as the number of significant strength tap weights becomes large, assuming no small subset of the weights dominate in strength. The number of significant tap weights is upper-bounded by the product WL_{tot} , where L_{tot} is a measure of the total multipath spread of the channel. We call a dense multipath channel tapped delay line model with $WL_{\text{tot}} \gg 1$ a *dense large-multipath* channel model.

The Gaussian noise method specializes results by Bello [15, 16] based on work of Turin [14] and Price [17, 18]. This method does not assume the combiner output decision variable is Gaussian. However, it does assume that the noise at the Rake correlator outputs consists of a set of i.i.d. complex Gaussian variables. As for the SNR method, the Gaussian noise method assumes that certain quadratic forms in the channel filtered tapped delay line weights

may be replaced by their averages and, as a consequence, requires a dense large-multipath channel model.

Sections 3.2.1 – 3.2.3 summarize the expressions for raw error rate using the SNR method, the Gaussian noise method, and exact method, respectively. Section 3.2.4 presents comparative plots of raw error rate vs. SNR for the three methods using the simplified indoor and outdoor channel models summarized in 3.1.4.

3.2.1 The SNR Method

In the SNR method, the real part of the Rake combiner output is approximated by a binary value plus a zero mean Gaussian noise. With this approximation, the channel raw bit error probability is

$$p_{rb} = \Phi\left(\sqrt{\rho_{out}}\right) \quad (3-48)$$

where ρ_{out} is the (decision variable) SNR and

$$\Phi(y) = \int_y^{\infty} \frac{1}{\sqrt{2\pi}} \exp\left(-\frac{x^2}{2}\right) dx \quad (3-49)$$

The sequence of decision variables at the combiner output for the SNR method are binary antipodal signal values of fixed level plus Gaussian noise. Consequently, the sequence of output decision variables is statistically identical to that of a hypothetical binary symmetric additive white Gaussian noise (AWGN) channel. Performance with error correction coding can then be determined from tabulated performances for codes used over AWGN channels. Thus, suppose a function $f_{code}(E_B/N_0)$ is available which relates decoder output bit error rate to E_B/N_0 ²³ for a hypothetical BPSK AWGN channel. Then the decoded bit error rate expressed in terms of ρ_{out} , the SNR of the hard decision variable, is given by

$$p = f_{code}\left(\rho_{out} / 2R_c\right) \quad (3-50)$$

²³ Ratio of energy per bit-to-noise power density. Also the ratio of input signal power to the noise power in a bandwidth equal to the throughput data rate.

where R_c is the code rate. However, it is readily seen that this expression applies equally to the channel model used in the SNR method²⁴ since the decision variable statistics are the same for the hypothetical AWGN channel output and the Rake output. A point of reference for subsequent calculations is the well known rate $\frac{1}{2}$, constraint length 7 convolutional code using 3 bit soft decision Viterbi decoding. For this code, a value of E_B/N_0 of approximately 5 dB²⁵ is required for a decoded error rate of 10^{-6} . For the rate $\frac{1}{2}$ code (3-50) reduces to $p = f_{\text{code}}(\rho_{\text{out}})$. Thus, a value of Rake output SNR of $\rho_{\text{out}} = 5$ dB is required for a decoded bit error rate of 10^{-6} provided the SNR method provides an accurate approximation. From (3-48), the raw bit error rate for $\rho_{\text{out}} = 5$ dB is $p_{\text{rb}} = .0377$.

In Appendix A, it is shown that for the SNR method, the output SNR can be expressed in the form (see (A-83))

$$\rho_{\text{out}} = \frac{2A^2 \rho^2}{R\gamma + B\rho} \quad (3-51)$$

where ρ is the energy/uncoded symbol divided by the input noise power density (also called E_s/N_0) and γ is the two-sided noise power bandwidth of the tap weight measurement filter. The coefficients A, B, have been evaluated using assumptions (1) – (4) of Section 3.1.3. However, we consider here only the specialized cases of the outdoor and indoor dense large-multipath channel models, for which the additional assumptions (1) – (4) of 3.1.4 apply.

Then, it is shown in Appendix A that

$$A = \chi \operatorname{Re} \left\{ \int_{-1-\frac{r}{2}}^{1+\frac{r}{2}} p(f, r) \operatorname{sinc}^2(fx) G_0(fx) e^{-j2\pi fx} df \right\} \quad (3-52)$$

²⁴ This expression does not account for the increase in error rate that occurs if differential encoding/decoding and transparent codes are used as the means of resolving the 180 degree ambiguity that is present in the channel due to decision-directed operation. However, this loss in performance amounts to only a small fraction of a dB and will be ignored in this report.

²⁵ From Figure 5.11 of report by J.P.Odenwalder [21].

$$B = \chi \left\{ \int_{-1-\frac{r}{2}}^{1+\frac{r}{2}} p(f, r) \text{sinc}^2(fx) |G_0(fx)|^2 df + \gamma \int_{-1-\frac{r}{2}}^{1+\frac{r}{2}} p(f, r) \text{sinc}^2(fx) df \right\} \quad (3-53)$$

where

$$\chi = \frac{\int_0^{R/W} \widehat{Q}(\xi) d\xi}{\int_0^{\infty} \widehat{Q}(\xi) d\xi} = 1 - e^{-\frac{R}{\tau}} \quad (3-54)$$

is the fraction of the tap weight power utilized by the R rake correlators. $G_0(f)$ is the normalized discrete tap weight estimation filter transfer function. This is related to the tap weight estimation filter $G(f)$ ²⁶ by

$$G_0(f) = \sum_{p=0}^{\infty} b_p e^{-j2\pi p f} = G\left(\frac{f}{T}\right) \quad (3-55)$$

x is a normalized Doppler shift parameter,

$$x = v_{\max} T \quad (3-56)$$

and τ is the normalized delay constant

$$\tau = \sigma W \quad (3-57)$$

For numerical evaluations, we use a “boxcar” tap weight measurement filter impulse response which averages over N_F samples. For this filter, $\gamma = 1/N_F$, $p(f, r)$ is the common normalized tap weight power spectrum given by (3-47) and specialized to the indoor and outdoor dense multipath channels by using (3-40) and (3-41), respectively.

3.2.2 The Gaussian Noise Method

In Appendix A it is shown that the raw bit error probability approximation for the Gaussian noise method is given by

²⁶ The tap weight filter has unity gain at $f = 0$, so that $\sum_{p=0}^{\infty} b_p = 1$.

$$P_{rb} = P_R \left(\sqrt{\frac{\rho}{\gamma}} [B - 2A\sqrt{\gamma}], \sqrt{\frac{\rho}{\gamma}} [B + 2A\sqrt{\gamma}] \right) \quad (3-58)$$

where the parameters ρ , γ , A , and B have already been defined in the previous section. The function

$$P_R(a, b) = Q\left(\frac{a}{\sqrt{2}}, \frac{b}{\sqrt{2}}\right) - \frac{1}{2} \exp\left(-\frac{a^2 + b^2}{4}\right) I_0\left(\frac{ab}{2}\right) + \exp\left(-\frac{a^2 + b^2}{4}\right) \left(\sum_{m=1}^{R-1} C_m(R) \left[\left(\frac{b}{a}\right)^m - \left(\frac{a}{b}\right)^m \right] I_m\left(\frac{ab}{2}\right) \right) \quad (3-59)$$

in which

$$Q(u, v) = \int_v^{\infty} x e^{-\frac{1}{2}(x^2 + u^2)} I_0(ux) dx \quad (3-60)$$

is Marcum's Q function [20] and

$$C_m(R) = \frac{1}{2^{2R-1}} \sum_{k=0}^{R-1-m} C_k^{2R-1} \quad (3-61)$$

where C_n^m is the binomial coefficient. Raw bit error rate calculations for the Gaussian noise method and the SNR method yield results so close that the differences are not visible on plots.

3.2.3 The Exact Method

In this section, we summarize the exact error probability evaluation for the special case in which both the tap weights and the noises at the correlator outputs may be approximated by zero mean complex Gaussian statistics. Then the combiner output decision variable assuming a fixed data bit, may be expressed as a Hermitian quadratic form q in zero mean complex Gaussian variables (see (5)). With the described statistics, the probability that the quadratic form $q < 0$ has been determined by Turin [15] for a general covariance matrix \mathbf{M} of the variables and a quadratic form matrix \mathbf{Q} . Thus, Turin shows that the characteristic function of q is given by

$$\phi_q(jt) \triangleq \overline{e^{jtq}} = \frac{1}{\text{Det}[\mathbf{I} - jt\mathbf{M}\mathbf{Q}]} \quad (3-62)$$

As pointed out by Turin, this is the reciprocal of a $2R^{\text{th}}$ degree polynomial in jt , the zeros of which lie at the reciprocals of the eigenvalues of the matrix $\mathbf{M}\mathbf{Q}$. The probability density function of q is given by

$$W(q) = \frac{1}{2\pi j} \int_{-j\infty}^{j\infty} \frac{1}{\text{Det}[\mathbf{I} - z\mathbf{M}\mathbf{Q}]} e^{-zq} dz \quad (3-63)$$

Integrating over $W(q)$, the raw bit error probability is given by the integral

$$p_{\text{rb}} = \Pr[q < 0] = \int_{-\infty}^0 W(q) dq = -\frac{1}{2\pi j} \int_{-j\infty}^{j\infty} \frac{1}{z\text{Det}[\mathbf{I} - z\mathbf{M}\mathbf{Q}]} dz \quad (3-64)$$

Again, as pointed out by Turin, it follows that once the eigenvalues of

$$\mathbf{P} = \mathbf{M}\mathbf{Q} \quad (3-65)$$

are determined, the integral in (A-64) may be determined by use of the residue theorem. The previous discussion shows that, in principle, the desired error probability can be determined for a quadratic form matrix \mathbf{Q} once the moment matrix \mathbf{M} is evaluated. To present this solution, we define the vector of variables

$$\mathbf{G} = [U_0, V_0, U_1, V_1, \dots, U_{R-1}, V_{R-1}] \quad (3-66)$$

where U_{k-1}, V_{k-1} are the complex weight and correlator output for the k^{th} Rake finger. Thus, the covariance matrix is given by

$$\mathbf{M} = \overline{\mathbf{G}^H \mathbf{G}} = \begin{bmatrix} \overline{U_0^* U_0} & \overline{U_0^* V_0} & \overline{U_0^* U_1} & \overline{U_0^* V_1} & \cdot & \cdot & \overline{U_0^* U_{R-1}} & \overline{U_0^* V_{R-1}} \\ \overline{V_0^* U_0} & \overline{V_0^* V_0} & \overline{V_0^* U_1} & \overline{V_0^* V_1} & \cdot & \cdot & \overline{V_0^* U_{R-1}} & \overline{V_0^* V_{R-1}} \\ \overline{U_1^* U_0} & \overline{U_1^* V_0} & \overline{U_1^* U_1} & \overline{U_1^* V_1} & \cdot & \cdot & \overline{U_1^* U_{R-1}} & \overline{U_1^* V_{R-1}} \\ \overline{V_1^* U_0} & \overline{V_1^* V_0} & \overline{V_1^* U_1} & \overline{V_1^* V_1} & \cdot & \cdot & \overline{V_1^* U_{R-1}} & \overline{V_1^* V_{R-1}} \\ \cdot & \cdot & \cdot & \cdot & \cdot & \cdot & \cdot & \cdot \\ \cdot & \cdot & \cdot & \cdot & \cdot & \cdot & \cdot & \cdot \\ \overline{U_{R-1}^* U_0} & \overline{U_{R-1}^* V_0} & \overline{U_{R-1}^* U_1} & \overline{U_{R-1}^* V_1} & \cdot & \cdot & \overline{U_{R-1}^* U_{R-1}} & \overline{U_{R-1}^* V_{R-1}} \\ \overline{V_{R-1}^* U_0} & \overline{V_{R-1}^* V_0} & \overline{V_{R-1}^* U_1} & \overline{V_{R-1}^* V_1} & \cdot & \cdot & \overline{V_{R-1}^* U_{R-1}} & \overline{V_{R-1}^* V_{R-1}} \end{bmatrix} \quad (3-67)$$

and the quadratic form of interest (see (2-5)) can be expressed as

$$\mathbf{q} = \mathbf{G}^H \mathbf{Q} \mathbf{G} \quad (3-68)$$

where \mathbf{Q} is a sparse matrix with the simple repetitive structure,

$$\mathbf{Q} = \begin{bmatrix} 0 & 1 & 0 & 0 & \cdot & \cdot & 0 & 0 \\ 1 & 0 & 0 & 0 & \cdot & \cdot & 0 & 0 \\ 0 & 0 & 0 & 1 & \cdot & \cdot & 0 & 0 \\ 0 & 0 & 1 & 0 & \cdot & \cdot & 0 & 0 \\ \cdot & \cdot & \cdot & \cdot & \cdot & \cdot & \cdot & \cdot \\ \cdot & \cdot & \cdot & \cdot & \cdot & \cdot & \cdot & \cdot \\ 0 & 0 & 0 & 0 & \cdot & \cdot & 0 & 1 \\ 0 & 0 & 0 & 0 & \cdot & \cdot & 1 & 0 \end{bmatrix} \quad (3-69)$$

This moment matrix has been evaluated in Appendix A utilizing the results in Section B.4.1 on the tap weight cross-power spectra and cross-correlation functions for the complex channel. With the normalizations used²⁷

$$\overline{U_n^* V_m} = \overline{\mu_n^* v_m} \quad (3-70)$$

$$\overline{U_n^* U_m} = \begin{cases} \overline{|\mu_n|^2} + 1; n = m \\ \overline{\mu_n^* \mu_m} ; n \neq m \end{cases} \quad (3-71)$$

²⁷ The complex noise in the correlator outputs and the tap weight estimates have been normalized to unity average magnitude-squared (see (A-102) – (A-110)).

$$\overline{V_n^* V_m} = \begin{cases} \overline{|v_n|^2} + 1; n = m \\ \overline{v_n^* v_m} ; n \neq m \end{cases} \quad (3-72)$$

where

$$\overline{v_n^* v_m} = \frac{\rho}{\sqrt{\gamma}} \int P_{nm}(f) \operatorname{sinc}^2(fT) G^*(f) e^{j2\pi f \left(\frac{n-m}{W} + T \right)} df \quad (3-73)$$

$$\overline{\mu_n^* \mu_m} = \frac{\rho}{\gamma} \int P_{nm}(f) \operatorname{sinc}^2(fT) |G(f)|^2 e^{j2\pi f \left(\frac{n-m}{W} \right)} df \quad (3-74)$$

$$\overline{v_n v_m} = \rho \int P_{nm}(f) \operatorname{sinc}^2(fT) e^{j2\pi f \left(\frac{n-m}{W} \right)} df \quad (3-75)$$

$P_{nm}(f)$ is given by (3-20) and $G(f)$ is the tap weight filter transfer function.

Using the normalized cross-power spectra (3-46) and power delay profile relationship (3-34), we can express the integrals in (3-73) - (3-74), in terms of normalized parameters and functions, as follows,

$$\overline{v_n^* v_m} = \frac{\rho}{\sqrt{\gamma}} \frac{e^{-\frac{n+m}{2\tau}}}{\tau} \int_{-1-\frac{r}{2}}^{1+\frac{r}{2}} p(f, r, m-n) \operatorname{sinc}^2(fx) G_0^*(fx) e^{j2\pi fx \left(1 + \frac{m-n}{N} \right)} df \quad (3-76)$$

$$\overline{\mu_n^* \mu_m} = \frac{\rho}{\gamma} \frac{e^{-\frac{n+m}{2\tau}}}{\tau} \int_{-1-\frac{r}{2}}^{1+\frac{r}{2}} p(f, r, m-n) \operatorname{sinc}^2(fx) |G_0(fx)|^2 e^{j2\pi fx \frac{m-n}{N}} df \quad (3-77)$$

$$\overline{v_n v_m} = \rho \frac{e^{-\frac{n+m}{2\tau}}}{\tau} \int_{-1-\frac{r}{2}}^{1+\frac{r}{2}} p(f, r, m-n) \operatorname{sinc}^2(fx) e^{j2\pi fx \frac{m-n}{N}} df \quad (3-78)$$

As mentioned, the raw error probability may, in principle, be determined by use of the residue theorem. However, this procedure becomes impractical in the current application where R is a very large number and the eigenvalues can be very close in value as the

distortion of the channel begins to degrade performance. We chose instead a single integral numerical evaluation of the error probability as outlined below.

Returning to (3-63), recasting the integral as an integration over the real variable t , and making a scale change, the PDF of the quadratic form defining the decision variable becomes

$$W(q) = \int_{-\infty}^{\infty} \frac{1}{\text{Det}[\mathbf{I} - j2\pi t \mathbf{M} \mathbf{Q}]} e^{-j2\pi t q} dt \quad (3-79)$$

Consider the raw error probability as the limit

$$p_{rb} = \lim_{a \rightarrow \infty} \int_{-a}^0 W(q) dq \quad (3-80)$$

Substituting (3-80) in (3-79), reversing the order of integration, and carrying out the integration over q ,

$$p_{rb} = \lim_{a \rightarrow \infty} \int_{-\infty}^{\infty} \frac{a \text{sinc}(at) e^{j\pi at}}{\text{Det}[\mathbf{I} - j2\pi t \mathbf{M} \mathbf{Q}]} dt \quad (3-81)$$

where

$$\text{sinc}(t) = \frac{\sin \pi t}{\pi t} \quad (3-82)$$

The limiting integration (3-81) was carried out using the numerical integration routines in *Mathematica*. This numerical procedure was checked against special cases for which exact analytical results are available.

3.2.4 Calculations

From arguments given previously, we expect the average channel methods to provide useful approximations to raw bit error rate when $\tau = \sigma W \gg 1$ and the required raw bit error rate is not very small. Section 3.2.4.1 presents illustrative calculations comparing raw error rate performance using the exact method with error rate predicted by the average channel methods for the decision-directed modem. Based on the SNR method and assuming the

dense large-multipath outdoor channel model, Section 3.2.4.2 presents some relevant calculations. The input SNR (E_s/N_0) required to achieve a decoded error rate of 10^{-6} is plotted versus multipath delay constant σ for the decision-directed modem. In addition, the optimal values of tap weight filter time constant T_F and number of Rake taps R used in the E_s/N_0 calculation are plotted versus σ . Section 3.2.4.3 presents a similar set of calculations for the dense large-multipath indoor channel. In both cases, the required values of E_s/N_0 are determined for both the non-delay-compensated and delay-compensated decision-directed modems. Section 3.2.4.4 compares the required values of E_s/N_0 for the delay-compensated decision directed modem evaluated in the previous two sections with corresponding calculations for the parallel and serial probe modems. In addition, optimized values of g , the relative power required for the parallel probe and optimized values of P , the period P of the serial probe in units of data symbols, are plotted vs σ for the indoor and outdoor channels.

3.2.4.1 Comparison of Exact Method and Average Channel Methods

For example calculations we use the outdoor dense large-multipath channel model at a center frequency $f_0 = 7.5$ GHz, a bandwidth $W = 2$ GHz, a symbol rate $D = 1/T = 1.5$ Mss, and a terminal velocity of 100 feet/sec. Figures 3-7 to 3-10, for $\sigma = 10, 20, 35$, and 50 ns (or $\tau = \sigma W = 20, 40, 70$, and 100) respectively, present plots of raw bit error probability vs E_b/N_0 for the three methods of error-rate estimation. We observe that the Gaussian noise method and the SNR method results are so close the differences are not visible on the plots. We also show the operating point at which the output SNR is 5 dB and the raw bit error rate prediction is .0377 for the SNR method. It will be recalled that assuming the validity of the SNR method, an output SNR of 5 dB yields a decoded error rate of 10^{-6} for a rate $1/2$ constraint level 7 convolutional code using 3 bit quantized soft decision decoding. For each graph, the number of Rake taps, R , and the tap weight filter integration time, $T_F = N_F T = N_F/d$, have been selected to minimize the required E_s/N_0 at this operating point. From these figures we see that the SNR method provides a close prediction of coded performance at $\sigma =$

10 ns with the prediction improving as σ increases. The same conclusion was arrived at for the indoor channel.

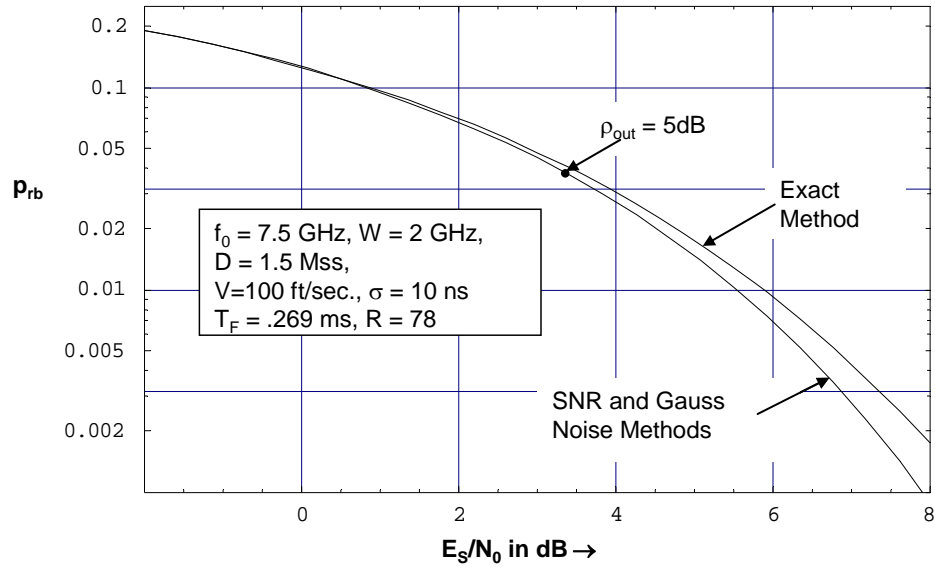


Figure 3-7. Raw Bit Error Probability as a Function of E_S/N_0 for an Example Outdoor Dense Large Multipath Channel Model with Multipath Delay Constant = 10 ns.

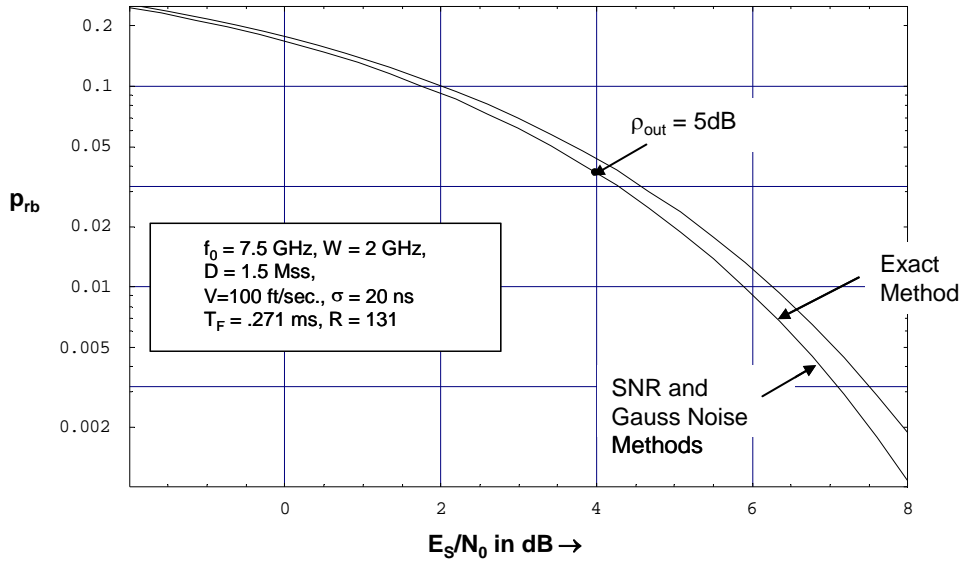


Figure 3-8. Raw Bit Error Probability as a Function of E_S/N_0 for an Example Outdoor Dense Large Multipath Channel Model with Multipath Delay Constant = 20 ns.

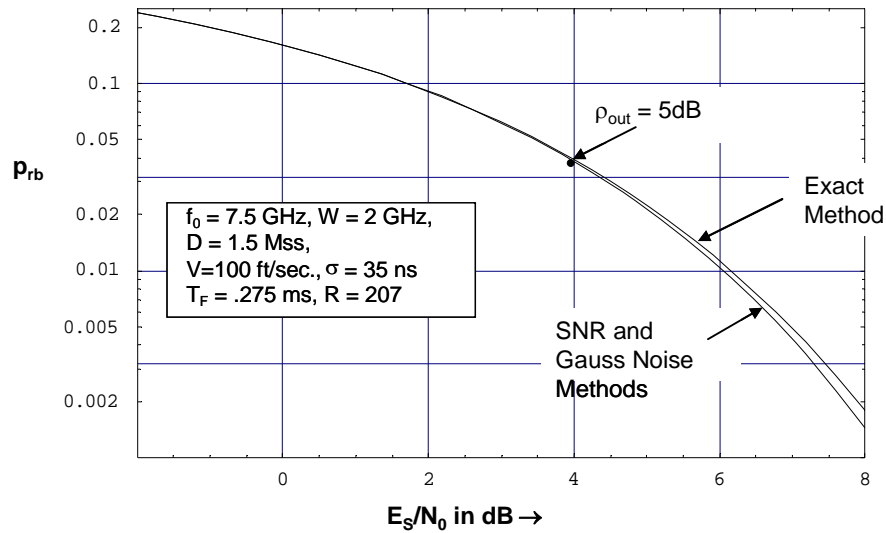


Figure 3-9. Raw Bit Error Probability as a Function of E_s/N_0 for an Example Outdoor Dense Large Multipath Channel Model with Multipath Delay Constant = 35 ns.

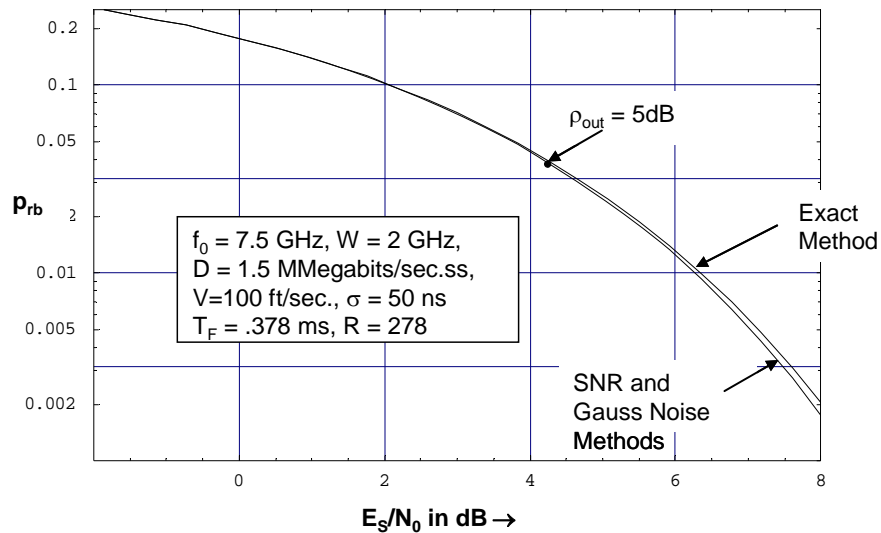


Figure 3-10. Raw Bit Error Probability as a Function of E_s/N_0 for an Example Outdoor Dense Large Multipath Channel Model with Multipath Delay Constant = 50 ns.

3.2.4.2 Performance for the Outdoor Dense Large Multipath Channel Model

The previous section has validated the use of the SNR method to evaluate modem performance for the dense large-multipath channel model. For the remainder of the performance analyses, we will use the SNR method. In this section, we plot the required

values of E_B/N_0 needed to obtain an output SNR of 5 dB for symbol rates of .15, 1.5, and 15 Mss as a function of σ . The parameters, R and T_F , are selected at each value of E_S/N_0 to maximize the output SNR. Both non-delay-compensated and delay-compensated modems are considered. Plots of these optimal values of R and T_F are also presented.

Figure 3-11 presents plots of required E_S/N_0 for an output SNR of 5 dB as a function of the multipath delay constant σ in the range of 10 to 300 ns for the outdoor channel. Six curves are presented. The three solid curves and the three dashed curves correspond to no delay compensation and delay compensation²⁸ calculations, respectively, for symbol rates of .15 Mss, 1.5 Mss, and 15 Mss, as in Figures 3-7 to 3-10, $f_0 = 7.5$ GHz, and $w = 2$ GHz. At each point on the curves, the parameters T_F and R have been optimized to minimize the required E_S/N_0 to achieve an output SNR of 5 dB. Figures 3-12 and 3--13, respectively, present the optimized values of T_F and R, respectively, as a function of σ .

We see from Figure 3-11 that as the symbol rate increases, the modem becomes more efficient, that is to say, at the same value of σ the required value of E_S/N_0 for an output SNR of 5 dB decreases. The minimum value of E_S/N_0 is 2 dB corresponding to the additive white Gaussian noise channel. As the symbol rate increases, the number of symbols averaged per unit time in the tap weight filter increases. Thus, the tap weights are less noisy for the same averaging time as the data rate increases. There are two consequences to this phenomenon. First, a larger number of taps R can be used for combining with increasing data rate because the tap weights are less noisy. Second, a shorter averaging time can be used with the higher data rate which leads to less time selective fading degradation. These results are visible in Figures 3-12 and 3-13.

²⁸ Appendix D includes an analysis of delay compensation.

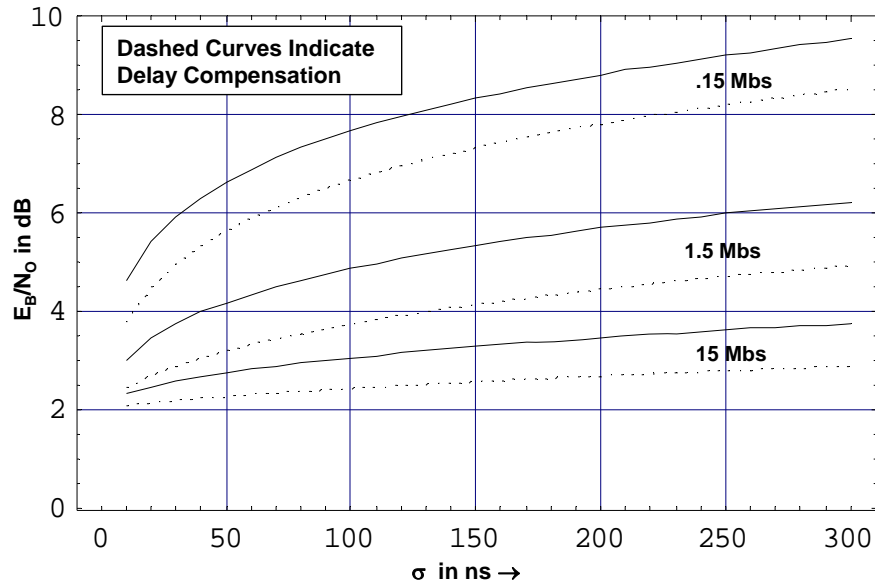


Figure 3-11. Plots of Required E_s/N_0 for 10^{-6} Decoded Error Rate as a Function of Multipath Delay Constant σ . Decision-Directed Modem with and without Delay Compensation. $f_0 = 7.5$ GHz, $W = 2$ GHz, $V = 100$ ft/sec., and Symbol Rates = .15, 1.5, and 15 Mss. Tap Weight Filter Time Constant T_F and Number of Rake Taps R Simultaneously Optimized for Each Point on Curves. Outdoor Dense Large-Multipath Channel.

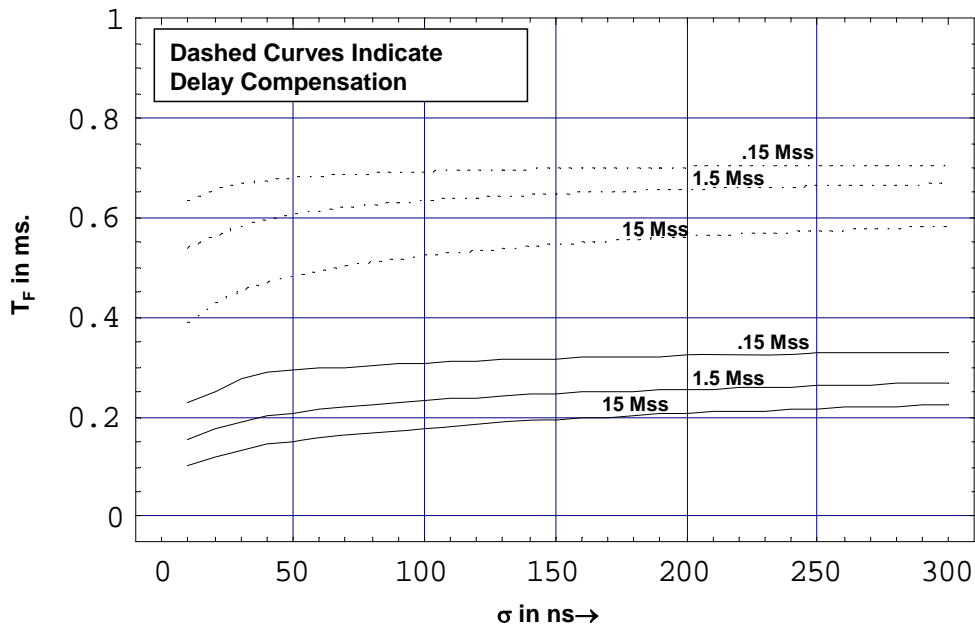


Figure 3-12. Optimal Values of Normalized Tap Weight Measurement Filter Time Constant T_F as a Function of Multipath Delay Constant σ Corresponding to Plots in Figure 3-11.

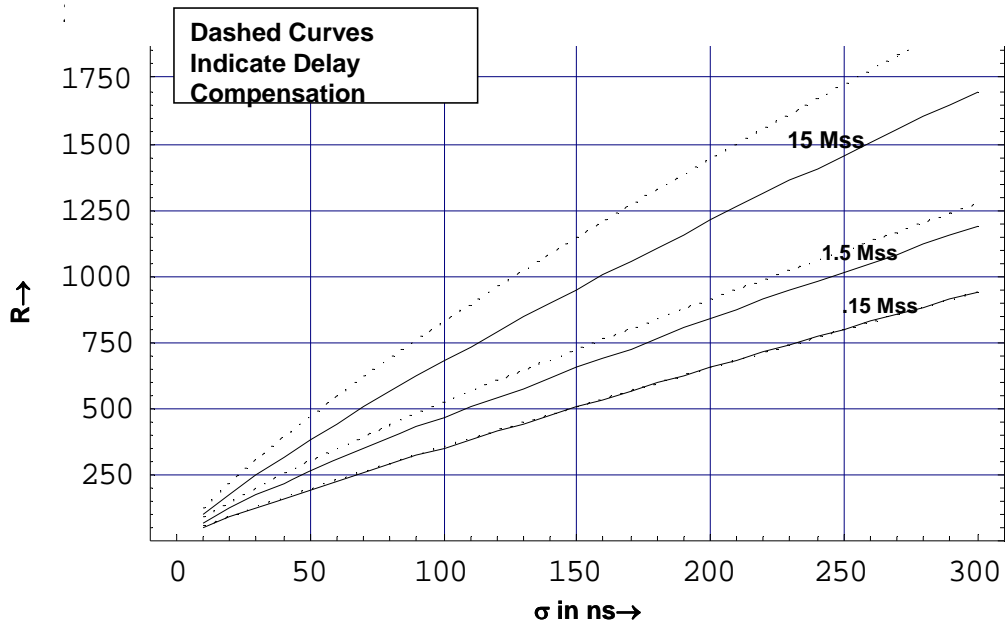


Figure 3-13. Optimal Value of the Number of Rake Taps R Corresponding to Plots in Figure 3-11.

Delay compensation improves performance particularly at the lower data rates where improvements in excess of 1 dB are indicated. With delay compensation, it is possible to use a larger value of T_F at the same data rate for the same degree of time selective distortion. The resulting improved channel measurement allows use of larger values of R . That is to say, the optimal values of T_F and R increase and this results in a lower value of required E_S/N_0 to achieve an output SNR of 5 dB.

The increasing degradation due to fast fading as the data rate decreases is clearly evident in Figure 3-11. Assuming delay compensation, at $\sigma = 300$ ns there is around 5.5 dB larger E_S/N_0 required at a symbol rate of .15 Mss than at 15 Mss to obtain an output SNR of 5 dB. At $\sigma = 50$ ns this drops to around 3.3 dB larger E_S/N_0 .

3.2.4.3 Calculations for the Indoor Dense Large Multipath Channel Model

Figures 3-14 through 3-16 present calculations for the indoor dense large multipath channel analogous to Figures 3-11 through 3-13 for the outdoor dense large multipath

channel. The only system parameter changed is the velocity, which is reduced from 100 ft/sec to 5 ft/sec, a brisk walking pace. In addition, the power spectra for the tapped delay line model weights change as shown in Section 3.1.4. However, the major impact on performance change relative to the outdoor example is the reduced velocity. This allows longer integration times for the Rake tap weight filters before time-selective fading becomes significant and thus improved channel measurement and lower required values of E_s/N_0 . Compare the larger optimized integration times in Figure 3-15 relative to those in Figure 3-12.

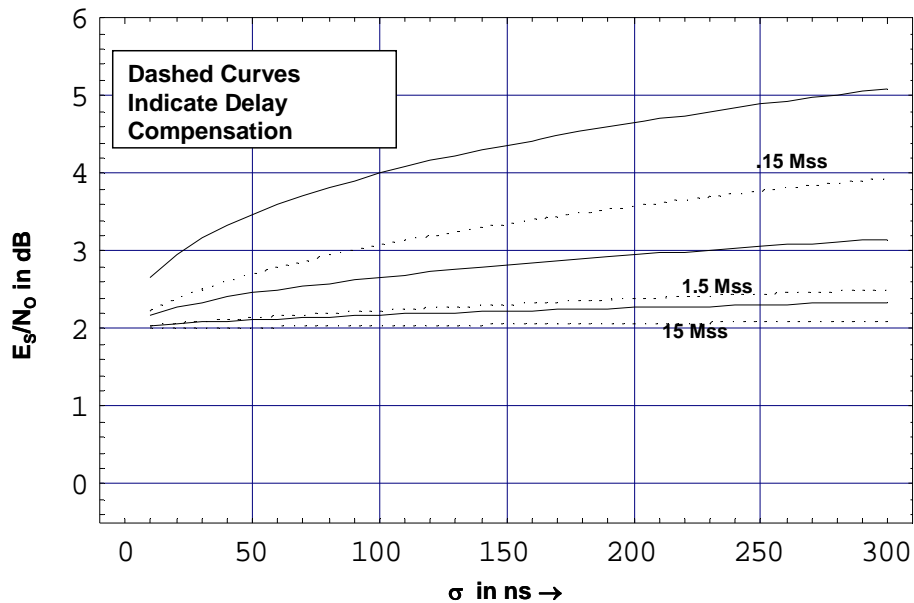


Figure 3-14. Plots of Required E_s/N_0 for 10^{-6} Decoded Error Rate as a Function of Multipath Delay Constant σ with and without Delay Compensation. $f_0 = 7.5$ GHz, $W = 2$ GHz, $V = 5$ ft/sec., and Symbol Rates = .15, 1.5, and 15 Mss. Normalized Tap Weight Filter Time Constant T_F and Number of Rake Taps R Optimized for Each Point on Curves. Indoor Dense Large-Multipath Channel.

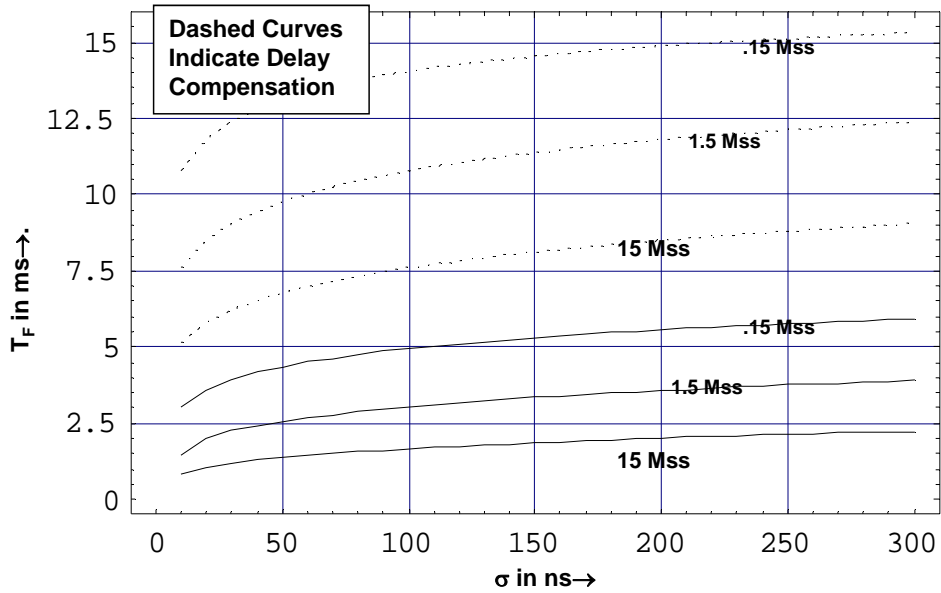


Figure 3-15. Optimal Value of Normalized Tap Weight Measurement Filter Time Constant T_F Corresponding to Plots in Figure 3-14.

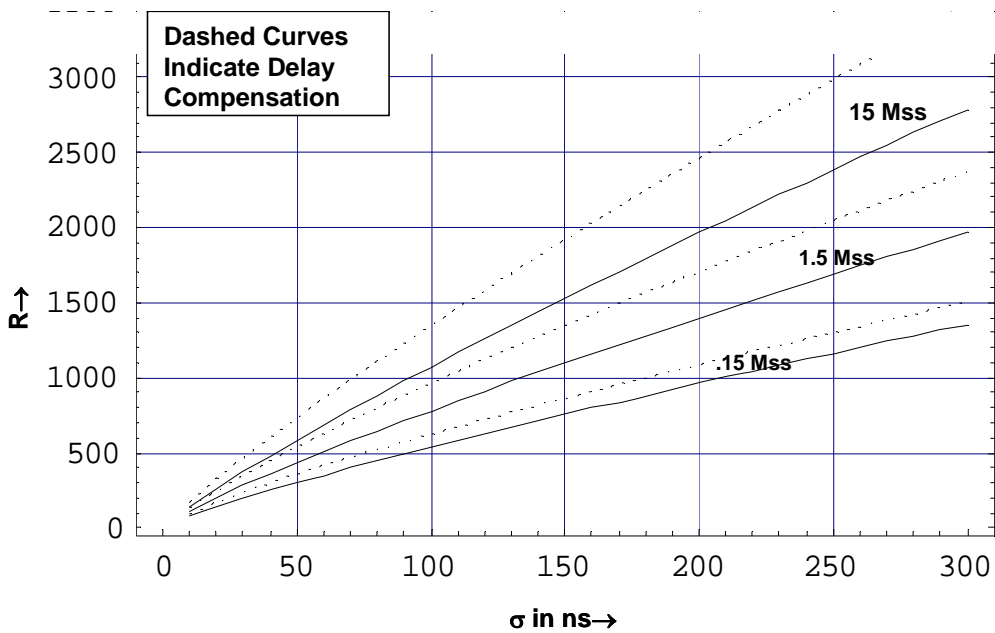


Figure 3-16. Optimal Value of the Number of Rake Taps R Corresponding to Plots in Figure 3-14.

The reduction in required E_s/N_0 is most notable at the lower data rates as may be seen by comparing Figure 3-11 with Figure 3-14.

3.2.4.4 Comparison of Decision-Directed, Parallel-Probe and Serial-Probe Modems.

The parallel-probe and serial-probe Rake modems are analyzed in Appendix D. Here, we compare the performances of the decision-directed, parallel-probe, and serial-probe modems assuming delay compensation. As in the previous sections, we assume the dense large multipath channel model and use the SNR method for performance prediction. Figures 3-17 through 3-19 present calculations for the outdoor channel model for symbol rates of 1.5, 15, and .15 Mss, respectively. For each figure, the required value of E_s/N_0 to obtain a decoded error rate of 10^{-6} is plotted vs. the multipath constant σ . In addition, the optimal values of normalized parallel-probe transmitted signal strength g and serial-probe modem probe period P (in units of data symbols) are plotted vs. σ . As in the previous sections, the time constant of the tap weight filter T_F , and the number of Rake taps R , are optimized for each value of σ . Figures 3-20 through 3-22 present the analogous set of calculations for the indoor channel model.

We observe that the performances of the optimized parallel-probe and serial-probe modems are so close as to be indistinguishable in 5 of the 6 cases plotted. In addition, we note that the decision-directed modem is always better, with increasing improvement as σ increases. The larger the impact of time-selective fading, as when lower data rates are used or the terminal velocity is higher, the greater the improvement of the decision-directed modem over the probe modems. Reduced requirements on E_s/N_0 for the decision-directed modem range from a fraction of a dB to well over 2 dB. Although the performance of the decision-directed modem does not include degradation due to decision-directed operation, this degradation is estimated to be a small fraction of a dB at the output SNR of 5 dB required to achieve a decoded bit error probability of 10^{-6} .

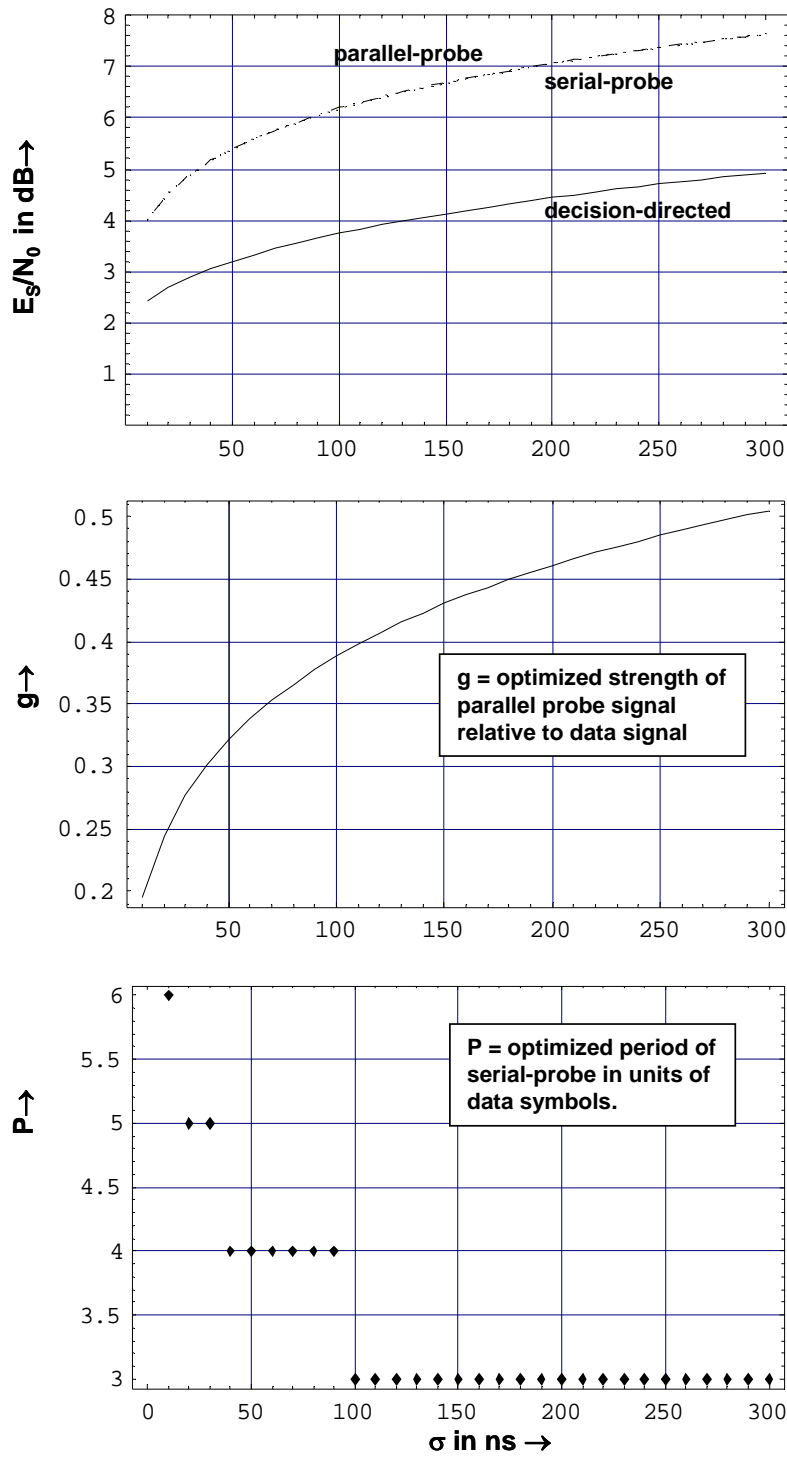


Figure 3-17. Comparison of Required E_s/N_0 to Obtain a Decoded Error Rate of 10^{-6} Over the Outdoor Channel for the Decision-Directed, Parallel-Probe, and Serial-Probe Modems at a Symbol Rate of 1.5 Mss. T_F , R , and Probe Parameters g and P Optimized at Each Value of σ . $f_0 = 7.5$ GHz, $W = 2$ GHz, and Relative Terminal Velocity of 100 ft./sec.

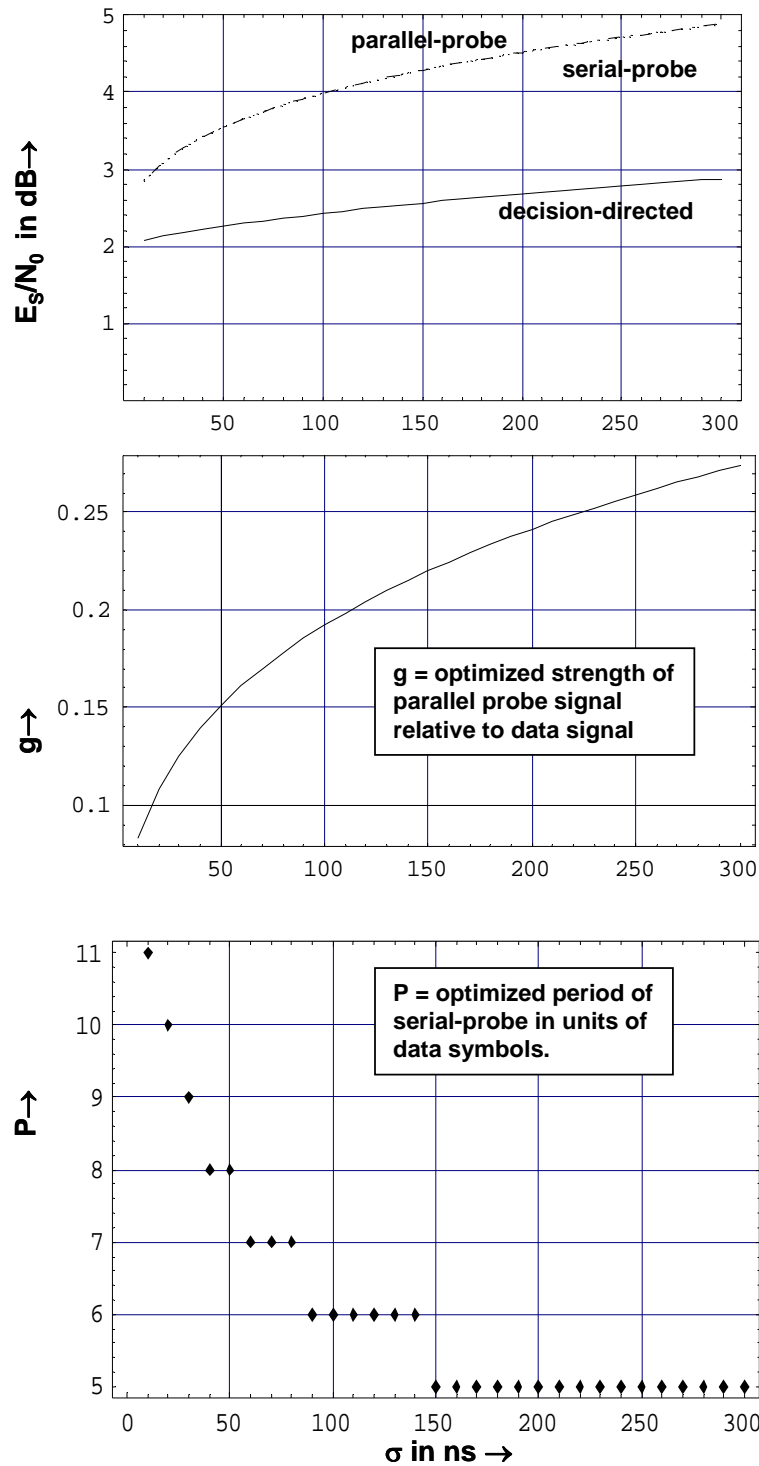


Figure 3-18. Comparison of Required E_s/N_0 to Obtain a Decoded Error Rate of 10^{-6} Over the Outdoor Channel for the Decision-Directed, Parallel-Probe, and Serial-Probe Modems at a Symbol Rate of 15 Mss. T_F , R , and Probe Parameters g and P Optimized at Each Value of σ . $f_0 = 7.5$ GHz, $W = 2$ GHz, and Relative Terminal Velocity of 100 ft./sec.

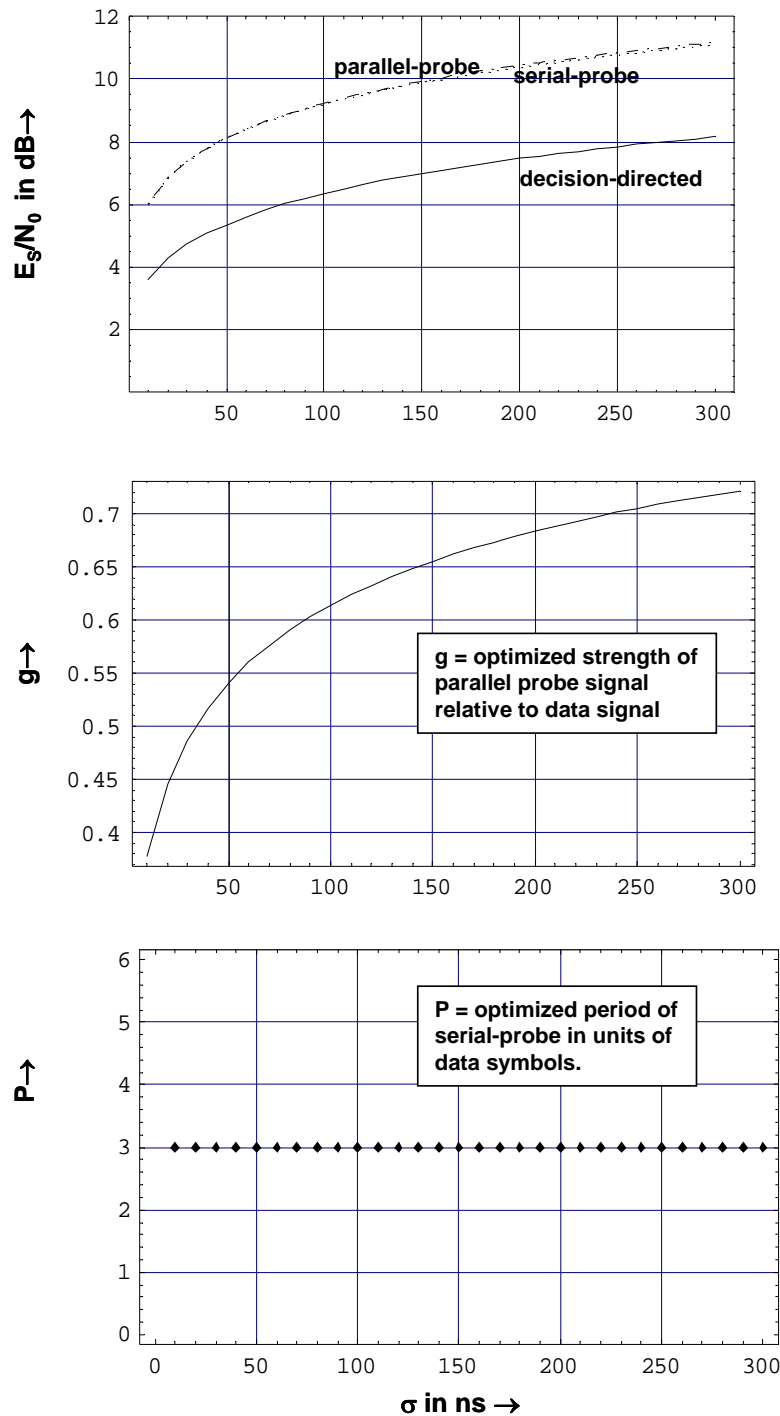


Figure 3-19. Comparison of Required E_s/N_0 to Obtain a Decoded Error Rate of 10^{-6} Over the Outdoor Channel for the Decision-Directed, Parallel-Probe, and Serial-Probe Modems at a Symbol Rate of .15 Mss. T_F , R , and Probe Parameters g and P Optimized at Each Value of σ . $f_0 = 7.5$ GHz, $W = 2$ GHz, and Relative Terminal Velocity of 100 ft./sec.

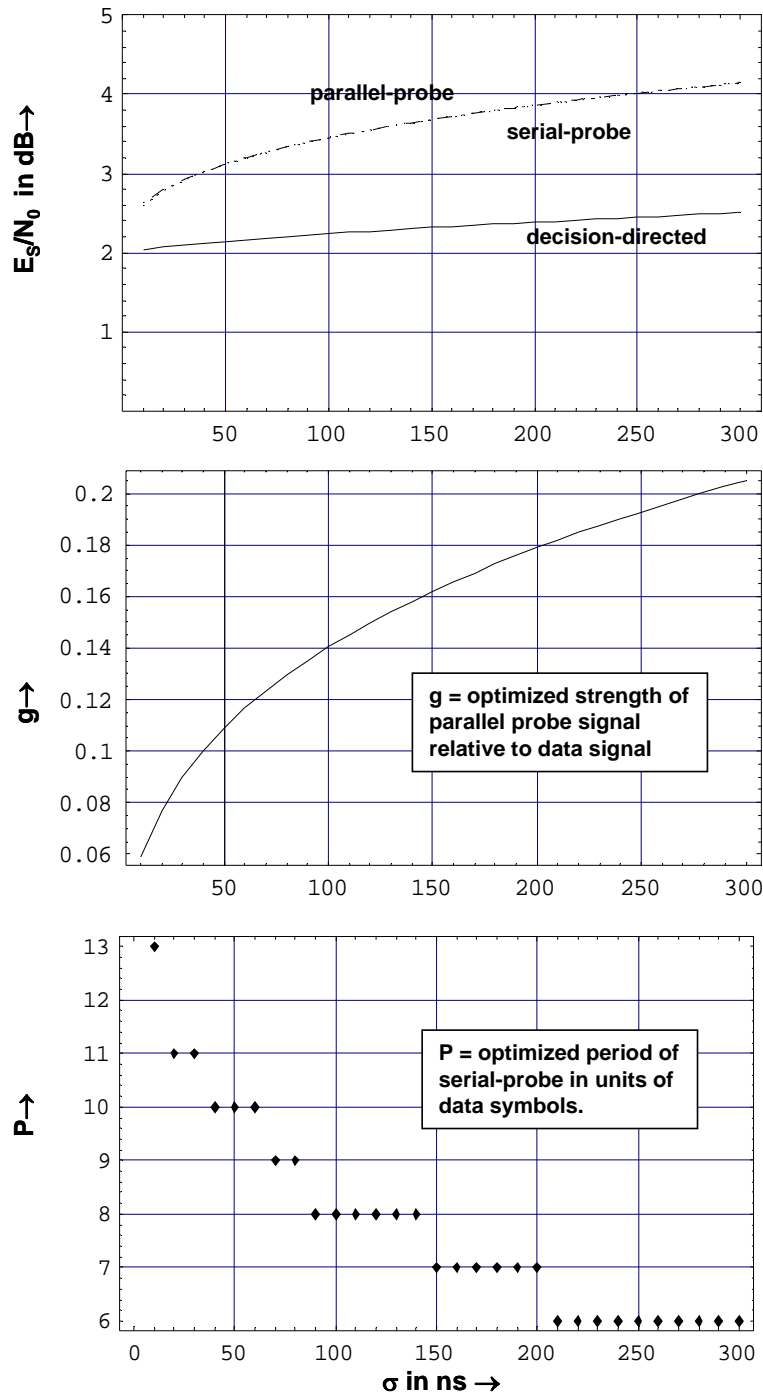


Figure 3-20. Comparison of Required E_s/N_0 to Obtain a Decoded Error Rate of 10^{-6} Over the Indoor Channel for the Decision-Directed, Parallel-Probe, and Serial-Probe Modems at a Symbol Rate of 1.5 Mss. T_F , R , and Probe Parameters g and P Optimized at Each Value of σ . $f_0 = 7.5$ GHz, $W = 2$ GHz, and Relative Terminal Velocity of 5 ft./sec.

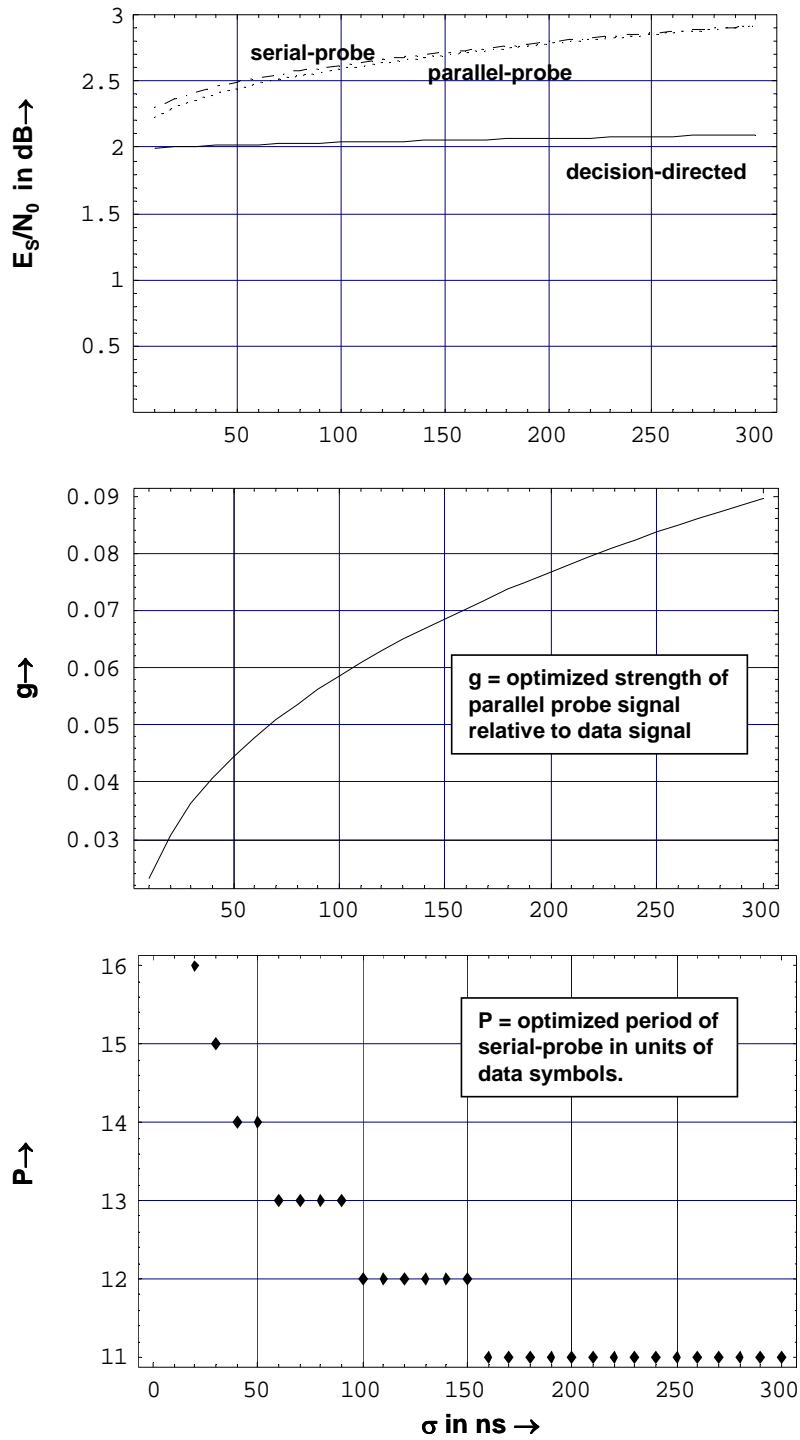


Figure 3-21. Comparison of Required E_s/N_0 to Obtain a Decoded Error Rate of 10^{-6} Over the Indoor Channel for the Decision-Directed, Parallel-Probe, and Serial-Probe Modems at a Symbol Rate of 15 Mss. T_F , R , and Probe Parameters g and P Optimized at Each Value of σ . $f_0 = 7.5$ GHz, $W = 2$ GHz, and Relative Terminal Velocity of 5 ft./sec.

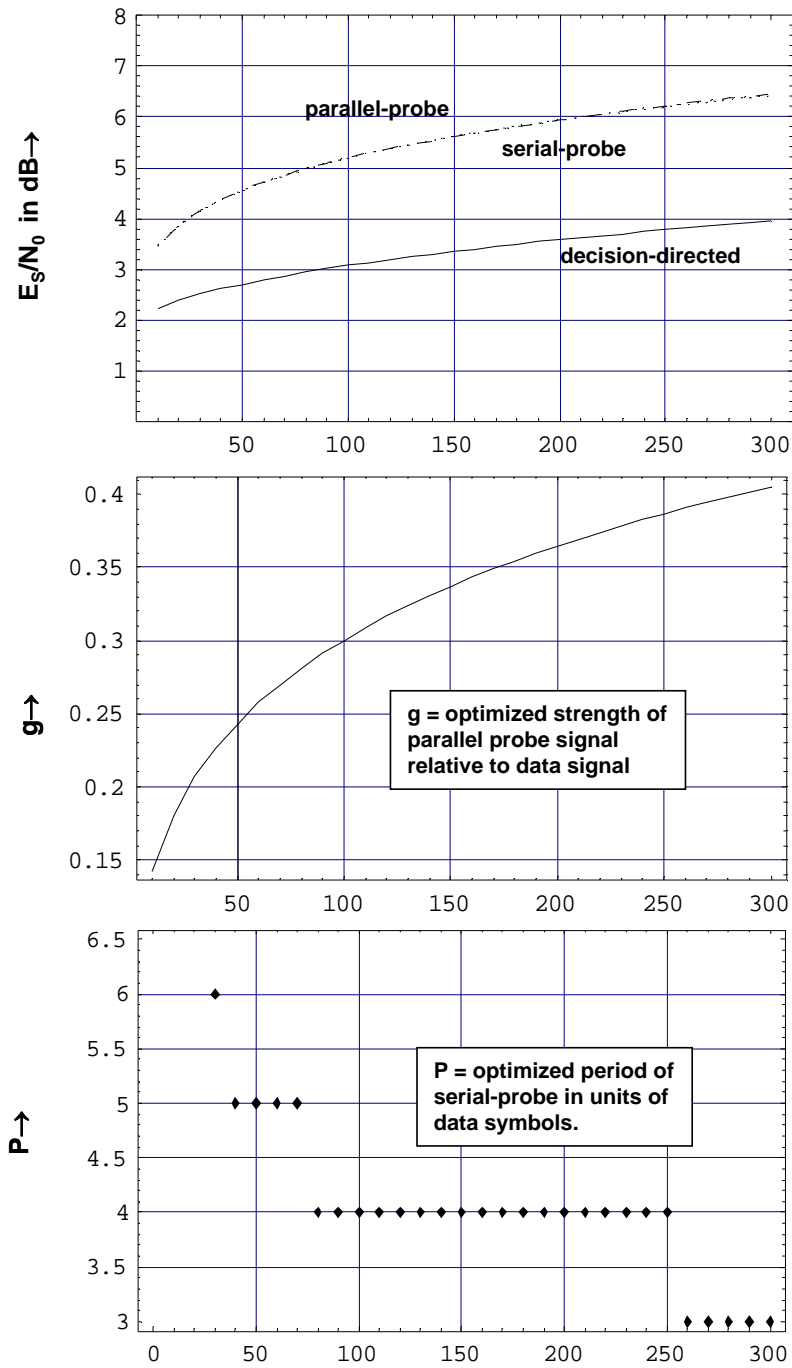


Figure 3-22. Comparison of Required E_s/N_0 to Obtain a Decoded Error Rate of 10^{-6} Over the Indoor Channel for the Decision-Directed, Parallel-Probe, and Serial-Probe Modems at a Symbol Rate of 1.5 Mss. T_F , R , and Probe Parameters g and P Optimized at Each Value of σ . $f_0 = 7.5$ GHz, $W = 2$ GHz, and Relative Terminal Velocity of 5 ft./sec.

4 Conclusions

As a result of this study, the following conclusions have been reached:

1. The DSSS/Rake modem is a viable method of communicating over dense multipath UWB channels with mobile terminals. The use of tracking loops with appropriate time and frequency discriminators provides the means of adapting to terminal mobility. These tracking loops, coupled with the Rake channel measurement subsystem, provide the means for coherent combining of multipath over a finite range of path delays of duration R/W , where W is the bandwidth of the transmitted signal and R is the number of Rake correlators. The channel measurement filter time constant T_F , and R , can be adjusted to minimize the required E_S/N_0 for a specified error rate performance.
2. The SNR and Gaussian Noise methods are sufficiently accurate for error rate performance prediction in links using error correction coding when the large multipath condition $WL_{tot} \gg 1$ applies.
3. Three methods of channel measurement were examined: the decision-directed, the parallel-probe, and the serial-probe methods. When the time constant of the channel measurement filters, the number of correlators in the Rake combiner, and the fraction of transmitter power devoted to channel measurement are optimized, the serial and parallel-probe modems show almost identical performance. The optimized decision-directed modem provides superior performance to the serial and parallel-probe modems with increasing improvement as multipath spread increases. The performance measure used was the required value of E_S/N_0 ²⁹ to achieve a decoded error

²⁹ assuming a rate $1/2$ constraint level 7 convolutional code using 3 bit quantized soft decision Viterbi decoding.

rate of 10^{-6} . The larger the impact of time-selective fading³⁰, the greater the improvement of the decision-directed modem over the probe modems. Reduced requirements on E_S/N_0 for the decision-directed modem range from a fraction of a dB to well over 2 dB.

4. Delay compensation improves performance, particularly at the lower data rates. With delay compensation, it is possible to use a larger value of channel measurement integration time, T_F , at the same data rate for the same degree of time-selective distortion. The resulting improved channel measurement allows use of larger values of R , the number of Rake correlators. That is to say, the optimal values of T_F and R increase and this results in a lower value of required E_S/N_0 to achieve a desired output SNR.
5. For lower bit rates, performance becomes increasingly degraded due to time-selective fading caused by relative terminal motion. This effect is most evident for the outdoor channels where higher velocities are possible. For the numerical examples, the outdoor relative terminal velocity chosen was 100 ft/sec. Assuming delay compensation, at a multipath delay constant $\sigma = 300$ ns, there is around 5.5 dB larger E_S/N_0 required at a symbol rate of .15 Mss than at 15 Mss to obtain a decoded error rate of 10^{-6} . At $\sigma = 50$ ns this drops to around 3.3 dB larger E_B/N_0 .
6. At sufficiently high data rates, it is necessary to consider performance limitations caused by self-noise. Self-noise is the residual signal appearing at a Rake correlator output due to all the other tap weight signals in the tapped delay line model. A sufficient condition for neglecting the contribution of self-noise is that the received SNR in the bandwidth W , ρ_I , be much less than

³⁰ as when lower data rates are used or the terminal velocity is higher.

a threshold Γ dependent upon the terminal equipment composite impulse response. With the assumed Gaussian shaped terminal equipment impulse response used, it is shown that $\Gamma = -7.35$ dB. For the numerical results obtained in this report, the input SNR is $\ll -7.35$ dB indicating that the impact of self-noise will be small or negligible for these cases. However, these calculations apply to the case of no noise excision. With an increasing percentage of the band excised, the threshold Γ decreases and for sufficiently high levels of excision, self-noise will have to be considered in the performance analysis.

7. This report develops for the first time a generic stochastic uniformly tapped delay line model of the mobile dense multipath UWB channel such as would be encountered in urban communications.. As the ratio of bandwidth to carrier frequency gets small (i.e., the NB case), it is shown that the tapped delay line model approaches a form that would result from the assumption of a WSSUS channel model. It is proposed that experimental PDPs including those proposed in the IEEE 802.15. Standard be used in the proposed tapped delay line model. Use of this model will allow inclusion of the effect of non ideal adaptive processing and multipath combining in the comparative performance analysis of mobile UWB modems in dense multipath. A number of simplifying assumptions have been made in the model development. However it is believed that these assumptions do not detract from use of the model in the comparative performance analysis of mobile UWB modems.

REFERENCES

- [1] M. Z. Win and R. B. Scholtz, "Impulse radio: How it works," *IEEE Communications Letters*, pp. 10-12, Jan. 1998.
- [2] M. Z. Win and R. B. Scholtz, "Ultra-Wide Bandwidth Time-Hopping Spread Spectrum Impulse Radio for Wireless Multiple-Access Communications," Vol. 48, No.4, April 2000.
- [3] M. Z. Win, G. Chrisikos, and N. R. Sollenberger, "Performance of Rake reception in dense multipath channels: Implications of spreading bandwidth and selection diversity order," *IEEE J. Select. Areas Commun.*, vol. 18, no. 8, pp. 1516-1525, Aug. 2000.
- [4] R. Price and P. Green, "A Communication technique for multipath channels," *PROC. IRE*, vol. 46, pp. 555-570; March, 1958.
- [5] P. A. Bello, "Characterization of Randomly Time-Variant Linear Channels," *IEEE Transactions on Communications*, vol. 11, Issue: 4, pp. 360 -39, Dec 1963.
- [6] P. A. Bello, "Correlation functions in a tapped delay line model of the orbital dipole channel," *IEEE Transactions on Information Theory*, Volume: 9 Issue: 1, pp. 2 -11, Jan 1963.
- [7] Project Westford, M.I.T. Lincoln Laboratory.
- [8] T. Kailath, "Sampling Models for Linear Time-Variant Filters," M.I.T. Research Laboratory of Electronics, Cambridge MA, Report No. 352, May 1959.
- [9] P. A. Bello, "Performance of four Rake modems over the non-disturbed Wideband HF channel," 1988 MILCOM Conference Record.
- [10] J. G. Proakis, P. R. Drouilhet, and R. Price, "Performance of Coherent Detection Systems Using Decision-Directed Channel Measurement," *IEEE Transactions of Communications Systems*, March 1964.
- [11] G. C. Clark, Jr., and J. B. Cain, *Error Correction Coding for Digital Communications*, Plenum Press, August 1982.
- [12] P. A. Bello and H. Raemer, "Performance of a Rake System Over the Orbital Dipole Channel," *Utica National Communication Symposium Record*, October 1962, pp. 46-53.
- [13] *Study of Adaptable Communications Systems*, Final Report on Contract No. AF30(602)-2461, Appendix C, Sylvania Electronic Systems., Volume 1 and 2, June 14, 1962.
- [14] G. L. Turin, "Some Computations of Error Rate for Selectively Fading Radio Channels," *NEC Vol.15* (1959), pp. 431-440.

- [15] P. A. Bello, "Binary error probabilities over selectively fading channels containing specular components," *IEEE Trans. on Commun. Technol.*, vol. 14, no. 4, pp. 400–406, Aug. 1966.
- [16] P. A. Bello, "Corrections to 'Binary error probabilities over selectively fading channels containing specular components'," *IEEE Trans. on Commun. Technol.*, vol. 14, no. 6, p. 857, Dec. 1966.
- [17] R. Price, "Error probabilities for adaptive multichannel reception of binary signals," *IRE Trans. Information Theory*, vol. IT-8, pp. 305-316, September 1962.
- [18] R. Price, "Some non-central F-distributions expressed in closed form," *Biometrika*, vol. 51, pts 1, 2, pp. 107-122, June 1964.
- [19] P. A. Bello, "On the approach of a filtered pulse train to a stationary Gaussian process," *IRE Trans. on Information Theory*, Vol. IT-7, Number 3, July 1961.
- [20] J. I. Marcum, "Table of Q Functions," Research Memo RM-339, The Rand Corp., Santa Monica, CA, January 1, 1950.
- [21] J. P. Odenwalder, Error Control Coding Handbook, prepared under Contract No. F44620-76-C-0056, by Linkabit Corporation, San Diego, CA, July 15, 1976.
- [22] M. Z. Win, and R. A. Scholtz, "Characterization of Ultra-Wide Bandwidth Wireless Indoor Channel: A Communication Theoretic View," *IEEE Journal on Selected Areas in Communications*, Vol. 20, No.9, December 2002, pp. 1613 – 1627.
- [23] P. A. Bello, Generic Channel Simulator, Final Report under Contract MDA904-95-C-2078, Reporting Period: 10 February 1995 - 10 February 1997. Available from www.eecs.umich.edu/genchansim/
- [24] W. R. Braun and U. Dersch, "A Physical Mobile Channel Model," *IEEE Trans. on Vehicular Technology*, Vol. 40, No.2, May 1991, pp. 472-482.
- [25] R. H. Clarke, "A Statistical Theory of Mobile Radio Reception," *BSTJ*, Vol. 47, 1968, pp. 957-1000.
- [26] W. C. Jakes, Ed., *Microwave Mobile Communications*, John Wiley, 1974.
- [27] R. H. Clarke and B. W. Conolly, "Statistics of Mobile-Radio Signals in 3-D Scattered Multipath Fields," *ICT '96 Istanbul Turkey* pp. 730-733 (1996).
- [28] R. H. Clarke and Wee Lin Khoo, "3-D mobile radio channel statistics," *IEEE Transactions on Vehicular Technology*, Vol. 46, Issue: 3, Aug. 1997, pp. 798-799.
- [29] R. E. Crochiere and L. R. Rabiner, *Multirate Digital Signal Processing*, Prentice Hall 1983.
- [30] P. A. Bello, "Selective Fading Limitations of the Kathryn Modem and Some System Design Considerations," *IEEE Trans. on Comm.*, Vol. 13, Issue 3, Sept. 1965, pp. 320-333.

- [31] R. Price, "Wideband analog communication through multipath by means of a pseudo-noise carrier," 1962 Spring Meeting (April 30 - May 3), URSI. [Documented: M.I.T. Lincoln Laboratory, Meeting Speech MS-539.
- [32] A. F. Molisch, K. Balakrishnan, C. C. Chong, S. Emami, A. Fort, J. Karedal, J. Kunisch, H. Schantz, U. Schuster, and K. Siwiak, "IEEE 802.15.4a channel model - final report," Sept., 2004. [Online]. Available: <http://www.ieee802.org/15/pub/TG4a.html>. See also: A. F. Molisch, J. R. Foerster, and M. Pendergrass, "Channel models for ultra-wideband personal area networks," *IEEE Wireless Commun. Mag.*, vol. 10, no. 6, pp. 14-21, Dec. 2003.
- [33] L.J.Greenstein, S.S.Ghassemzadeh, S.C.Hong, and Vahid Tarokh, "Comparison Studies of UWB Indoor Channel Models", to be published in *IEEE Trans. on Wireless Comm.*, vol. 6, no. 1, January 2007.
- [34] J. Foerster, "Channel modeling sub-committee report final," IEEE P802.15-02/490r1, Feb. 2003.
- [35] S. S. Ghassemzadeh, R. Jana, C. W. Rice W. Turin, and V. Tarokh, "Measurement and modeling of an indoor UWB channel," *IEEE Trans. Commun.*, vol. 52, no. 10, pp. 1786-1796, Oct. 2004.
- [36] D. Cassioli, M. Z. Win, and A. Molisch, "The ultra-wide bandwidth indoor channel: From statistical model to simulations," *IEEE J. Select Areas Commun.*, vol. 20, no. 6, pp. 1247-1257, Aug. 2002.
- [37] S. S. Ghassemzadeh, L. J. Greenstein, T. Sveinsson, A. Kavcic, and V. Tarokh, "UWB indoor delay profile model for residential and commercial environments," *IEEE Veh. Technol. Conf.-Fall*, Oct. 2003, vol. 5, pp. 3120-3125.
- [38] S. S. Ghassemzadeh, L. J. Greenstein, T. Sveinsson, and V. Tarokh, "UWB delay profile models for residential and commercial indoor environments," *IEEE Trans. Veh. Technol.*, vol. 54, no. 4, pp. 1235-1244, July 2005.
- [39] R. Addler, D. Cheung, E. Green, M. Ho, Q. Li, C. Prettie, L. Rusch, and K. Tinsley, "UWB channel measurements for the home environment," *UWB Intel Forum*, 2001.
- [40] S. S. Ghassemzadeh, L. J. Greenstein, T. Sveinsson, and V. Tarokh, "An impulse response model for residential wireless channels," in *Proc. IEEE Global Commun. Conf.*, Dec. 2003, vol. 3, pp. 1211-1215.

Distribution List

Internal

E050

Nissen, C. A.

E130

Graff, A. J.

E131

Blanco, M. A.

Hamalainen, J. R

Marsicano, D. V.

E132

Girard, M. M.

Low, J.

E142

vonTobel, B. J.

E146

Robbins, D. P.

E500

Johnson, B. L.

E530

Bello, P. A. (10)

Bronez, Thomas P.

Hopkinson, T. M.

Howland, James W.

Landry, R.

Marshall, James W.

Palo, E. A.

Tromp, L. D.

E537

Grace, K. H.

E536

Capozza, P. T.

Correia, Jeffrey T.

Lathrop, C. W.

E539

Parl, Steen A.

E53A

Muhonen, J.

Rasmussen, J. L.

Zinkovitch, P. M.

E532

McDonald, K. F.

Appendix A Performance Analysis

A.1 Introduction

This appendix presents a performance analysis of the decision-directed Rake modem described in Section 2. Section A.2 formulates the input to the modems, including the effect of the propagation medium. Central to this formulation is the use of a tapped delay line channel model with time varying weights analyzed in Appendix B. Section A.3 characterizes the Rake combiner output for the decision-directed Rake modem, neglecting the effect of decision errors. Approaches to error rate evaluation are developed in Section A.4 using the statistical properties of the tap weights derived in Appendix B. Appendix D analyzes the performance of the decision-directed, serial-probe, and parallel-probe DSSS/Rake modems with delay compensation. Section A.5 summarizes the derivation of a sufficient condition for neglect of self-noise. Self-noise is the residual signal appearing at the p^{th} correlator output due to all the other tap weight signals in the tapped delay line model.

A.2 Sampled Signal at Modem Input

Starting with an impulse train input signal, the received signal may be regarded as being formed by passing the transmitted signal through five filters in cascade: a chip pulse-forming filter, a transmitter filter which confines the transmitted signal to a bandwidth of W Hz, a propagation medium “filter” including any terminal equipment and antenna filtering, a noise whitening filter³¹, and receiver anti-alias filter. These five filtering operations may be combined, for analysis purposes, into one composite filter with complex low-pass impulse response $h(t, \xi)$.

³¹ The noise whitening filter can be analog or digital. For simplicity of presentation, and without loss of generality, we assume it is analog.

Since we assume the transmitted signal to be limited to a bandwidth of W Hz, this composite filter, in turn, may be represented by a tapped delay line with taps spaced $\Delta = 1/W$ apart and complex weights equal to sampled values of the composite channel impulse response³². Figure 2-1 shows this representation, due to the bandwidth limitation, the p -th complex tap weight is given by

$$h_p(t) = \frac{1}{W} h\left(t, \frac{p}{W}\right) \quad (\text{A-1})$$

For simplicity of notation, we assume that the synchronization process sets the first arriving path at the first tap of the tapped delay line model. This representation has been called the “excess-delay” tapped delay line model³³. A maximum delay of $(M-1)\Delta$ is shown (M taps) to characterize the total multipath spread of the channel, $L_{\text{tot}} = M\Delta$.

We now formulate an expression for the received sampled signal fed to the Rake demodulator. With the definition of the composite channel filter incorporating the chip pulse forming filter and successive band limiting filtering operations in the transmitter, the transmitted signal, $z(t)$, can be represented as the hypothetical impulse train

$$z(t) = \sum a_q m_q \delta\left(t - \frac{q}{W}\right) \quad (\text{A-2})$$

a_q is the q -th DSPN chip modulation, and m_q is the data modulation superimposed on the q -th DSPN chip. The data modulation is at a much slower rate than the chip modulation, i.e.,

$$m_{q+kN} = d_k; \quad 0 < q < N-1 \quad (\text{A-3})$$

where d_k is the data modulation for the k -th data symbol. Each symbol spans a sequence of N DSPN chips so that the time duration of a data symbol is

$$T = N/W \quad (\text{A-4})$$

³² For the real low-pass case, these weights are real and W is replaced by $2W$ (see Section B.1).

³³ The excess-delay tapped delay line channel model is discussed in Section B.3 of Appendix B.

If $z_i(t)$ is the input to a time variant filter with impulse response³⁴ $h(t, \xi)$, the output is given by

$$w_o(t) = \int z_i(t - \xi)h(t, \xi)d\xi \quad (\text{A-5})$$

To obtain $s(t)$, the signal component of the received process prior to receiver sampling, we pass the impulse train (A-2) through the composite filter, with the result

$$s(t) = \sum a_q m_q h\left(t, t - \frac{q}{W}\right) \quad (\text{A-6})$$

The noise component of the received process is determined as the output response of the receiver filter to the input noise. Assuming the receiver incorporates noise whitening filters, the input noise to the Rake demodulator will be white. We use $\eta(t)$ to represent the complex noise at the input to the Rake demodulator. Thus, the received signal including noise is given by

$$w(t) = s(t) + \eta(t) \quad (\text{A-7})$$

A.3 Rake Combiner Output

Figure 2-3 presents a block diagram of the decision-directed coherent Rake modem. The (complex) sampled input process is correlated with delayed versions of the locally generated PN sequence³⁵. The correlation operation involves conjugate multiplication followed by an I&D over successive groups of N input samples. Each I&D output is multiplied by an estimated tapped delay line model weight and the results summed to produce the Rake combiner output. This output is fed to a decoder and also to a hard decision device. The hard decisions are used in the estimation of the tapped delay line model weight as discussed below.

³⁴ There are many ways to represent the input/output relationship for a time variant random channel [5]. To distinguish $h(t, \xi)$ from other possible relationships in [5], $h(t, \xi)$ is called the Input Delay Spread function.

³⁵ Alternate versions exist in which the complex digital input and the local PN sequence exchange positions (as in [9]) or in which the input signal and reference are both delayed.

Ideally, each correlator suppresses all multipath components except one of the M shown in Figure 2-1 and, as a result, produces an output identical to that for a hypothetical channel having only one of the tap weight multipliers. Thus, the successive I&D outputs for a particular correlator ideally produce a data signal proportional to one of the composite channel tap weight multipliers. A tap weight measurement circuit attempts to measure this complex time variant channel tap weight. Multiplication of each I&D output by the conjugate of the corresponding tap weight measurement followed by summation of all products then approximates predetection or coherent combining of multipath components.

The tap weight measurement circuit shown in Figure 2-4 is a decision-directed procedure in which an attempt is made to cancel the data modulation on the I&D output through feedback of hard data decisions (with a delay to compensate for an assumed decision delay of T). If the data modulation were cancelled, the noise-free component left would be proportional to the desired channel tap weight multiplier. Averaging with a long time constant digital filter can reduce the noise level sufficiently to make the predetection combining effective.

In this section we will develop analytic expressions for the combiner output which include the non-idealities associated with tap weight measurement and the basic correlation operation. These non-idealities include additive noise, time-selective fading, and “self noise.” Self- noise is due to the residual signal components at an I&D output due to undesired multipath components. These cannot be suppressed completely due to the random nature of the PN sequence and the finite integration time of the I&D.

The output of the first correlator is formed by multiplication of the received input signal samples by samples of the locally generated PN sequence, followed by summation over N samples. This multiplication and I&D operation is repeated continually, generating a complex output every $T = N/W$ seconds. We represent the multiplication process as a multiplication of the input (A-7) by the conjugate PN impulse train

$$I(t - \tau) = \sum_n a_n^* \delta\left(t - \tau - \frac{n}{W}\right) \quad (\text{A-8})$$

where the variable τ denotes a timing offset relative to the timing of the sampling at the transmitter. Thus, the input to the integrator is represented as

$$I(t - \tau) w(t) = \sum a_n^* w\left(\tau + \frac{n}{W}\right) \delta\left(t - \tau - \frac{n}{W}\right) \quad (\text{A-9})$$

The I&D operation over the k^{th} block of N samples for the first correlator is then

$$\begin{aligned} y_{0k} &= \frac{1}{N} \int_{\tau + \frac{k}{W}N}^{\tau + \frac{k}{W}N + \frac{N-1}{W}} \sum a_n^* w\left(\tau + \frac{n}{W}\right) \delta\left(t - \tau - \frac{n}{W}\right) dt \\ &= \frac{1}{N} \sum_{n=kN}^{kN+N-1} a_n^* w\left(\tau + \frac{n}{W}\right) \end{aligned} \quad (\text{A-10})$$

Successive correlators use delayed versions of the impulse train (A-8) which leads to the following generic expression for the I&D output of the k^{th} block of N samples for the p^{th} correlator output ($p = 0$ corresponds to the first correlator)

$$y_{pk} = \frac{1}{N} \sum_{n=kN}^{kN+N-1} a_n^* w\left(\tau + \frac{p}{W} + \frac{n}{W}\right) \quad (\text{A-11})$$

We now consider separately the signal and noise components of the I&D output,

$$y_{pk} = s_{pk} + n_{pk} \quad (\text{A-12})$$

where s_{pk} is the signal component and n_{pk} is the noise component.

Using (A-6) in (A-11) we determine that

$$s_{pk} = \frac{1}{N} \sum_{q=-\infty}^{\infty} \sum_{n=kN}^{kN+N-1} a_n^* a_q m_q h\left(\tau + \frac{p}{W} + \frac{n}{W}, \tau + \frac{p}{W} + \frac{n}{W} - \frac{q}{W}\right) \quad (\text{A-13})$$

We express s_{pk} as the sum of two components, the first corresponding to terms in the summations for which $n = q$ and the second, the self-noise term, to terms for which $n \neq q$,

$$s_{pk} = \frac{d_k}{N} \sum_{n=kN}^{kN+N-1} h\left(\tau + \frac{p}{W} + \frac{n}{W}, \tau + \frac{p}{W}\right) + x_{pk} \quad (\text{A-14})$$

In forming the first term, (A-3) has been used. Note that it has been assumed the data block epochs are tied to the timing of the PN sequence, so the receiver can start the I&D at the beginning of a data block given that the local PN sequence is synchronized properly (i.e. $n = q$). It has also been assumed that the PN chip symbols, $\{a_n\}$ are BPSK symbols so that $|a_k|^2 = 1$.

The self-noise term is given by

$$x_{pk} = \frac{1}{N} \sum_{q=-\infty}^{\infty} \sum_{n=kN}^{kN+N-1} a_n^* a_q m_q h\left(\tau + \frac{p}{W} + \frac{n}{W}, \tau + \frac{p}{W} + \frac{n}{W} - \frac{q}{W}\right); n \neq q \quad (\text{A-15})$$

Based upon analysis in [9] for a related DSSS/Rake modem, it may be determined that for input SNRs in the bandwidth W , much less than a threshold $\Gamma = -7.3$ dB, self-noise may be neglected at the Rake combiner output. We assume this inequality valid and neglect the impact of self-noise. However, as discussed in A-5, the -7.3 dB is predicated on the assumption of no interference excision and with excision the threshold is smaller.

Finally, the noise term at the correlator output is given by

$$n_{pk} = \frac{1}{N} \sum_{n=kN}^{kN+N-1} a_n^* \eta\left(\tau + \frac{p}{W} + \frac{n}{W}\right) \quad (\text{A-16})$$

The strength of the noise term is given by

$$\begin{aligned} \overline{|n_{pk}|^2} &= \frac{1}{N^2} \sum_{m=kN}^{kN+N-1} \sum_{r=kN}^{kN+N-1} a_m a_r^* \overline{\eta\left(\tau + \frac{p}{W} + \frac{r}{W}\right) \eta^*\left(\tau + \frac{p}{W} + \frac{m}{W}\right)} \\ &= \frac{1}{N} \overline{|\eta|^2} \end{aligned} \quad (\text{A-17})$$

Although the results can be generalized, to simplify the analysis, we have assumed white noise input and a brick-wall receiver filter of bandwidth W . Then

$$\overline{|\eta|^2} = 2WN_0 \quad (\text{A-18})$$

where N_0 is the one-sided power density of the noise and

$$\overline{n_{pk}^* n_{qk}} = \frac{1}{N^2} \sum_{m=kN}^{kN+N-1} \sum_{r=kN}^{kN+N-1} \overline{a_m a_r^* \eta\left(\tau + \frac{p}{W} + \frac{r}{W}\right) \eta^*\left(\tau + \frac{q}{W} + \frac{m}{W}\right)} = \begin{cases} 0; p \neq q \\ \frac{WN_0}{N}; p = q \end{cases} \quad (\text{A-19})$$

We now reconsider the expression (A-14) for s_{pk} neglecting the self-noise term, x_{pk} . Making the valid assumption that the composite impulse response $h(t, \xi)$ changes very little for changes in t of the order of $1/W$, the summation in (A-14) over n is well approximated by an integral as follows

$$s_{pk} = \frac{d_k}{T} \int_{kT}^{kT+T} h\left(\tau + \frac{p}{W} + t, \tau + \frac{p}{W}\right) dt \quad (\text{A-20})$$

Thus, s_{pk} is proportional to a short-term time average of the time variant impulse response over a time duration T for a particular value of the delay variable, $\xi = \tau + \frac{p}{W}$.

Consider now the role of the synchronization timing variable τ . This variable is controlled by the chip synchronization loop to “center” the measured multipath components over the available correlators in order that most or all of the multipath components are combined by the Rake processing. In effect, τ is chosen so that the “excess delay” channel is measured as has been mentioned. Thus, it is sufficient to absorb τ in our definition of the excess delay channel with the understanding of the role that it has played. Then, using (A-1), we may simplify (A-20) to

$$s_{pk} = d_k \frac{W}{T} \int_{kT}^{kT+T} h_p\left(t + \frac{p}{W}\right) dt = d_k \frac{W}{T} \int_{-T/2}^{T/2} h_p\left(t + kT + \frac{T}{2} + \frac{p}{W}\right) dt \quad (\text{A-21})$$

where $h_p(t)$ is the p 'th tap weight in the tapped delay line channel model. If we define a filtered version of the tap weight

$$\tilde{h}_p(t) = \int_{-\infty}^{\infty} h_p(t-s) \frac{1}{T} \text{Rect}\left[\frac{s}{T}\right] dt \quad (\text{A-22})$$

where

$$\text{Rect}[t] = \begin{cases} 1; |t| < 1/2 \\ 0; |t| \geq 1/2 \end{cases} \quad (\text{A-23})$$

Then the signal component at the correlator output may be expressed as

$$s_{pk} = d_k W \tilde{h}_p\left(kT + \frac{T}{2} + \frac{p}{W}\right) \quad (\text{A-24})$$

and the k^{th} I&D output for the p^{th} correlator, including self-noise, represented as

$$y_{pk} = d_k W \tilde{h}_p\left(kT + \frac{T}{2} + \frac{p}{W}\right) + n_{pk} + x_{pk} \quad (\text{A-25})$$

We analyze now the processing used to estimate the complex weight of the p^{th} multipath component. The conjugate of this estimate is multiplied by the correlator output prior to forming the Rake multipath combiner output. Since this estimate is a discrete filtered version of the corresponding I&D output (A-25), assuming data cancellation, it will also be representable in terms of a desired signal component, a self-noise component, and an additive noise component. In the case of a decision-directed operation, it will contain an additional perturbation due to decision errors fed back to the data cancellation circuit.

Assuming perfect decision-directed data cancellation, the tap weight estimation is given by the filtering operation (see Figure A-2),

$$g_{pk} = \sum_{m=0}^{\infty} b_m d_{k-m-1}^* y_{p,k-m-1} \quad (\text{A-26})$$

where the impulse response of the discrete filter is

$$g_w(t) = \sum_{m=0}^{\infty} b_m \delta(t - mT) \quad (\text{A-27})$$

For illustration, we note two common choices of impulse response, the exponential impulse response,

$$b_m = (1-a)a^m; \quad a < 1 \quad (\text{A-28})$$

corresponding to a first-order recursive filter, and the “boxcar” filter response,

$$b_m = \begin{cases} \frac{1}{N_F}; & 0 \leq m \leq N_F - 1 \\ 0; & \text{elsewhere} \end{cases} \quad (\text{A-29})$$

To simplify notation, it is assumed that the impulse response of the tap weight estimation filter has been normalized to unity dc gain,

$$\sum_{m=0}^{\infty} b_m = 1 \quad (\text{A-30})$$

Using (A-26) in (A-25) we may represent the weight as

$$g_{pk} = W \hat{h}_p \left(kT + \frac{T}{2} + \frac{p}{W} \right) + \hat{x}_{pk} + \hat{n}_{pk} \quad (\text{A-31})$$

in which³⁶

$$\hat{h}_p(t) = \tilde{h}_p(t) \otimes g_w(t-T) = h_p(t) \otimes \frac{1}{T} \text{Rect} \left[\frac{t}{T} \right] \otimes g_w(t-T) \quad (\text{A-32})$$

where \otimes denotes convolution, and the self-noise and additive noise components at the tap weight estimator output are given by,

$$\hat{x}_{pk} = \sum_{m=0}^{\infty} b_m d_{k-m-1}^* x_{p,k-m-1} \quad (\text{A-33})$$

$$\hat{n}_{pk} = \sum_{m=0}^{\infty} b_m n_{p,k-m-1} \quad (\text{A-34})$$

³⁶ $t - T$ is used in the argument of $g(\cdot)$ to account for the delay of T used in the feedback data cancellation.

It should be noted that \hat{n}_{qk} and n_{qk} are statistically independent because \hat{n}_{qk} is functionally dependent only on the set $\{n_{q,k-1}, n_{q,k-2}, n_{q,k-3}, \dots\}$, which may be seen to depend upon mutually exclusive portions of the input noise. In fact, \hat{n}_{pk} and n_{qk} also very nearly depend upon mutually exclusive portions of the input noise, especially if the former represents an average over many I&D cycles or if the number of correlators is $\ll N$. In any case, \hat{n}_{pk} and n_{qk} are uncorrelated for all p and q , as are \hat{n}_{pk} and \hat{n}_{qk} ($p \neq q$) as is evident from (A-19).

The Rake combiner complex output for the k -th symbol is thus given by

$$C_k = \sum_{p=0}^{R-1} g_{pk}^* y_{pk} \quad (\text{A-35})$$

where we have assumed that the Rake combiner has R taps. Using (A-25), and (A-31) in (A-35),

$$C_k = \sum_{p=0}^{R-1} \left(W \hat{h}_p^* \left(kT + \frac{T}{2} + \frac{p}{W} \right) + \hat{x}_{pk}^* + \hat{n}_{pk}^* \right) \left(d_k W \tilde{h}_p \left(kT + \frac{T}{2} + \frac{p}{W} \right) + x_{pk} + n_{pk} \right) \quad (\text{A-36})$$

For coherent demodulation and BPSK data and chip modulation, only the real part of C_k is used. This real part can be separated into a signal and a noise part

$$q_k = \text{Re}(C_k) = S_k + N_k \quad (\text{A-37})$$

where

$$S_k = d_k W^2 \text{Re} \left\{ \sum_{p=0}^{R-1} \hat{h}_p^* \left(kT + \frac{T}{2} + \frac{p}{W} \right) \tilde{h}_p \left(kT + \frac{T}{2} + \frac{p}{W} \right) \right\} \quad (\text{A-38})$$

$$N_k = \text{Re} \left\{ \sum_{p=0}^{R-1} \left(\hat{x}_{pk}^* x_{pk} + \hat{n}_{pk}^* n_{pk} + W \hat{h}_p^* \left(kT + \frac{T}{2} + \frac{p}{W} \right) (x_{pk} + n_{pk}) + x_{pk} \hat{n}_{pk}^* + n_{pk} \hat{x}_{pk}^* + d_k W \tilde{h}_p \left(kT + \frac{T}{2} + \frac{p}{W} \right) (\hat{x}_{pk}^* + \hat{n}_{pk}^*) \right) \right\} \quad (\text{A-39})$$

and $d_k = \pm 1$.

A.4 Error Probability Evaluation

Error probability evaluation is considered in this section. We consider first in section A.4.1 two approximations to the error probability, which we call *average channel* approximations. They are valid asymptotically as the number of significant strength tap weights on the channel tapped delay line model becomes large, assuming a dense large-multipath channel. Section A.4.2 presents an exact evaluation technique that assumes the tap weights and noises are zero mean complex Gaussian variables.

A.4.1 Average Channel Methods

Two average channel methods, called the *SNR method* and the *Gaussian noise method*, will be analyzed. We consider the SNR method first.

A.4.1.1 The SNR Method

If the number of terms in the summation in (A-39) is sufficiently large and we regard the channel tap weights as given processes (we call this the *frozen channel* hypothesis), the sum of the real parts of the noise terms may be assumed approximately normally distributed due to the application of the Central Limit Theorem. Thus, for purposes of estimating error rates conditioned on the channel, it is reasonable to approximate N_k as a normally distributed random variable. Since the noise and self-noise terms are zero mean and uncorrelated, N_k will also be zero mean. Then the basic parameter for determination of the channel error rate, conditioned on the channel fluctuations, is the combiner output SNR for the k^{th} channel symbol,

$$\rho_{\text{out},k} = \frac{S_k^2}{N_k^2} \quad (\text{A-40})$$

where $\overline{N_k^2}$ is an average over the input noise fluctuations alone. Assuming that the input noise is stationary, the variation of $\rho_{\text{out},k}$ with k will be due to variations in S_k and in $\overline{N_k^2}$ caused by channel fluctuations. With the dense large multipath assumption, these

fluctuations cause small percentage variations in S_k and $\overline{N_k^2}$. The proposed SNR method ignores these fluctuations and, at a particular point in the derivation, replaces certain quadratic forms involving filtered tap weights by averages³⁷.

In the SNR method, the decision variable $\text{Re}(C_k)$ is assumed well approximated by a binary value plus zero mean Gaussian noise so that the channel raw bit error probability is

$$p_{\text{rb}} = \phi(\sqrt{\rho_{\text{out}}}) \quad (\text{A-41})$$

where ρ_{out} is the (decision variable) SNR and

$$\phi(y) = \int_y^\infty \frac{1}{\sqrt{2\pi}} \exp\left(-\frac{x^2}{2}\right) dx \quad (\text{A-42})$$

The sequence of decision variables at the combiner output for the SNR method are binary antipodal signal values of fixed level plus Gaussian noise. Consequently, the sequence of output decision variables is statistically identical to that of a hypothetical binary symmetric AWGN channel. Performance with error correction coding can then be determined from tabulated performances for codes used over AWGN channels. Thus, suppose a function f_{code} (E_b/N_o) is available which relates decoder output bit error rate to E_b/N_o ³⁸ for a hypothetical BPSK AWGN channel. Then it is readily shown that the decoded bit error rate expressed in terms of ρ_{out} , the SNR of the hard decision variable, is given by

$$p = f_{\text{code}}(\rho_{\text{out}} / 2R_c) \quad (\text{A-43})$$

³⁷ However, if the statistics of these quadratic forms in the tap weights can be determined or measured, one may evaluate the bit error probability as an average of the frozen channel bit error probability over the quadratic form statistics. For the case of a large scatter multipath, we may apply the Central Limit Theorem and approximate the quadratic forms by normally distributed variables. We do not explore these alternatives as the increased accuracy in error rate estimation is likely to be too small to justify the effort for the dense, large-multipath case considered here.

³⁸ Ratio of energy per bit to noise power density. Also the ratio of input signal power to the noise power in a bandwidth equal to the throughput data rate.

where R_c is the code rate. However, it is readily seen that this expression applies equally to the channel model used in the SNR method³⁹ since the decision variable statistics are the same for the hypothetical AWGN channel and the SNR method channel.

Consider first the situation in which time-selective distortion is absent, the tap weight measurement is perfect, and self-noise is negligible, i.e.

$$\hat{h}_p \left(kT + \frac{T}{2} + \frac{p}{W} \right) = \tilde{h}_p \left(kT + \frac{T}{2} + \frac{p}{W} \right) = h_p \left(kT + \frac{p}{W} \right) \quad (\text{A-44})$$

$$\hat{x}_{pk} = x_{pk} = \hat{n}_{pk} = 0 \quad (\text{A-45})$$

Then,

$$S_k = d_k W^2 \sum_{p=0}^{R-1} \left| h_p \left(kT + \frac{p}{W} \right) \right|^2 \quad (\text{A-46})$$

$$N_k = \text{Re} \left\{ W \sum_{p=0}^{R-1} h_p^* \left(kT + \frac{p}{W} \right) n_{pk} \right\} \quad (\text{A-47})$$

Assuming the input complex noise has circular symmetry and using (A-18) and (A-19), we find the average output noise conditioned on the channel fluctuations is given by

$$\overline{|N_k|^2} = W^2 \sum_{p=0}^{R-1} \left| h_p \left(kT + \frac{p}{W} \right) \right|^2 \frac{WN_0}{N} \quad (\text{A-48})$$

so that the output SNR conditioned on the channel fluctuations assuming perfect tap weight measurement is given by

$$\rho_{\text{out},k} = N \frac{W \sum_{p=0}^{R-1} \left| h_p \left(kT + \frac{p}{W} \right) \right|^2}{N_0} \cong \rho_{0k} \quad (\text{A-49})$$

³⁹ This expression does not account for the increase in error rate that occurs if differential encoding/decoding and transparent codes are used as the means of resolving the 180 degree ambiguity that is present in the channel due to decision directed operation. However, this loss in performance amounts to only a small fraction of a dB and will be ignored in this report.

We now compare (A-49) to the input SNR conditioned on the channel fluctuations. (A-6) presents the expression for the input signal $s(t)$. The mean absolute squared value of this input signal conditioned on the channel fluctuations is given by

$$\overline{|s(t)|^2} = \sum \sum \overline{a_q^* m_q^* a_p m_p} h^* \left(t, t - \frac{q}{W} \right) h \left(t, t - \frac{p}{W} \right) \quad (\text{A-50})$$

By hypothesis, the chip modulations are independent and of unit amplitude. Thus,

$$\overline{|s(t)|^2} = \sum_p \left| h^2 \left(t, t - \frac{p}{W} \right) \right| \quad (\text{A-51})$$

The sum in (A-51) may be expressed as a convolution of the magnitude squared impulse response with an impulse train

$$\overline{|s(t)|^2} = \int |h^2(t, \xi)| \sum_p \delta \left(t - \xi - \frac{p}{W} \right) d\xi \quad (\text{A-52})$$

If we replace the impulse train in (A-52) by the corresponding Fourier series

$$\sum_p \delta \left(t - \xi - \frac{p}{W} \right) = W \sum_m e^{j2\pi m W(t - \xi)} \quad (\text{A-53})$$

we obtain the convolution series

$$\overline{|s(t)|^2} = \sum_m \int |h^2(t, \xi)| W e^{j2\pi m W(t - \xi)} d\xi = W \int |h^2(t, \xi)| d\xi \quad (\text{A-54})$$

All terms in the summation vanish except the $m = 0$ term, because, by hypothesis, the impulse response $h(t, \xi)$ is band limited to W Hz along the ξ axis and thus $|h(t, \xi)|^2$ is confined to the bandwidth $(-W, W)$. The terms in the sum (A-54) for $m \neq 0$ have spectral locations orthogonal to this latter interval and thus, the corresponding convolutions vanish. The input SNR in a bandwidth W along the ensemble at the time instant t , is thus given by the ratio

$$\rho_{\text{in}}(t) = \frac{\int |h^2(t, \xi)| d\xi}{N_0} = \frac{\sum_{p=-\infty}^{\infty} \left| h\left(t, \frac{p}{W}\right) \right|^2}{WN_0} = \frac{W \sum_{p=-\infty}^{\infty} |h_p(t)|^2}{N_0} = \frac{\rho(t)}{N} \quad (\text{A-55})$$

where use has been made of the sampling expansion

$$h(t, \xi) = \sum_{p=-\infty}^{\infty} h\left(t, \frac{p}{W}\right) \text{sinc } W\left(\xi - \frac{p}{W}\right) \quad (\text{A-56})$$

and the tap-weight definition (A-1). $\rho(t)$ is the SNR in a bandwidth of $1/T$ at time t , where T is the symbol duration. The last equation in (A-55) shows that $\rho(t)$ is N times the input SNR in a bandwidth W .

The large scatter multipath assumption leads to the use of the approximations

$$\sum_{p=-\infty}^{\infty} |h_p(t)|^2 \cong E \left[\sum_{p=-\infty}^{\infty} |h_p(t)|^2 \right] = \sum_{p=-\infty}^{\infty} \overline{|h_p(t)|^2} \cong \sum_{p=0}^{\infty} \overline{|h_p(t)|^2} \quad (\text{A-57})$$

The lower limit in the last approximation stems from the assumption of an excess delay channel model. Using the dense large-multipath assumption also leads to the approximation

$$\sum_{p=0}^{R-1} \left| h_p\left(kT + \frac{p}{W}\right) \right|^2 \approx E \left[\sum_{p=0}^{R-1} \left| h_p\left(kT + \frac{p}{W}\right) \right|^2 \right] = \sum_{p=0}^{R-1} \overline{\left| h_p\left(kT + \frac{p}{W}\right) \right|^2} \quad (\text{A-58})$$

We assume the time variations of the impulse response are wide-sense stationary and use the definition from section B.4.1 for the average strength of the p 'th tap weight

$$\overline{|h_p(t)|^2} = \frac{Q_p}{W} = \frac{1}{W} \hat{Q}\left(\frac{p}{W}\right) \quad (\text{A-59})$$

In (A-59) we have postulated a hypothetical function $\hat{Q}(\xi)$ which, when sampled at $\xi=p/W$, is proportional to Q_p . Adopting terminology commonly used in similar situations in the open literature, we have denoted $\hat{Q}(\xi)$ the *power delay profile*. In accordance with the *smooth* assumption, $\hat{Q}(\xi)$ varies little as ξ changes by $1/W$, so that Q_p varies little as p

changes by 1. Using the smooth assumption and the dense large-multipath assumption leads to the approximations

$$\sum_{p=0}^{\infty} \overline{|h_p(t)|^2} \cong \int_0^{\infty} \widehat{Q}(\xi) d\xi \quad (\text{A-60})$$

$$\sum_{p=0}^{R-1} \overline{\left| h_p \left(kT + \frac{p}{W} \right) \right|^2} \cong \int_0^{R/W} \widehat{Q}(\xi) d\xi \quad (\text{A-61})$$

Thus, dropping the k subscript, we arrive at the output SNR approximation

$$\rho_{\text{out}} = 2N\rho_{\text{in}} \frac{\int_0^{R/W} \widehat{Q}(\xi) d\xi}{\int_0^{\infty} \widehat{Q}(\xi) d\xi} = 2\rho \frac{\int_0^{R/W} \widehat{Q}(\xi) d\xi}{\int_0^{\infty} \widehat{Q}(\xi) d\xi} \cong \rho_0 \quad (\text{A-62})$$

If R is large enough, the ratio in the last factor will approach 1 and ρ_{out} becomes equal to 2ρ . However, as we will show next, when noise is included in the tap weight estimation, too large a value of R becomes undesirable, eventually resulting in a decrease in output SNR.

Now consider the case wherein the tap weight estimates are noisy but there is still no time-selective distortion. Thus, (A-44) is still valid. Ignoring self-noise, the output noise term is now given by

$$N_k = \text{Re} \left\{ \sum_{p=0}^{R-1} \left(\widehat{n}_{pk}^* n_{pk} + W h_p^* \left(kT + \frac{T}{2} + \frac{p}{W} \right) n_{pk} + W h_p \left(kT + \frac{T}{2} + \frac{p}{W} \right) \widehat{n}_{pk}^* \right) \right\} \quad (\text{A-63})$$

Using the Central Limit Theorem (generalized to the complex Gaussian case⁴⁰), the summation may be approximated as a complex Gaussian variable when the number of terms in the summation is large, as assumed here. Since the mean squared value of the real part of a complex Gaussian variable equals one-half of the mean absolute squared value of the variable, we may use

⁴⁰ Analogous to the proof by Bello [19].

$$\overline{N_k^2} = \frac{1}{2} \overline{\left| \sum_{p=0}^{R-1} \left(\hat{n}_{pk}^* n_{pk} + W h_p^* \left(kT + \frac{T}{2} + \frac{p}{W} \right) n_{pk} + W h_p \left(kT + \frac{T}{2} + \frac{p}{W} \right) \hat{n}_{pk}^* \right) \right|^2} \quad (\text{A-64})$$

As pointed out after (A-34), n_{pk} and \hat{n}_{pk} are statistically independent and \hat{n}_{pk} and n_{qk} are uncorrelated for all p and q . We assume that the average $\overline{\hat{n}_{pk}^* \hat{n}_{qk} n_{pk}}$ is zero for all p and q . This moment property would be true if the noise variables were complex Gaussian variables, which we do not assume for the SNR method. With the noise averages described, all cross-product terms obtained by squaring in (A-64) will vanish after averaging. Thus, (A-64) simplifies to

$$\begin{aligned} \overline{N_k^2} = \frac{1}{2} \sum_{p=0}^{R-1} \overline{|\hat{n}_{pk}|^2 |n_{pk}|^2} + \frac{W^2}{2} \sum_{p=0}^{R-1} \overline{|n_{pk}|^2} \left| h_p \left(kT + \frac{T}{2} + \frac{p}{W} \right) \right|^2 \\ + \frac{W^2}{2} \sum_{p=0}^{R-1} \overline{|\hat{n}_{pk}|^2} \left| h_p \left(kT + \frac{T}{2} + \frac{p}{W} \right) \right|^2 \end{aligned} \quad (\text{A-65})$$

Using (A-17) - (A-19) and (A-34),

$$\frac{\overline{|\hat{n}_{pk}|^2}}{\left(\frac{2WN_0}{N} \right)} = \sum_{m=0}^{\infty} |b_m|^2 \triangleq \gamma \quad (\text{A-66})$$

where, with the normalization $\sum_{m=0}^{\infty} b_m = 1$, it may be shown that γ is the *two-sided* noise

bandwidth of the tap weight filter normalized the symbol rate $1/T$. Thus,

$$\overline{N_k^2} = \frac{W^2 N_0^2}{N^2} (\gamma 2R + \rho_{0k} (1 + \gamma)) \quad (\text{A-67})$$

Using (A-66), (A-49), and (A-46), we obtain the general expression for output SNR for noisy tap weights, when self noise is neglected and there is no time-selective distortion:

$$\rho_{\text{out},k} = \frac{\rho_{0k}^2}{(\gamma 2R + \rho_{0k} (1 + \gamma))} \quad (\text{A-68})$$

By hypothesis, in the SNR method, the fluctuations in ρ_{0k} , (A-49), are assumed small enough to be neglected. Thus replacing ρ_{0k} by the average value of ρ_{0k} , as in A.4.1.1, we obtain the output SNR expression

$$\rho_{\text{out}} = \frac{\rho_0^2}{(\gamma 2R + \rho_0(1 + \gamma))} = \frac{2\chi^2 \rho^2}{(\gamma R + \chi(1 + \gamma)\rho)} \quad (\text{A-69})$$

where ρ_0 is given by (A-62) and

$$\chi = \frac{\int_0^{R/W} \widehat{Q}(\xi) d\xi}{\int_0^{\infty} \widehat{Q}(\xi) d\xi} \quad (\text{A-70})$$

Note from (A-69) that as R increases, the factor χ increases, approaching unity when R/W exceeds the multipath spread. In the absence of the term γR in the denominator ρ_{out} would increase to a limiting value of 2ρ . However, the presence of the term γR causes an eventual reduction in ρ_{out} with increasing R . Thus, there is an optimum value of R .

Finally we consider the case wherein time-selective distortion is present, the tap weight measurements are noisy, and self noise is neglected. In this case, we use the more general expressions (A-38) and (A-39) for the signal and noise, respectively, at the combiner output with the self-noise set to zero in the latter expression. Following the same procedure as in the derivations for the case of no time-selective fading case, the combiner SNR output for the k^{th} I&D is readily found to be given by the following expression

$$\rho_{\text{out},k} = \frac{2A_k^2 \rho_k^2}{R\gamma + B_k \rho_k} \quad (\text{A-71})$$

where

$$\rho_k \triangleq N \frac{W \sum_{p=0}^{\infty} \left| h_p \left(kT + \frac{T}{2} \right) \right|^2}{2N_0} \quad (\text{A-72})$$

$$A_k = \text{Re} \left[\frac{\sum_{p=0}^{R-1} \hat{h}_p \left(kT + \frac{T}{2} + \frac{p}{W} \right) \tilde{h}_p^* \left(kT + \frac{T}{2} + \frac{p}{W} \right)}{\sum_{p=0}^{\infty} \left| h_p \left(kT + \frac{T}{2} \right) \right|^2} \right] \quad (\text{A-73})$$

$$B_k = \frac{\gamma \sum_{p=0}^{R-1} \left| \tilde{h}_p \left(kT + \frac{T}{2} \right) \right|^2 + \sum_{n=0}^{R-1} \left| \hat{h}_p \left(kT + \frac{T}{2} \right) \right|^2}{\sum_{n=0}^{\infty} \left| h_p \left(kT + \frac{T}{2} \right) \right|^2} \quad (\text{A-74})$$

The SNR method assumes the dense large-multipath model which leads to the approximation of replacing the sums in (A-72) through (A-74) by ensemble averages. We have already determined the ensemble average (see (A-60)),

$$\sum_{p=0}^{\infty} \overline{|h_p|^2} \cong \int_0^{\infty} \hat{Q}(\xi) d\xi \triangleq 1 \quad (\text{A-75})$$

In (A-75) we have normalized the area under $\hat{Q}(\xi)$ as unity to simplify subsequent notation. From (A-73) and (A-74) we see that we need to evaluate $\overline{\hat{h}_p \tilde{h}_p^*}$, the complex correlation between \hat{h}_p and \tilde{h}_p , and the average magnitude squared values $\overline{|\hat{h}_p|^2}$ and $\overline{|\tilde{h}_p|^2}$. (A-22) and (A-32) show that $\hat{h}_p(t)$ and $\tilde{h}_p(t)$ are filtered versions of $h_p(t)$. Thus, assuming that the tap weights are statistically stationary processes, it is readily determined that these averages are

$$\overline{\hat{h}_p \tilde{h}_p^*} = \int P_{pp}(f) \text{sinc}^2(fT) G(f) e^{-j2\pi fT} df \quad (\text{A-76})$$

$$\overline{|\hat{h}_p|^2} = \int P_{pp}(f) \text{sinc}^2(fT) |G^2(f)| df \quad (\text{A-77})$$

$$\overline{|\tilde{h}_p|^2} = \int P_{pp}(f) \text{sinc}^2(fT) df \quad (\text{A-78})$$

where $G(f)$ is the transfer function of the tap weight filter,

$$G(f) = \sum_{n=0}^{\infty} b_n e^{-j2\pi n f T} \quad (\text{A-79})$$

and $P_{pp}(f)$ (using the notation from Appendix B) denotes the power spectrum of the p 'th tap weight, $h_p(t)$.

To carry out numerical evaluations, it is necessary to determine or postulate tap weight correlation functions or spectra. This has been done in Appendix B. Section 3.1.3 summarizes the assumptions used to derive the tap weight cross-correlation functions and cross-power spectra for the tap weights. With these assumptions, it is shown in Appendix B (see (B-55), that

$$P_{pp}(f) = \frac{1}{W} \hat{Q}\left(\frac{p}{W}\right) \int F\left(v, \frac{p}{W}\right) \frac{1}{|v|_r} E\left(-\frac{f+v}{vr}\right) dv \quad (\text{A-80})$$

where the functions in (A-80) are defined by (3-21) through (3-24). It is convenient to express this power spectrum in the form

$$P_{pp}(f) = \frac{1}{W} \hat{S}\left(\frac{p}{W}, f\right) \quad (\text{A-81})$$

In (A-81) we have used a hypothetical function $\hat{S}(\xi, f)$ which, when sampled at $\xi=p/W$, is proportional to $P_{pp}(f)$. We call the function $\hat{S}(\xi, f)$, the *power spectrum delay profile*⁴¹. With the *smooth* assumption used throughout the report, $\hat{S}(\xi, f)$ varies little with ξ over a delay change of the order of $1/W$. In fact, it is readily seen that

$$\hat{Q}(\xi) = \int \hat{S}(\xi, f) df \quad (\text{A-82})$$

⁴¹ $\hat{S}(\xi, f)$ is not to be confused with $S(\xi, f)$, the (delay-Doppler) scattering function of a WSSUS channel. Only with the smooth assumption and a narrow band channel do these functions become equal (assuming both are normalized to unit volume).

Using (A-76) through (A-81) in (A-71) through (A-74), we obtain the following expression for the SNR

$$\rho_{\text{out}} = \frac{2A^2 \rho^2}{R\gamma + B\rho} \quad (\text{A-83})$$

Where

$$\begin{aligned} A &= \text{Re} \left\{ \int s \left(f, \frac{R}{W} \right) \text{sinc}^2 fT G(f) e^{-j2\pi fT} df \right\} \\ B &= \int s \left(f, \frac{R}{W} \right) \text{sinc}^2 fT |G^2(f)| df + \gamma \int s \left(f, \frac{R}{W} \right) \text{sinc}^2 fT df \end{aligned} \quad (\text{A-84})$$

in which we have defined the integrated spectrum

$$s \left(f, \frac{R}{W} \right) = \int_0^{R/W} \widehat{S}(\xi, f) d\xi \quad (\text{A-85})$$

Note that,

$$\int s \left(f, \frac{R}{W} \right) df = \int \int_0^{R/W} \widehat{S}(\xi, f) d\xi df = \int_0^{R/W} \widehat{Q}(\xi) d\xi = \chi \quad (\text{A-86})$$

If R is large enough to encompass all the multipath spread

$$s \left(f, \frac{R}{W} \right) \cong \int_0^{\infty} \widehat{S}(\xi, f) d\xi \triangleq P(f) \quad (\text{A-87})$$

We call the function $P(f)$ the *average tap weight power spectrum*. From (A-75) and (A-82) the area under $P(f)$ is unity. When (A-86) is valid

$$\begin{aligned} A &= \text{Re} \left\{ \int P(f) \text{sinc}^2 fT G(f) e^{-j2\pi fT} df \right\} \\ B &= \int P(f) \text{sinc}^2 fT |G^2(f)| df + \gamma \int P(f) \text{sinc}^2 fT df \end{aligned} \quad (\text{A-88})$$

Section 3.1.4 summarizes the assumptions used in the specialization of the tap weight cross-correlation functions and cross-power spectra to two scenarios: outdoor base-station to

urban mobile and indoor fixed terminal to mobile terminal assuming a dense multipath model. For these scenarios, the power spectrum delay profile can be expressed in the factored form.

$$\widehat{S}(\xi, f) = \widehat{Q}(\xi) \frac{1}{v_{\max}} p\left(\frac{f}{v_{\max}}, r\right) \quad (\text{A-89})$$

The normalized tap weight power spectrum $p(f, r)$ is given by (3-47). For the two scenarios we use an exponentially decreasing power delay profile

$$\widehat{Q}(\xi) = \frac{1}{\sigma} e^{-\frac{\xi}{\sigma}}; \sigma \geq 0 \quad (\text{A-90})$$

where σ is the delay at which the power delay profile decreases by the factor e . With the above relationships, the coefficients A and B are given by the integrals

$$A = \chi \operatorname{Re} \left\{ \int_{-1-\frac{r}{2}}^{1+\frac{r}{2}} p(f, r) \operatorname{sinc}^2(fx) G_0(fx) e^{-j2\pi fx} df \right\} \quad (\text{A-91})$$

$$B = \chi \left\{ \int_{-1-\frac{r}{2}}^{1+\frac{r}{2}} p(f, r) \operatorname{sinc}^2(fx) |G_0(fx)|^2 df + \gamma \int_{-1-\frac{r}{2}}^{1+\frac{r}{2}} p(f, r) \operatorname{sinc}^2(fx) df \right\} \quad (\text{A-92})$$

where

$$\chi = \frac{\int_0^{R/W} \widehat{Q}(\xi) d\xi}{\int_0^{\infty} \widehat{Q}(\xi) d\xi} = 1 - e^{-\frac{R}{\tau}} \quad (\text{A-93})$$

is the fraction of the tap weight power utilized by the R rake correlators. The normalized discrete tap weight filter transfer function,

$$G_0(f) = \sum_{p=0}^{\infty} b_p e^{-j2\pi p f} = G\left(\frac{f}{T}\right) \quad (\text{A-94})$$

the normalized Doppler shift parameter,

$$\mathbf{x} = \mathbf{v}_{\max} \mathbf{T} \quad (\text{A-95})$$

and the normalized delay constant

$$\tau = \sigma W \quad (\text{A-96})$$

For numerical evaluations, we use a ‘‘boxcar’’ tap weight measurement filter which averages over N_f samples and has a two-sided noise bandwidth $\gamma = 1/N_f$.

Having come this far with the proposed SNR method, a word of caution is in order. We repeat (A-38) below, which presents the expression for S_k , the signal component of the combiner output

$$S_k = d_k W^2 \text{Re} \left\{ \sum_{p=0}^{R-1} \hat{h}_p^* \left(kT + \frac{T}{2} + \frac{p}{W} \right) \tilde{h}_p \left(kT + \frac{T}{2} + \frac{p}{W} \right) \right\} \quad (\text{A-97})$$

We are assuming binary data so that $d_k = \pm 1$. In the absence of time selective distortion the real part of the sum in (A-87) is positive. However, it is possible that the real part will become negative due to the decorrelation introduced between \hat{h}_p and \tilde{h}_p by the tap weight and I&D filtering. Thus, assuming that $d_k=1$, the probability of raw bit error for the frozen channel for the k 'th data bit (see (A-40)) is given by

$$(p_{\text{rb}})_k = \begin{cases} \phi(\sqrt{\rho_{\text{out},k}}); \text{Re} \left\{ \sum_{p=0}^{R-1} \hat{h}_p^* \left(kT + \frac{T}{2} + \frac{p}{W} \right) \tilde{h}_p \left(kT + \frac{T}{2} + \frac{p}{W} \right) \right\} > 0 \\ 1 - \phi(\sqrt{\rho_{\text{out},k}}); \text{Re} \left\{ \sum_{p=0}^{R-1} \hat{h}_p^* \left(kT + \frac{T}{2} + \frac{p}{W} \right) \tilde{h}_p \left(kT + \frac{T}{2} + \frac{p}{W} \right) \right\} < 0 \end{cases} \quad (\text{A-98})$$

Strictly speaking, evaluation of the average of $(p_{\text{rb}})_k$ over the channel fluctuations must include consideration of the two conditions in (A-98). The SNR approach replaces the real part of the sum by the average of the real part, assuming that the sum fluctuates little from the average. Thus, the effect on performance of the non-zero probability that the real part may go negative (sometimes called the ‘‘irreducible’’ error probability) is neglected. For the SNR method to be useful, the irreducible error probability must be much less than the raw bit error

probability computed from the SNR method. This will be true for the dense large-multipath channel model wherein the effective diversity of the channel is very large.

To summarize, assuming the irreducible error rate is negligible, the raw channel bit error rate according to the SNR method is given by

$$p_{\text{rb}} = \phi\left(\sqrt{\rho_{\text{out}}}\right)$$

where ρ_{out} is the SNR at the real part of the Rake combiner output, given by

$$\rho_{\text{out}} = \frac{2A^2\rho^2}{R\gamma + B\rho}$$

ρ is the ratio of the received signal power to the noise power in a bandwidth $1/T$ where T is the symbol duration.⁴² To the extent that the SNR method models raw bit error performance for values of ρ_{out} of interest, the decoded error rate is given by

$$p = f_{\text{code}}\left(\rho_{\text{out}}/2R_c\right)$$

where $f_{\text{code}}(E_b/N_0)$ describes the AWGN performance of the decoder.

A.4.1.2 The Gaussian Noise Method

In the SNR method, the noise at each correlator I&D output was not assumed to be complex Gaussian, although certain moment properties of Gaussian noise were assumed to be valid in the derivations⁴³. In this section we assume that correlator output noises are independent⁴⁴ complex Gaussian stochastic variables. Using results from Bello [15, 16], based on work of Turin [14] and Price [17, 18], we determine the bit error probability for the frozen channel case. This bit error probability is expressible in closed form or as a double

⁴² The parameter ρ is also termed E_s/N_0 , the energy per received symbol divided by the noise power density.

⁴³ See the discussion following (A-64).

⁴⁴ The case of dependent complex noises at the correlator outputs can be handled but with an increase in complexity for numerical evaluations.

integral where the channel dependence appears as two quadratic forms in the filtered channel model tap weights.

This situation is analogous to the SNR method in which the frozen channel bit error probability was expressed in closed form wherein the channel dependence appeared in three quadratic forms involving filtered channel tap weights. Thus, as for the SNR method, if the statistics of these quadratic forms in the tap weights can be determined or measured, one may evaluate the bit error probability as an average of the frozen channel bit error probability over the quadratic form statistics. For the case of dense large-multipath, we may apply the Central Limit Theorem and approximate the quadratic forms by normally distributed variables. Or, using the average channel method, which also requires a dense large-multipath channel model for validity, but is less accurate, we may replace the quadratic forms by averages.

We consider binary PSK data transmission and analyze the bit error probability for the k 'th data symbol where, without loss of generality, we assume $d_k = 1$. Then, the error probability is given by the probability that the real part of the combiner output is negative, or, equivalently, that the quadratic form

$$q_k = \text{Re} \left\{ \sum_{p=0}^{R-1} q_{pk} \right\} < 0 \quad (\text{A-99})$$

where

$$q_{pk} = \mathbf{g}_{pk}^* y_{pk} = \left[\mathbf{W} \hat{\mathbf{h}}_p \left(kT + \frac{T}{2} + \frac{p}{W} \right) + \hat{\mathbf{n}}_{pk} \right]^* \left[\mathbf{W} \tilde{\mathbf{h}}_p \left(kT + \frac{T}{2} + \frac{p}{W} \right) + \mathbf{n}_{pk} \right] \quad (\text{A-100})$$

\mathbf{g}_{pk} (A-31) is the p 'th tap weight estimate for the k 'th correlator I&D output and y_{pk} (A-25) is the p 'th correlator output for the k 'th I&D. Referring to the discussion below (A-34), we note that $\hat{\mathbf{n}}_{pk}$ and \mathbf{n}_{qk} are uncorrelated for all p and q . With our assumption of complex Gaussian statistics, they are also statistically independent. Thus q_k is a Hermitian quadratic form in independent non-zero-mean complex Gaussian variables when the channel

is regarded as frozen. The results in [15, 16]⁴⁵ may be applied to determine the probability that the quadratic form is negative with the channel frozen. Then, including consideration of the irreducible error probability, the raw bit error probability is given by

$$(\mathbf{p}_{\text{rb}})_k = \begin{cases} \Pr[q_k < 0]; \text{Re} \left\{ \sum_{p=0}^{R-1} \hat{h}_p^* \left(kT + \frac{T}{2} + \frac{p}{W} \right) \tilde{h}_p \left(kT + \frac{T}{2} + \frac{p}{W} \right) \right\} > 0 \\ 1 - \Pr[q_k < 0]; \text{Re} \left\{ \sum_{p=0}^{R-1} \hat{h}_p^* \left(kT + \frac{T}{2} + \frac{p}{W} \right) \tilde{h}_p \left(kT + \frac{T}{2} + \frac{p}{W} \right) \right\} < 0 \end{cases} \quad (\text{A-101})$$

We now use the results in [15, 16] to obtain an expression for $\Pr[q_k < 0]$. To simplify the notation, we normalize g_{pk} and y_{pk} so that the noise components in these terms have unit average magnitude squared values. These normalizations do not affect $\Pr[q_k < 0]$ since they result in multiplying q_k by a positive number. From (A-16) and (A-19) we note that

$$\overline{|n_{pk}|^2} = \frac{2WN_0}{N}; \quad \overline{|\hat{n}_{pk}|^2} = \frac{2WN_0}{N} \gamma \quad (\text{A-102})$$

Thus we replace g_{pk} and y_{pk} by the normalized variables

$$U_{pk} = \mu_{pk} + z_{pk} \quad (\text{A-103})$$

$$V_{pk} = v_{pk} + w_{pk} \quad (\text{A-104})$$

where z_{pk} , w_{pk} are the normalized noises,

$$\overline{|z_{pk}|^2} = \overline{|w_{pk}|^2} = 1 \quad (\text{A-105})$$

and

$$\mu_{pk} = \sqrt{\frac{WN}{2N_0\gamma}} \hat{h}_p \left(kT + \frac{T}{2} + \frac{p}{W} \right) \quad (\text{A-106})$$

$$v_{pk} = \sqrt{\frac{WN}{2N_0}} \tilde{h}_p \left(kT + \frac{T}{2} + \frac{p}{W} \right) \quad (\text{A-107})$$

⁴⁵ Some typographical errors in [15] were corrected in [16]. However we note three additional typographical errors: (67), the lower left hand term in the matrix change, $+\frac{2}{\alpha+\beta}$ to $-\frac{2}{\alpha+\beta}$, (34) change λ to λI , and in (36) and (37) use upper case S.

At this point, we temporarily simplify the notation and drop the k subscript with the understanding the results are for the frozen channel. Thus

$$\Pr[q < 0] = \Pr\left[\sum_{p=1}^{R-1} (U_p^* V_p + U_p V_p^*) < 0\right] \quad (\text{A-108})$$

in which

$$U_p = \mu_p + z_p \quad (\text{A-109})$$

$$V_p = v_p + w_p \quad (\text{A-110})$$

[15, 16] present an expression for the probability that the more general quadratic form

$$\begin{aligned} q &= \sum_{p=0}^{R-1} \left(f |U_p|^2 + g |V_p|^2 + c U_p^* V_p + c^* U_p V_p^* \right) \\ &= \sum_{p=0}^{R-1} \begin{bmatrix} U_p^* & V_p^* \end{bmatrix} \mathbf{Q} \begin{bmatrix} U_p \\ V_p \end{bmatrix} \end{aligned} \quad (\text{A-111})$$

is negative where \mathbf{Q} is the matrix of the quadratic form

$$\mathbf{Q} = \begin{bmatrix} f & c \\ c^* & g \end{bmatrix} \quad (\text{A-112})$$

In [15, 16], it is assumed terms (z_p, w_p) are complex Gaussian and independent for different p but possibly statistically dependent for the same p . The covariance matrix of these variables is given by

$$\mathbf{M} = \begin{bmatrix} m_U & m_{UV} \\ m_{UV}^* & m_V \end{bmatrix} \quad (\text{A-113})$$

For the special case in this report we see that

$$\mathbf{Q} = \begin{bmatrix} 0 & 1 \\ 1 & 0 \end{bmatrix} \quad (\text{A-114})$$

$$\mathbf{M} = \begin{bmatrix} 1 & 0 \\ 0 & 1 \end{bmatrix} \quad (\text{A-115})$$

In [15, 16] it is shown that the probability the general quadratic form \mathbf{Q} in (A-111) is negative, assuming a general covariance matrix \mathbf{M} , is

$$\Pr[q < 0] = P_R(a, b, r) = \int_0^\infty W_R(x, a) \left(\int_0^{xr} W_R(y, b) dy \right) dx \quad (\text{A-116})$$

where

$$r = \sqrt{\frac{\alpha}{\beta}} \quad (\text{A-117})$$

$$W_R(y, b) = \frac{1}{b^{R-1}} y^R \exp\left[-\frac{(y^2 + b^2)}{2}\right] I_{R-1}(by) \quad (\text{A-118})$$

$I_{R-1}(\cdot)$ is the modified Bessel function of the first kind and order $R-1$ and the parameters a , b are given by

$$a = \sqrt{\sum_{p=0}^{R-1} \mathbf{S}_p^H \mathbf{Q}_a \mathbf{S}_p} \quad (\text{A-119})$$

$$b = \sqrt{\sum_{p=0}^{R-1} \mathbf{S}_p^H \mathbf{Q}_b \mathbf{S}_p} \quad (\text{A-120})$$

in which H stands for conjugate-transpose, \mathbf{S}_p is the column vector of means

$$\mathbf{S}_p = \begin{bmatrix} \mu_p \\ \nu_p \end{bmatrix} \quad (\text{A-121})$$

and the matrices

$$\mathbf{Q}_a = 2 \left(\frac{\beta \mathbf{M}^{-1} - \mathbf{Q}}{\alpha + \beta} \right) \quad (\text{A-122})$$

$$\mathbf{Q}_b = 2 \left(\frac{\alpha \mathbf{M}^{-1} + \mathbf{Q}}{\alpha + \beta} \right) \quad (\text{A-123})$$

For the simpler quadratic form of interest to this report, α and β are given by (see [15, 16]) (65) and (66))

$$\alpha = \sqrt{\text{Re}^2 \{m_{UV}\} + \det \mathbf{M}} - \text{Re} \{m_{UV}\} \quad (\text{A-124})$$

$$\beta = \sqrt{\text{Re}^2 \{m_{UV}\} + \det \mathbf{M}} + \text{Re} \{m_{UV}\} \quad (\text{A-125})$$

In our case, the moment matrix is the identity matrix which leads to

$$\alpha = \beta = 1; r = 1 \quad (\text{A-126})$$

and

$$\mathbf{Q}_a = \begin{bmatrix} 1 & -1 \\ -1 & 1 \end{bmatrix} \quad (\text{A-127})$$

$$\mathbf{Q}_b = \begin{bmatrix} 1 & 1 \\ 1 & 1 \end{bmatrix} \quad (\text{A-128})$$

Using (A-121), (A-127), and (A-128) in (A-119) and (A-120),

$$a = \sqrt{\sum_{p=0}^{R-1} |\mu_p - v_p|^2} \quad (\text{A-129})$$

$$b = \sqrt{\sum_{p=0}^{R-1} |\mu_p + v_p|^2} \quad (\text{A-130})$$

As pointed out in [16] the double integral (A-116) has been expressed by Price[17, 18] in terms of a single integral plus a closed form set of terms. Specializing Price's results, the desired probability may be expressed in the form

$$\begin{aligned} P_R(a, b) = & Q\left(\frac{a}{\sqrt{2}}, \frac{b}{\sqrt{2}}\right) - \frac{1}{2} \exp\left(-\frac{a^2 + b^2}{4}\right) I_0\left(\frac{ab}{2}\right) + \\ & \exp\left(-\frac{a^2 + b^2}{4}\right) \left(\sum_{m=1}^{R-1} C_m(R) \left[\left(\frac{b}{a}\right)^m - \left(\frac{a}{b}\right)^m \right] I_m\left(\frac{ab}{2}\right) \right) \end{aligned} \quad (\text{A-131})$$

where

$$Q(u, v) = \int_v^{\infty} x e^{-\frac{1}{2}(x^2 + u^2)} I_0(ux) dx \quad (\text{A-132})$$

is Marcum's Q function [] and

$$C_m(R) = \frac{1}{2^{2R-1}} \sum_{k=0}^{R-1-m} C_k^{2R-1} \quad (\text{A-133})$$

in which C_n^m is the binomial coefficient.

We now examine the parameters a and b. Returning to the k subscript, and using the definition of the parameters A_k and B_k in (A-72) through (A-74), we find

$$a_k^2 = \frac{\rho_k}{\gamma} [B_k - 2\sqrt{\gamma} A_k] \quad (\text{A-134})$$

$$b_k^2 = \frac{\rho_k}{\gamma} [B_k + 2\sqrt{\gamma} A_k] \quad (\text{A-135})$$

Then using the average channel approach with the large scatter multipath assumption, we replace each quadratic form by its average, yielding the result

$$a^2 = \frac{\rho}{\gamma} [B - 2A\sqrt{\gamma}] \quad (\text{A-136})$$

$$b^2 = \frac{\rho}{\gamma} [B + 2A\sqrt{\gamma}] \quad (\text{A-137})$$

where A, B are given by (A-84) or (A-91) and (A-92). In these expressions it is important to note that, as in the previous sections, $\sum_{m=0}^{\infty} b_m$ has been normalized to unity. Ignoring the

irreducible error probability, the raw bit error probability is given by

$$P_{rb} = P_R \left(\sqrt{\frac{\rho}{\gamma} [B - 2A\sqrt{\gamma}]}, \sqrt{\frac{\rho}{\gamma} [B + 2A\sqrt{\gamma}]} \right) \quad (\text{A-138})$$

A.4.2 Exact Error Probability for Complex Gaussian Tap Weights and Noise

In this section, we present an exact error probability evaluation for the special case in which both the tap weights and the noises at the correlator outputs may be approximated by zero mean complex Gaussian statistics. We use the normalized variables defined in the preceding section. Then the combiner output may be expressed as a Hermitian quadratic form, q_k , in zero mean complex Gaussian variables. Assuming $d_k=1$, the error probability is

the probability that $q_k < 0$. (A-103) – (A-110) apply, but now the variables (μ_{pk}, v_{pk}) , and thus the variables (U_{pk}, V_{pk}) , are zero mean complex Gaussian variables. We drop the k subscript at this point since we assume statistically stationary statistics for the tap weights and noise.

With the described statistics, the probability that the quadratic form $q < 0$ has been determined by Turin [14] for a general covariance matrix of the variables in the quadratic form and for a more general quadratic form than needed for our problem. To present this solution, we define the vector of normalized I&D output variables

$$\mathbf{G} = [U_0, V_0, U_1, V_1, \dots, U_{R-1}, V_{R-1}] \quad (\text{A-139})$$

and the covariance matrix

$$\mathbf{M} = \overline{\mathbf{G}^H \mathbf{G}} = \begin{bmatrix} \overline{U_0^* U_0} & \overline{U_0^* V_0} & \overline{U_0^* U_1} & \overline{U_0^* V_1} & \cdot & \cdot & \overline{U_0^* U_{R-1}} & \overline{U_0^* V_{R-1}} \\ \overline{V_0^* U_0} & \overline{V_0^* V_0} & \overline{V_0^* U_1} & \overline{V_0^* V_1} & \cdot & \cdot & \overline{V_0^* U_{R-1}} & \overline{V_0^* V_{R-1}} \\ \overline{U_1^* U_0} & \overline{U_1^* V_0} & \overline{U_1^* U_1} & \overline{U_1^* V_1} & \cdot & \cdot & \overline{U_1^* U_{R-1}} & \overline{U_1^* V_{R-1}} \\ \overline{V_1^* U_0} & \overline{V_1^* V_0} & \overline{V_1^* U_1} & \overline{V_1^* V_1} & \cdot & \cdot & \overline{V_1^* U_{R-1}} & \overline{V_1^* V_{R-1}} \\ \cdot & \cdot & \cdot & \cdot & \cdot & \cdot & \cdot & \cdot \\ \cdot & \cdot & \cdot & \cdot & \cdot & \cdot & \cdot & \cdot \\ \overline{U_{R-1}^* U_0} & \overline{U_{R-1}^* V_0} & \overline{U_{R-1}^* U_1} & \overline{U_{R-1}^* V_1} & \cdot & \cdot & \overline{U_{R-1}^* U_{R-1}} & \overline{U_{R-1}^* V_{R-1}} \\ \overline{V_{R-1}^* U_0} & \overline{V_{R-1}^* V_0} & \overline{V_{R-1}^* U_1} & \overline{V_{R-1}^* V_1} & \cdot & \cdot & \overline{V_{R-1}^* U_{R-1}} & \overline{V_{R-1}^* V_{R-1}} \end{bmatrix} \quad (\text{A-140})$$

The quadratic form of interest can be expressed as

$$q = \mathbf{G}^H \mathbf{Q} \mathbf{G} \quad (\text{A-141})$$

where \mathbf{Q} is a Hermitian symmetric matrix defining the quadratic form. Turin's results apply to a general Hermitian matrix. In our case, \mathbf{Q} is a sparse matrix with the simple repetitive structure,

$$\mathbf{Q} = \begin{bmatrix} 0 & 1 & 0 & 0 & \cdot & \cdot & 0 & 0 \\ 1 & 0 & 0 & 0 & \cdot & \cdot & 0 & 0 \\ 0 & 0 & 0 & 1 & \cdot & \cdot & 0 & 0 \\ 0 & 0 & 1 & 0 & \cdot & \cdot & 0 & 0 \\ \cdot & \cdot & \cdot & \cdot & \cdot & \cdot & \cdot & \cdot \\ \cdot & \cdot & \cdot & \cdot & \cdot & \cdot & \cdot & \cdot \\ 0 & 0 & 0 & 0 & \cdot & \cdot & 0 & 1 \\ 0 & 0 & 0 & 0 & \cdot & \cdot & 1 & 0 \end{bmatrix} \quad (\text{A-142})$$

Turin shows that the characteristic function of q is given by

$$\phi_q(jt) \triangleq e^{\overline{j}tq} = \frac{1}{\text{Det}[\mathbf{I} - jt\mathbf{M}\mathbf{Q}]} \quad (\text{A-143})$$

As pointed out by Turin, this is the reciprocal of a $2R^{\text{th}}$ degree polynomial in jt , the zeros of which lie at the reciprocals of the eigenvalues of the matrix $\mathbf{M}\mathbf{Q}$. The probability density function of q is given by

$$W(q) = \frac{1}{2\pi j} \int_{-j\infty}^{j\infty} \frac{1}{\text{Det}[\mathbf{I} - z\mathbf{M}\mathbf{Q}]} e^{-zq} dz \quad (\text{A-144})$$

Integrating over $W(q)$, the raw bit error probability is given by the integral

$$p_{\text{rb}} = \Pr[q < 0] = \int_{-\infty}^0 W(q) dq = -\frac{1}{2\pi j} \int_{-j\infty}^{j\infty} \frac{1}{z\text{Det}[\mathbf{I} - z\mathbf{M}\mathbf{Q}]} dz \quad (\text{A-145})$$

Again, as pointed out by Turin, it follows that once the eigenvalues of

$$\mathbf{P} = \mathbf{M}\mathbf{Q} \quad (\text{A-146})$$

are determined, the integral in (A-145) may be determined by use of the residue theorem.

The previous discussion shows that in principle the desired error probability can be determined once the moment matrix \mathbf{M} is evaluated. Thus, we now consider the evaluation of the moment matrix utilizing the results in Section B.4.1 of Appendix B on the tap weight cross-power spectra and cross-correlation functions for the complex channel. With use of the normalizations (A-103) – (A-107) we see that

$$\overline{U_p^* V_q} = \overline{\mu_p^* v_q} \quad (\text{A-147})$$

$$\overline{U_p^* U_q} = \begin{cases} \overline{|\mu_p|^2} + 1; p = q \\ \mu_p^* \mu_q; p \neq q \end{cases} \quad (\text{A-148})$$

$$\overline{V_p^* V_q} = \begin{cases} \overline{|v_p|^2} + 1; p = q \\ v_p^* v_q; p \neq q \end{cases} \quad (\text{A-149})$$

where

$$\overline{\mu_p^* v_q} = \frac{E_s/N_0}{\sqrt{\gamma}} \overline{\hat{h}_p^* \left(kT + \frac{T}{2} + \frac{p}{W} \right) \tilde{h}_q \left(kT + \frac{T}{2} + \frac{q}{W} \right)} \quad (\text{A-150})$$

$$\overline{\mu_p^* \mu_q} = \frac{E_s/N_0}{\gamma} \overline{\hat{h}_p^* \left(kT + \frac{T}{2} + \frac{p}{W} \right) \hat{h}_q \left(kT + \frac{T}{2} + \frac{q}{W} \right)} \quad (\text{A-151})$$

$$\overline{v_p^* v_q} = E_s/N_0 \overline{\tilde{h}_p^* \left(kT + \frac{T}{2} + \frac{p}{W} \right) \tilde{h}_q \left(kT + \frac{T}{2} + \frac{q}{W} \right)} \quad (\text{A-152})$$

These normalizations, which do not change the raw bit error probability, allow the covariance matrix \mathbf{M} to be expressed as the sum of the unit matrix \mathbf{I} and the covariance matrix of the normalized variables.

Equations (A-22) and (A-32) show that $\hat{h}_p(t)$ and $\tilde{h}_p(t)$ are filtered versions of $h_p(t)$, the p^{th} tap weight of the complex channel. Thus, assuming that the tap weights are statistically stationary processes, it is readily determined that the averages in (A-150) through (A-152) may be expressed by the following integrals,

$$\overline{\hat{h}_p^*(t) \tilde{h}_q(t + \tau)} = \int P_{pq}(f) \text{sinc}^2(fT) G^*(f) e^{j2\pi f(\tau+T)} df \quad (\text{A-153})$$

$$\overline{\hat{h}_p^*(t) \hat{h}_q(t + \tau)} = \int P_{pq}(f) \text{sinc}^2(fT) |G(f)|^2 e^{j2\pi f\tau} df \quad (\text{A-154})$$

$$\overline{\tilde{h}_p^*(t) \tilde{h}_q(t + \tau)} = \int P_{pq}(f) \text{sinc}^2(fT) e^{j2\pi f\tau} df \quad (\text{A-155})$$

where $G(f)$ is the transfer function of the tap weight filter, and $P_{pq}(f)$ is the cross-power spectral density between the p^{th} and q^{th} tap weights. $P_{pq}(f)$ is given by the Fourier transform

$$P_{pq}(f) = \int R_{pq}(\tau) e^{-j2\pi f\tau} d\tau \quad (\text{A-156})$$

where

$$R_{pq}(\tau) = \overline{h_p^*(t)h_q(t+\tau)} \quad (\text{A-157})$$

is the cross-correlation function between the p^{th} and q^{th} tap weights. Using (A-153) through (A-155) in (A-150) through (A-152) provides the necessary elements of the covariance matrix \mathbf{M} :

$$\overline{\mu_p^* v_q} = \frac{\rho}{\sqrt{\gamma}} \int P_{pq}(f) \text{sinc}^2(fT) G^*(f) e^{j2\pi f \left(\frac{q-p}{W} + T\right)} df \quad (\text{A-158})$$

$$\overline{\mu_p^* \mu_q} = \frac{\rho}{\gamma} \int P_{pq}(f) \text{sinc}^2(fT) |G(f)|^2 e^{j2\pi f \left(\frac{q-p}{W}\right)} df \quad (\text{A-159})$$

$$\overline{v_p^* v_q} = \rho \int P_{pq}(f) \text{sinc}^2(fT) e^{j2\pi f \left(\frac{q-p}{W}\right)} df \quad (\text{A-160})$$

We consider now the special cases of the outdoor and indoor dense multipath channels. Using the normalized cross-power spectra (3-46) and power delay profile relationship (3-34), we can express the integrals in (A-158) through (A-160), in term of normalized parameters and functions, as follows,

$$\overline{\mu_n^* v_m} = \frac{\rho}{\sqrt{\gamma}} \frac{e^{-\frac{n+m}{2\tau}}}{\tau} \int_{-1-\frac{r}{2}}^{1+\frac{r}{2}} p(f, r, m-n) \text{sinc}^2(fx) G_0^*(fx) e^{j2\pi fx \left(1 + \frac{m-n}{N}\right)} df \quad (\text{A-161})$$

$$\overline{\mu_n^* \mu_m} = \frac{\rho}{\gamma} \frac{e^{-\frac{n+m}{2\tau}}}{\tau} \int_{-1-\frac{r}{2}}^{1+\frac{r}{2}} p(f, r, m-n) \text{sinc}^2(fx) |G_0(fx)|^2 e^{j2\pi fx \frac{m-n}{N}} df \quad (\text{A-162})$$

$$\overline{v_n^* v_m} = \rho \frac{e^{-\frac{n+m}{2\tau}}}{\tau} \int_{-1-\frac{r}{2}}^{1+\frac{r}{2}} p(f, r, m-n) \text{sinc}^2(fx) e^{j2\pi fx \frac{m-n}{N}} df \quad (\text{A-163})$$

According to (A-145), the raw bit error probability for the exact calculation assuming complex Gaussian tap weights and noise, may be expressed as

$$p_{\text{rb}} = \Pr[q < 0] = \int_{-\infty}^0 W(q) dq = -\frac{1}{2\pi j} \int_{-j\infty}^{j\infty} \frac{1}{z \text{Det}[\mathbf{I} - z\mathbf{M}\mathbf{Q}]} dz \quad (\text{A-164})$$

In principle, this integral may be determined by use of the residue theorem because the determinant is a $2R^{\text{th}}$ degree polynomial in z , the zeros of which lie at the reciprocals of the eigenvalues of the matrix \mathbf{MQ} . However, this procedure becomes impractical in the current application where R is a very large number and the eigenvalues can be very close in value as the distortion of the channel begins to degrade performance. We choose instead a single integral numerical evaluation of the error probability as outlined below.

Returning to (A-144), recasting the integral as an integration over the real variable t , and making a scale change, the PDF of the quadratic form defining the decision variable becomes

$$W(q) = \int_{-\infty}^{\infty} \frac{1}{\text{Det}[\mathbf{I} - j2\pi t\mathbf{MQ}]} e^{-j2\pi tq} dt \quad (\text{A-165})$$

Consider the raw error probability as the limit

$$p_{\text{rb}} = \lim_{x \rightarrow \infty} \int_{-x}^0 W(q) dq \quad (\text{A-166})$$

Substituting (A-164) in (A-165), reversing the order of integration, and carrying out the integration over q ,

$$p_{\text{rb}} = \lim_{x \rightarrow \infty} \int_{-\infty}^{\infty} \frac{x \text{sinc}(xt) e^{j\pi xt}}{\text{Det}[\mathbf{I} - j2\pi t\mathbf{MQ}]} dt \quad (\text{A-167})$$

where

$$\text{sinc}(t) = \frac{\sin \pi t}{\pi t} \quad (\text{A-168})$$

To estimate p_{rb} , we use a sufficiently large but finite value of x until the desired number of significant figures in the integral is achieved. This numerical procedure was checked against special cases for which exact analytical results are available. It has been found that very accurate results (> 6 significant digits) were obtained for $x \geq 200\pi$, using the integration routines in *Mathematica*.

A.5 Self-Noise

Up to this point we have neglected self-noise. Self-noise is the residual signal appearing at the p^{th} correlator output due to all the other tap weight signals in the tapped delay line model. In this section, adapting results from [9]⁴⁶, we examine the contribution of self-noise to the Rake combiner output. A sufficient condition is derived under which the effect of self-noise is small compared to that of additive noise at the Rake combiner output. To simplify the derivation, the effect of time-selective fading is neglected. Since under normal operation the modem is designed to operate so that the effect of time-selective fading is small, this assumption is not felt to reduce the usefulness of the result.

Self-noise at the p^{th} correlator output for the k^{th} I&D time, x_{pk} , is given by (see (A-15)),

$$x_{pk} = \frac{1}{N} \sum_{q=-\infty}^{\infty} \sum_{n=kN}^{kN+N-1} a_n^* a_q m_q h\left(\tau + \frac{p}{W} + \frac{n}{W}, \tau + \frac{p}{W} + \frac{n}{W} - \frac{q}{W}\right); n \neq q \quad (\text{A-169})$$

where τ is the synchronization timing variable, and $h(t, \xi)$ is the bandlimited time-variant impulse response. As discussed below (A-20), this variable is controlled by the chip synchronization loop to “center” the measured multipath components over the available correlators in order that most or all of the multipath components are combined by the Rake processing. From an analysis point of view, we may set $\tau = 0$ with the understanding that the “excess delay” channel is measured and $p = 0$ is the first correlator that produces non-zero output.

Further simplification is possible if we assume that the time variant impulse response $h(t, \xi)$ varies little with t over the time interval $(kN, kN+N-1)$. In fact, when examining the channel estimation filters’ outputs, we will make an even stronger assumption, i.e., that $h(t, \xi)$ varies little with t over a time duration equal to the channel estimation filters’ time

⁴⁶ The notation used in [9] differs from that used here. Among other differences, [9] considers more general PSK data and chip modulation. In addition, the implementation of the Rake processing is different, the input signal being delayed instead of the local PN references. While [9] treats the WBHF channel, the evaluations for self-noise are appropriate for the present analysis which neglects time-selectivity. There are numerous typos and some corrections in [9] which are being documented.

constant. This is the condition of negligible time selectivity used for the derivations in this section. Using this condition, the excess delay channel model and the tapped delay line weight definition (A-1), (A-168) can be simplified to

$$x_{pk} = \frac{W}{N} \sum_{q=-\infty}^{\infty} \sum_{n=kN}^{kN+N-1} a_n^* a_q m_q h_{p+n-q}(kT); n \neq q \quad (\text{A-170})$$

Rearranging the summations

$$x_{pk} = W \sum_s h_{p+s}(kT) C_{ks}; s \neq 0 \quad (\text{A-171})$$

where

$$C_{ks} = \frac{1}{N} \sum_{q=0}^{N-1} a_{q+kN}^* a_{q+kN-s} m_{q+kN-s} \quad (\text{A-172})$$

Recall that the signal component at the p^{th} correlator output is proportional to $h_p(kT)$, the p^{th} weight in the tapped delay line channel model evaluated at $t=kT$. (A-170) shows that the self-noise at the p^{th} correlator output is given by the weighted sum of the tapped delay line weights for the other correlator outputs. The weights (for $s \neq 0$) are zero-mean random variables equal to finite cross-correlations between the locally generated PN sequence and the transmitted data-modulated PN sequence.

Ignoring time selectivity and using (A-33), (A-34), (A-38), and (A-39), the signal and noise components of the real part of the combiner output for the k^{th} I&D output, S_k and N_k , respectively, are given by

$$S_k = d_k W^2 \text{Re} \left\{ \sum_{p=0}^{R-1} |h_p(kT)|^2 \right\} \quad (\text{A-173})$$

$$N_k = \text{Re} \left\{ \sum_{p=0}^{R-1} \left(\hat{x}_{pk}^* x_{pk} + \hat{n}_{pk}^* n_{pk} + W h_p^*(kT) (x_{pk} + n_{pk}) \right. \right. \\ \left. \left. + x_{pk} \hat{n}_{pk}^* + n_{pk} \hat{x}_{pk}^* + d_k W h_p(kT) (\hat{x}_{pk}^* + \hat{n}_{pk}^*) \right) \right\} \quad (\text{A-174})$$

where \hat{x}_{pk} is the self-noise component of the tap weight measurement filter for the p^{th} correlator and the k^{th} I&D output (see(A-33)). The noise term N_k has 8 components, 5 of

which are dependent on the self-noise terms. In [9], the mean squared value of all 8 terms were evaluated to determine under what conditions the self-noise terms would make a small contribution to the mean squared value of N_k by comparison to the contributions of the three terms which are dependent upon the input noise alone. It was found that satisfaction of the following inequality

$$\rho_i \ll \Gamma \quad (\text{A-175})$$

where

$$\Gamma = \frac{1}{2} \frac{|R_0|^2}{\sum_{s \neq 0} |R_s|^2} \quad (\text{A-176})$$

is sufficient to make the self-noise contribution small compared to the additive noise contribution. In (A-174) ρ_i is the input SNR in the bandwidth W and R_s is the following discrete auto-correlation function of the tap weights

$$R_s = \sum_{p=-\infty}^{\infty} h_p^*(kT) h_{p+s}(kT) = \frac{1}{W^2} \sum_{p=-\infty}^{\infty} h^* \left(kT, \frac{p}{W} \right) h \left(kT, \frac{p+s}{W} \right) \quad (\text{A-177})$$

Due to the limitation of $h(kT, \xi)$ to the band $-W/2 < f < W/2$, we may express R_s as the integral

$$R_s = \frac{1}{W} \int_{-W/2}^{W/2} |T(f, kT)|^2 e^{j2\pi f \frac{s}{W}} df \quad (\text{A-178})$$

and we may express the sum

$$\sum_s |R_s|^2 = \frac{1}{W} \int_{-W/2}^{W/2} |T(f, kT)|^4 df \quad (\text{A-179})$$

Thus Γ may be expressed

$$\Gamma = \frac{1}{2} \frac{\mu}{1 - \mu} \quad (\text{A-180})$$

where

$$\mu = \frac{\left[\frac{1}{W} \int_{-W/2}^{W/2} |T(f, kT)|^2 df \right]^2}{\frac{1}{W} \int_{-W/2}^{W/2} |T(f, kT)|^4 df} \quad (\text{A-181})$$

Consider the simplified dense large-multipath channels defined in Section B.5 and introduced in Section 3.1.4. It was arbitrarily assumed that the energy density spectrum of the reference channel impulse response has a Gaussian shape. Performance evaluations for these channels are presented in Section 3.2. We first evaluate the self-noise inequality for the reference channel alone, i.e., the case of no multipath. In this case

$$|T(f, kT)|^2 = \frac{1}{W} E\left(\frac{f}{W}\right) \quad (\text{A-182})$$

where $E(f)$ is the Gaussian-shaped normalized energy density spectrum of the reference channel impulse response given by (3-42). Using (A-181) in (A-180) we find that

$$\mu_0 = \frac{\left[\int_{-1/2}^{1/2} E(f) df \right]^2}{\int_{-1/2}^{1/2} |E(f)|^2 df} \quad (\text{A-183})$$

and

$$\Gamma_0 = \frac{\left[\int_{-1/2}^{1/2} E(f) df \right]^2}{\int_{-1/2}^{1/2} |E(f)|^2 df - \left[\int_{-1/2}^{1/2} E(f) df \right]^2} \quad (\text{A-184})$$

where we have used the subscript 0 to denote the absence of multipath. For the Gaussian shaped $E(f)$, $\mu_0 = .538$ and $\Gamma_0 = .581$ and the self-noise inequality becomes $\rho_i \ll .581$ without multipath.

With the inclusion of multipath, the transfer function $T(f, t)$ becomes a random process and μ becomes a random variable. Exact analytic evaluation of the statistics of μ is not possible. While a simulation approach to evaluation is practical, we consider only an approximate analytic approach which is useful for the case of dense large-multipath channels. For this case, $T(f, t)$ may be approximated by a complex Gaussian process with many fluctuations or “degrees of freedom” in $T(f, kT)$ vs f over the bandwidth W . As a result of these fluctuations, the integrals in the numerator and denominator of (A-178), which are frequency averages, should fluctuate little relative to their mean values. We propose then to

replace the integrals by their mean values. To this end, we need to determine the averages

$$m_n(f) = \overline{|T(f, kT)|^{2n}}; n = 1, 2 \quad (\text{A-185})$$

Assuming that the transfer function is a complex Gaussian process, it is readily determined that

$$m_2(f) = 2m_1^2(f) \quad (\text{A-186})$$

so it is necessary to determine only $m_1(f)$ and our approximate expression for μ is given by

$$\mu \approx \frac{\left[\frac{1}{W} \int_{-W/2}^{W/2} m_1(f) df \right]^2}{\frac{2}{W} \int_{-W/2}^{W/2} m_1^2(f) df} \quad (\text{A-187})$$

It is readily determined that

$$m_1(f) = \overline{|T(f, kT)|^2} = E(f) \quad (\text{A-188})$$

Thus, with the dense large-multipath channel

$$\mu = \frac{\mu_0}{2} \quad (\text{A-189})$$

and

$$\Gamma = \frac{1}{2} \frac{\mu_0}{2 - \mu_0} \quad (\text{A-190})$$

With the Gaussian shaped energy density spectrum for the reference channel impulse response $\mu \approx .269$, $\Gamma = .184$ (-7.36 dB) and the self-noise inequality becomes $\rho_i \ll .184$.

Whether self-noise can be neglected by comparison to additive noise depends not only on ρ_i but also on the shape of $E(f)$. Thus, if $E(f)$ is selected rectangular in shape instead of Gaussian, we see that $\mu_0=1$ and the self-noise inequality for no multipath becomes $\rho_i < \infty$.

This result is to be expected apriori because with a rectangular shape and no multipath, there is only a single tap weight in the tapped delay line model of the channel and no self-noise is present. However, with multipath, $\mu \approx .5$ and $\rho_i \ll .5$ is required to neglect self-noise. The presence of interference excision will affect the shape of $E(f)$ and thus will modify the self-noise inequality, resulting in the need for smaller values of ρ_c to neglect self-noise.

It should be understood that even if the inequality should be violated, performance of the system can be satisfactory as long as the sum of the additive noise and self-noise contributions are small enough compared to the desired signal. Assuming the self-noise contributions to the combiner output may be approximated as Gaussian, the criterion of 5dB output SNR is still valid to obtain 10^{-6} decoded error rate with self-noise. Note that self-noise will produce an irreducible error rate, i.e., an error rate floor at infinite E_b/N_0 . As long as this floor is small enough, self-noise will be unimportant.

The performance calculations carried out in Section 3.2 assume symbol rates $D = .15$, 1.5 , and 15 Mss, a bandwidth $W=2$ GHz, and a center frequency of 7.5 GHz. Figures 3-11 and 3-14 present plots of required E_s/N_0 in dB to achieve an output SNR of 5dB (and thus a decoded error rate of 10^{-6}) vs the multipath delay constant σ in the range 10 to 300 ns. Figure 3-11 applies to the outdoor dense large-multipath channel model with relative terminal velocity of 100 ft/sec and Figure 3-14 applies to the indoor dense large-multipath channel with relative terminal velocity of 5 ft/sec. Table A-1 presents the input SNRs (in the bandwidth W) corresponding to these values of E_s/N_0 for symbol rates of $D = .15$, 1.5 , and 15 Mss.

Table A-1
Input Signal to Noise Ratio (dB) in the Bandwidth W

σ (ns)	D(Mss) for Outside Channel			D(Mss) for Inside Channel		
	.15	1.5	15	.15	1.5	15
10	-37.47	-28.81	-19.17	-39.01	-29.21	-19.25
300	-32.73	-26.32	-18.37	-37.30	-28.74	-19.15

In all cases, the input SNR is $\ll \Gamma = -7.36$ dB indicating that the impact of self-noise will be small or negligible for all the cases analyzed. However, these calculations apply to the case of no excision. With enough excision, the high data rate case is likely to be noticeably affected.

Appendix B Tapped Delay Line Model for the UWB Channel

All physical channels and signals have an essentially finite number of degrees of freedom due to restrictions on time duration, fading rate, bandwidth, etc. As a result, canonic mathematical models can be defined for such channels [5][8] based upon the sampling theorem. In this report, we will use one particular canonic model, which represents the channel as a uniformly tapped delay line with time-variant weights. The Rake modem performance analysis carried out in this report makes use of this tapped delay line model.

In this report, we focus our attention on the band-pass channel which is represented as a complex low-pass channel. Results have also been carried out with a real low-pass channel model but have been excluded from this report for simplicity. Section B.1 derives the tapped delay line model for the complex formulation. Section B.2 relates the characteristics of the tapped delay line model time variant weights to the UWB channel impulse response presented in Section 2. In Section B.3, the "excess delay" channel model is formulated. In this model, the time variant delays of the multipath components are reduced by a reference time-variant delay. The reference delay will be the direct path delay if the direct path is of sufficient strength. It is the excess path delay channel which is actually measured and utilized by the Rake demodulator.

Section B.4 derives statistical properties of the tapped delay line model for a dense multipath environment wherein the tap weights are represented as a set of quasi-stationary correlated complex Gaussian processes. A complete statistical description of the channel is then provided by the appropriate covariance matrices of the tap weight processes. The calculation of cross-correlation functions and cross-power spectra of the tap weights is carried out. It is found that these functions are dependent upon the bandwidth ratio $r = W/f_0$.

In the limit of small r , the correlation functions exhibit the behavior corresponding to a WSSUS channel.

B.1 Canonic Tapped Delay Line Model

It is assumed that the time-variant channel is band limited⁴⁷ with a center frequency f_0 . As a consequence, via the Sampling Theorem, the complex envelope of the time variant impulse response of the channel, $h(t, \xi)$, may be represented in the form

$$h(t, \xi) = \sum_n h\left(t, \frac{n}{W}\right) \text{sinc}\left(W\left(\xi - \frac{n}{W}\right)\right) \quad (\text{B-1})$$

where W is equal to or greater than the actual (two-sided) bandwidth of the channel. Using (B-1) and assuming the input signal bandwidth is equal to or less than W Hz, we obtain the tapped delay line input/output representation, where $x(t)$ is the input and $y(t)$ is the output,

$$y(t) = \sum_n h_n(t) x\left(t - \frac{n}{W}\right) \quad (\text{B-2})$$

where,

$$h_n(t) = \frac{1}{W} h\left(t, \frac{n}{W}\right) \quad (\text{B-3})$$

$h_n(t)$ is the time-variant weight associated with the tap delay n/W .

The derivation for the real low-pass case follows the same procedure. However, the tap weights are real and the taps on the tapped delay line are separated by $1/2W$, where W is the low pass bandwidth. An equation analogous to (B-3) holds, in which the real low-pass impulse response is used and W is replaced by $2W$. Note that a complex representation of the real channel is possible as above with complex tap weights spaced $1/W$ apart, by choosing the center frequency as $W/2$.

⁴⁷ To be more precise, it is assumed that the time-variant transfer function of the complex low-pass channel, $T(f, t)$, defined as the Fourier Transform of $h(t, \xi)$ with respect to the delay variable ξ , is zero for $|f| \leq W/2$. This will occur if the real band pass transmitter filter is band-limited to $|f - f_0| \leq W/2$.

B.2 Behavior of Tap Weights for the UWB Channel

Using (3-11) in (B-3) we find the n 'th tap weight for the UWB channel is given by

$$h_n(t) = \frac{1}{W} \sum_{k=0}^K a_k e^{j\phi_k} e^{-j2\pi f_0 \xi_k(t)} g_0\left(\frac{n}{W} - \xi_k(t)\right) \quad (\text{B-4})$$

Note that there are three sources of time variation in $h_n(t)$, the path weight a_k , the phase shift ϕ_k and the path delay $\xi_k(t)$. We have not explicitly indicated the time variations of a_k and ϕ_k because these variations are usually much slower than the variations introduced by $\xi_k(t)$.

Also note that the contribution to the n^{th} tap weight due to a multipath component with an increasing or decreasing delay $\xi_k(t)$ not only produces an increasing or decreasing phase shift $2\pi f_0 \xi_k(t)$ but also, as discussed in detail below, produces a pulse $g_0\left(\frac{n}{W} - \xi_k(t)\right)$. As a result, each tap weight consists of a sum of randomly arriving overlapping random pulses in a dense multipath environment. The spectral spread of the tap weight process is due primarily to the combined variation in phase of $e^{-j2\pi f_0 \xi_k(t)}$ and to the spectral spread of the individual pulses $\{g_0\left(\frac{n}{W} - \xi_k(t)\right)\}$. The character of the individual pulses is made evident by using two terms in Taylor series expansion in t of the time variant delay and assuming that this linear variation in $\xi_k(t)$ is a good approximation over an interval of time equal to the duration of the pulse $g_0\left(\frac{n}{W} - \xi_k(t)\right)$. Such pulses are then scaled and time shifted replicas of the reference pulse $\bar{g}_0(t)$. This approximation has been examined via simulation for a mobile moving at constant speed and surrounded by dense randomly-placed reflectors⁴⁸. It was found to be valid for most of the reflectors. Exceptions occur when passing by a reflector where the Doppler shift changes sign.

In evaluation of the correlation functions and power spectra of the tap weights, we make extensive use of this linear approximation. Consider first the direct path ($k = 0$). If we define $v_0(t)$ as the rate of change of the distance between transmitter and receiver, then

⁴⁸ Unpublished work by author.

$$\frac{d}{dt} \xi_0(t) = \frac{v_0(t)}{c} \quad (\text{B-5})$$

where c is the velocity of light. Let \vec{u}_0 denote a unit vector pointed from the receiver to the transmitter and \vec{v}_R, \vec{v}_T denote the velocity vectors of the receiver and transmitter, then

$$v_0 = \vec{u}_0 \bullet (\vec{v}_R - \vec{v}_T) = v_R \cos d_0 - v_T \cos b_0 \quad (\text{B-6})$$

where $\vec{x} \bullet \vec{y}$ denotes the dot-product of the vectors \vec{x}, \vec{y} and v_R, v_T are the transmitter and receiver speeds. d_0, b_0 are the angles between the vectors \vec{v}_R, \vec{v}_T , respectively, and \vec{u}_0 . For a constant v_0

$$\xi_0(t) = \tau_0 + \frac{v_0}{c} t \quad (\text{B-7})$$

where τ_0 is the value of $\xi_0(t)$ at $t = 0$.

Using analogous definitions for the multipath components

$$\frac{d}{dt} \xi_k(t) = \frac{v_k(t)}{c} ; k = 1, 2, \dots, K \quad (\text{B-8})$$

where $v_k(t)$ is the rate of change of the k^{th} path distance between transmitter and receiver.

Consider⁴⁹ the case of a multipath component generated by one or more stationary reflectors. If \vec{u}_k denotes a unit vector pointing along the virtual line-of-sight from the image of the transmitter to the receiver, v_k can be expressed as

$$v_k = \vec{u}_k \bullet (\vec{v}_R - \vec{v}_T) = v_R \cos d_k - v_T \cos b_k \quad (\text{B-9})$$

where d_k, b_k are the angles between \vec{u}_k and the transmitter (image) and receiver velocity vectors, respectively. For a constant rate of change of distance

$$\xi_k(t) = \tau_k + \frac{v_k}{c} t \quad (\text{B-10})$$

where τ_k is the value of $\xi_k(t)$ at $t = 0$.

Using (B-9) and (B-10) in (B-4), the tap weight for the case of linear variation in delay may be represented in the form

⁴⁹ One may generalize the formulation to include motion of reflecting objects.

$$h_n(t) = \frac{1}{W} \sum_{k=0}^K a_k e^{j\phi_k} e^{-j2\pi v_k t} g_0\left(-\frac{v_k}{f_0} t - \tau_k + \frac{n}{W}\right) \quad (\text{B-11})$$

where we have defined the Doppler shift at the carrier frequency f_0 caused by motion of the k^{th} reflector as,

$$v_k = f_0 \frac{v_k}{c} = f_0 \left(\frac{v_R}{c} \cos d_k - \frac{v_T}{c} \cos b_k \right) = \frac{v_R}{\lambda_0} \cos d_k - \frac{v_T}{\lambda_0} \cos b_k \quad (\text{B-12})$$

where λ_0 is the wavelength at the carrier frequency and, to simplify notation, we have incorporated the phase shift

$$\theta_k = -2\pi f_0 \tau_k \quad (\text{B-13})$$

in the phase shift ϕ_k .

Examination of (B-11) shows that the n^{th} tap weight is the sum of randomly delayed, severely stretched, and frequency-shifted versions of the reference impulse response. We will examine the frequency band occupied by this set of pulses, ignoring the additional spreading caused by the time variation of the other parameters. The reference impulse response is stretched by a factor $f_0/v_k = c/v_k$ and shifted in frequency by v_k Hz. Thus, if the reference impulse response occupies the band $\left(-\frac{W}{2} \leq f \leq \frac{W}{2}\right)$, the bandwidth of the k^{th} stretched reference impulse response $B_k = r |v_k|$, and the k^{th} multipath contribution to the tap weight occupies the band $\left(v_k - \frac{r}{2} |v_k| \leq f \leq v_k + \frac{r}{2} |v_k|\right)$, where we have defined $r = W/f_0$ as the bandwidth ratio. $r \ll 1$ denotes narrowband operation, while $r \geq .25$ denotes UWB operation. B_k is bounded as follows

$$B_k = \left| \frac{v_R}{c} \cos d_k - \frac{v_T}{c} \cos b_k \right| W \leq \frac{v_R + v_T}{c} W \quad (\text{B-14})$$

The upper bound in (B-14) corresponds to the case of the direct path with platforms approaching head-on, assuming a channel bandwidth of W Hz.

v_k will vary randomly over the set of reflectors. If (v_{\min}, v_{\max}) are the minimum and maximum Doppler shift, respectively, then the spectral spread of the tap weights covers the

frequency band $\left(v_{\min} - \frac{r}{2} |v_{\min}| \leq f \leq v_{\max} + \frac{r}{2} |v_{\max}| \right)$. If $v_{\min} = -v_{\max}$ the band spread becomes $\left(-v_{\max} \left(1 + \frac{r}{2} \right) \leq f \leq v_{\max} \left(1 + \frac{r}{2} \right) \right)$. In the narrow band limit the band occupied reduces to $(v_{\min} \leq f \leq v_{\max})$.

If v is the sum of the transmitter and receiver platforms' speeds in miles/hour and W is the channel bandwidth in GHz, B_k is upper-bounded by $1.49vW$ Hz. For $v = 700$ mph and $W = 2$ GHz, this upper bound is around 2 kHz. For indoor channels and a fast walking speed of 4 mph, the upper bound is around 11.4 Hz. The magnitude of the Doppler shift is given by B_k/r . Assuming $v_{\min} = -v_{\max}$, $r = 1$, and $v = 700$ mph, the spectrum of the tap weights lies within the band $(-3 < f < 3)$ kHz while for $v = 4$ mph, the band reduces to $(-17.1 < f < 17.1)$ Hz.

We examine now the behavior of the n^{th} tap weight, $h_n(t)$, with n . Consider first the contribution due to the direct path alone ($k=0$),

$$a_0(t) e^{-j2\pi f_0 \xi_0(t)} g_0\left(\frac{n}{W} - \xi_0(t)\right) \quad (\text{B-15})$$

Let us assume that the reference direct path impulse response $g_0(\xi)$ is non-zero over the interval $\{t_1 \leq \xi \leq t_2\}$, then (B-15) will be non-zero over the interval $\{t_{n2}, t_{n1}\}$, where

$$\frac{n}{W} - \xi_0(t_{n1}) = t_1 \quad (\text{B-16})$$

$$\frac{n}{W} - \xi_0(t_{n2}) = t_2 \quad (\text{B-17})$$

For a relevant example, assume linear variation as in (B-8). Then

$$t_{n1} = \frac{c}{v_0} \left(\frac{n}{W} - \tau_0 - t_1 \right) \quad (\text{B-18})$$

$$t_{n2} = \frac{c}{v_0} \left(\frac{n}{W} - \tau_0 - t_2 \right) \quad (\text{B-19})$$

If we define the duration of the direct path impulse response as

$$L_0 = t_2 - t_1 \quad (\text{B-20})$$

then the duration of $\bar{h}_n(t)$ is given by

$$d_0 = \frac{c}{v_0} L_0 \quad (\text{B-21})$$

The previous equations show that for the direct path alone, the tap weight time variations for the different taps are time-shifted replicas, with adjacent tap weight time variations shifted by $\delta_1 = \frac{c}{v_0} \left(\frac{1}{W} \right)$ sec. Thus, if the tap weights are examined as a function of n at a particular value of t , what will be seen is a sampled version of the direct path impulse response, with samples separated by $1/W$. The number of non-zero samples is approximately WL_0 . As time progresses, the pattern of samples will shift with a certain "velocity." From the foregoing discussion, the time interval for the pattern to move one tap is δ_1 . Thus for $W = 2$ GHz and $v_0 = 700$ mph, $\delta_1 = .49$ ms, and for $v_0 = 4$ mph, $\delta_1 = 86$ ms.

Due to the linearity of the channel we can superpose the individual multipath contributions, each of which exhibits the same general type of behavior as the direct path contribution. The pattern for each path will "move" along the tapped delay line with a different velocity resulting in reinforcements and cancellations. A global shift in time will generally be observed for the resulting complex pattern.

It is important to note that each tap weight is essentially dependent on a subset of the multipath components. Assume $g_0(\xi)$ is effectively non-zero over a finite interval, $\{0 \leq \xi \leq L_0\}$. Then, $g_0\left(\frac{n}{W} - \xi_k(t)\right)$ will be non-zero only for the set of values of k , say $\alpha(n/W)$, for which $\{n/W - L_0 \leq \xi_k(t) \leq n/W\}$, or assuming linear variation in time, (B-10), and $t = 0$, the set of values of k for which $\{n/W - L_0 \leq \tau_k \leq n/W\}$. The set $\alpha(n/W)$ will change with time because of the relative motion of reflectors and terminals.

The number of adjacent tap weights influenced by the k^{th} reflection, N_a , is of interest also, since this determines the tap spacing required for tap weights to become uncorrelated. N_a is equal to the number of “non-zero” samples of the reference impulse response $g_0(\xi)$ when sampled at the rate W/second . Since no waveform can be both band-limited and time-limited, calculating N_a requires an arbitrary definition of duration for $g_0(\xi)$. N_a can range from around 3-4 for a Gaussian shape to a large number for an oscillatory impulse response.

B.3 Excess Delay Channel

The Rake modem attempts to measure the tap weights of the channel and coherently combine the direct signal and multipath contributions to the received signal as represented by the complex tap weights of the tapped delay line model of the channel. The Rake modem must cope with the pattern shift without using a huge shift register to accommodate the large time shifts of the pattern. It does this by adjusting the time scale of a replica transmitted signal used in the Rake correlation processing. This adjustment is done by an appropriate time discriminator and delay-tracking loop.

When synchronization occurs, the measured tap weight pattern, although time variant, will have a stable global position, minimizing the number of tap weights necessary in the Rake combining process. The system can obtain synchronization from the direct path if it is strong enough. "Excess" path delay has been used frequently in the literature to describe channel multipath values relative to the direct path delay. We will use the term "excess path delay channel" to represent the channel tapped delay line model in which time variant path delays are measured relative to the time-variant direct path delay. If there is no significant direct path, then another reference position may be used by the synch system. However, for simplicity, we will still use the term excess delay channel to describe the resulting measured channel.

From the foregoing analyses, it is clear that we have modeled the received complex signal due to the k^{th} multipath component as the result of cascading two time-variant

operations in the following order: a filter with impulse response $a_k(t)g_0(\xi)$ and a time variable delay which can be modeled by the time variant impulse response, $\exp(-j2\pi f_0 \xi_k(t))\delta(\xi - \xi_k(t))$. The assumption has been made that the time variations of $a_k(t)$ and $\phi_k(t)$ are negligible within a time interval equal to the duration of L_k , the k^{th} path impulse response.

We now make the further assumption that the time variation of $\xi_k(t)$ is negligible over the same time interval. Then it is possible to reverse the order of the two operations with negligible error on the output signal. Furthermore, we can divide the time variant delay operation $\exp(-j2\pi f_0 \xi_k(t))\delta(\xi - \xi_k(t))$ into two successive delay operations. The first delay we define as a reference delay $\xi_{\text{ref}}(t)$ which is common to all paths, and the second as the excess delay given by

$$\tilde{\xi}_k(t) = \xi_k(t) - \xi_{\text{ref}}(t) \quad (\text{B-22})$$

It follows that the channel may be represented as the cascade of the time variable delay $\xi_{\text{ref}}(t)$, represented by the impulse response $\exp(-j2\pi f_0 \xi_{\text{ref}}(t))\delta(\xi - \xi_{\text{ref}}(t))$ with the excess delay channel having impulse response

$$\tilde{h}(t, \xi) = \frac{1}{W} \sum_{k=0}^K a_k e^{j\phi_k} e^{-j2\pi f_0 \tilde{\xi}_k(t)} g_0(\xi - \tilde{\xi}_k(t)) \quad (\text{B-23})$$

The n^{th} tap weight for the excess delay channel is thus given by

$$\tilde{h}_n(t) = \frac{1}{W} \sum_{k=0}^K a_k e^{j\phi_k} e^{-j2\pi f_0 \tilde{\xi}_k(t)} g_0\left(\frac{n}{W} - \tilde{\xi}_k(t)\right) \quad (\text{B-24})$$

The input to the excess delay channel, $x_{\text{ref}}(t)$, is the output of the reference delay channel, i.e.,

$$x_{\text{ref}}(t) = e^{-j2\pi f_0 \xi_{\text{ref}}(t)} x(t - \xi_{\text{ref}}(t)) \quad (\text{B-25})$$

Delay and Doppler tracking loops at the receiver attempt to construct a replica of $x_{\text{ref}}(t)$. This replica is used in the Rake receiver to correlate against the incoming signal.

The tap weights of the excess delay channel will generally fluctuate more slowly than the original channel. Representing the path delays and the reference delay as having linear variations with time reveals this behavior. Then instead of (B-11) we have

$$\tilde{h}_n(t) = \frac{1}{W} \sum_{k=0}^K a_k e^{j\tilde{\phi}_k} e^{-j2\pi\tilde{v}_k t} g_0\left(-\frac{\tilde{v}_k}{f_0} t - \tilde{\tau}_k + \frac{n}{W}\right) \quad (\text{B-26})$$

where the Doppler shift on the k'th received multipath component for the excess delay channel is given by

$$\tilde{v}_k = v_k - v_{\text{ref}} \quad (\text{B-27})$$

$$\tilde{\tau}_k = \tau_k - \tau_{\text{ref}} \quad (\text{B-28})$$

$$\tilde{\theta}_k = -2\pi f_0 \tilde{\tau}_k \quad (\text{B-29})$$

$$\tilde{\phi}_k = \tilde{\theta}_k + \phi_k \quad (\text{B-30})$$

In defining the foregoing parameters, we have assumed linear time variation of the reference delay, so that

$$\xi_{\text{ref}} = \tau_{\text{ref}} + \frac{v_{\text{ref}}}{c} t \quad (\text{B-31})$$

$$v_{\text{ref}} = \frac{v_{\text{ref}}}{\lambda_0} \quad (\text{B-32})$$

Subtraction of the Doppler shift of the reference channel from the Doppler shifts of the multipath signals of the original channel, (B-27), will generally cause the fluctuation rate of the tap weights of the excess delay channel to be less than that of the original channel.

B.4 Statistical Modeling of Tap Weights

Our objective in this study is to evaluate the DSSS/Rake modem under limiting dynamic conditions in order to obtain a performance envelope, rather than to develop a precise Urban Mobile UWB channel model. In fact, due to the non-stationary spatial and temporal characteristics of the channel, there can be no precise stochastic Urban Mobile channel

model, whether narrow band or UWB. At best, one may attempt to define a set of scenarios which bound the expected distortion characteristics of the channel and evaluate the modem performance over these scenarios. This procedure is sufficient for evaluating the effectiveness of a modem used over the channel.

In this report, we focus on a scenario which may be called *dense urban non-resolvable multipath* or simply *dense large-multipath*. In this scenario, there is no direct path and no strong discrete path. Thus, the modem is required to operate over a channel consisting of a continuum of unresolvable paths with W so large that the number of required tap weights is very large. It is believed these assumptions provide a conservative evaluation the DSSS/Rake modem for use with the Mobile UWB channel.

With the dense large-multipath scenario, each tap weight is composed of contributions from a large number of reflectors, with no single reflector predominating. Then application of the Central Limit Theorem can be used to justify a complex Gaussian statistical representation for the tap weights. In the case of the real low-pass channel, the scatter multipath scenario leads to a real Gaussian statistical model for the tap weights. Other scenarios should be considered such as the discrete/scatter model in which a few discrete strong scatterers are added to the dense multipath model. In addition, non-stationary scenarios should be considered in which the mobile passes nearby strong reflectors.

Assuming the scatter multipath scenario and the applicability of the Central Limit Theorem, the statistical behavior of the tap weights is then completely specified by the covariance matrix of the tap weights. This information allows a rigorous evaluation of error probabilities for the DSSS/Rake modem as discussed in Section A.4. Simpler approximate evaluations are also presented in Section A.4 that do not require the complex Gaussian assumption for the tap weights.

This section is devoted primarily to the computation of the cross-correlation functions and cross-power spectra of the tap weights. We consider here only the complex low-pass formulation for the band pass channel.

To evaluate correlation functions and power spectra of the tap weights, it is necessary to define statistical properties of the parameters in (B-11). The analysis is carried out for the excess delay channel. However, to simplify notation, we do not include the tilde symbols on variables. We make the following assumptions⁵⁰:

- (1) The arrival times $\{\tau_k\}$ follow a Poisson distribution with an average arrival rate of $\beta(n/W)$ per second for $k \in \alpha(n/W)$ ⁵¹. The set $\alpha(n/W)$ is the set of k values contributing to the n th tap weight.
- (2) The phases $\{\phi_k\}$ are independent of other parameters and i.i.d. with uniform PDF over $(0, 2\pi)$.
- (3) The path-amplitude a_k and Doppler shift v_k of the k^{th} multipath component are assumed to have a PDF $D(a, v, n/W)$ for $k \in \alpha(n/W)$ and to be statistically independent over k .

Assumption (1) should not be confused with the arrival time distributions of multipath in some descriptions of PDP's where simple Poisson distributions do not fit [32]. In this study we used a tapped delay line model with time varying tap weights $\{h_n(t)\}$ to model the channel. The PDP is defined here as the average strength of the tap weights vs. tap delay n/W , $\left\{ \overline{|h_n(t)|^2}; n = 0, 1, \dots \right\}$. On the other hand, the term "Poisson Arrival" in

assumption (1) refers to a sequence of delay parameters $\{\tau_k\}$ *versus* k associated with a

⁵⁰ For clarity, the parameters a_k , v_k , and τ_k could be changed to a_{kn} , v_{kn} , and τ_{kn} since the sum over k is for a subset of $k \in \alpha(n/W)$. We have avoided this clarification to simplify notation.

⁵¹ The set $\alpha(n/W)$ is defined at the end of Section B.2.

particular value of n . To put the comparison in general terms, assumption (1) is concerned with modeling the effect of the time-variation variable t , while the PDP's are concerned with modeling the effect of the delay variation variable ξ , on $h(t,\xi)$ the time variant impulse response of the channel. The choice of Poisson arrival in assumption (1) and the i.i.d. assumption in (3) are used strictly for mathematical convenience. These assumptions should not detract from use of the model for comparative evaluation of the effect of mobility on UWB modems.

In the following analysis, we need to define the aperiodic auto-correlation function and energy density function of the direct path reference impulse response. In this connection, it is convenient to define a reference impulse response, $g(t)$, normalized to unit bandwidth ($W = 1$) and unit “energy”⁵²

$$\int |g(t)|^2 dt = 1 \quad (\text{B-33})$$

In terms of this normalized reference impulse response, the actual reference pulse is given by

$$g_0(t) = \sqrt{\varepsilon W} g(Wt) \quad (\text{B-34})$$

where ε is the “energy” of the reference impulse response, i.e.,

$$\int |g_0(t)|^2 dt = \varepsilon \quad (\text{B-35})$$

We choose the convenient normalization

$$\varepsilon = W \quad (\text{B-36})$$

This is the value that ε would have if $G_0(f)$, the Fourier Transform of $g_0(t)$, were set equal to unity amplitude over the bandwidth W .

⁵² The energy of the corresponding real waveform would be 2.

The aperiodic auto-correlation function of $g_0(t)$ is given by

$$C_0(\tau) = \int g_0^*(\xi) g_0(\xi + \tau) d\xi \quad (\text{B-37})$$

This may be expressed as

$$C_0(\tau) = WC(W\tau) \quad (\text{B-38})$$

where

$$C(\tau) = \int g^*(\xi) g(\xi + \tau) d\xi \quad (\text{B-39})$$

is the aperiodic auto-correlation function of the normalized reference impulse response. For convenience we repeat (B-11) which presents the expression for the n^{th} tap weight as a sequence of randomly arriving random pulses

$$h_n(t) = \frac{1}{W} \sum_{k=0}^K a_k e^{j\phi_k} e^{-j2\pi v_k t} g_0\left(-\frac{v_k}{f_0} t - \tau_k + \frac{n}{W}\right) \quad (\text{B-40})$$

Using (B-11), the auto-correlation function of the n^{th} tap weight is given by the expectation,

$$\begin{aligned} R_{nn}(\tau) &= E\left[h_n^*(t) h_n(t + \tau)\right] \\ &= \frac{1}{W^2} \sum_{l=0}^K \sum_{k=0}^K E\left[a_k a_l e^{j(\phi_l - \phi_k)} e^{-j2\pi v_k \tau} g_0^*\left(-\frac{v_k}{f_0} t - \tau_k + \frac{n}{W}\right) g_0\left(-\frac{v_l}{f_0} t - \frac{v_l}{f_0} \tau - \tau_l + \frac{n}{W}\right)\right] \end{aligned} \quad (\text{B-41})$$

Due to the assumed independence and uniform distribution of the phases, the cross-product terms vanish in the expectation, yielding

$$R_{nn}(\tau) = \frac{1}{W^2} \sum_{k \in \alpha\left(\frac{n}{W}\right)} E\left[a_k^2 e^{-j2\pi v_k \tau} g_0^*\left(-\frac{v_k}{f_0} t - \tau_k + \frac{n}{W}\right) g_0\left(-\frac{v_k}{f_0} t - \frac{v_k}{f_0} \tau - \tau_k + \frac{n}{W}\right)\right] \quad (\text{B-42})$$

Averaging over the variables $\{a_k, v_k\}$ conditioned on the $\{\tau_k\}$ we obtain

$$R_{nn}(\tau) = \frac{1}{W^2} \iint a^2 W\left(v, a, \frac{n}{W}\right) e^{-j2\pi v \tau} E\left[\sum_{k \in \alpha\left(\frac{n}{W}\right)} g_0^*\left(-\tau_k + \frac{n}{W}\right) g_0\left(-\tau_k + \frac{n}{W} - \frac{v}{f_0} \tau\right)\right] da dv \quad (\text{B-43})$$

The sum may be recognized as a Monte Carlo integration with the approximate value

$$\sum_{k \in \alpha\left(\frac{n}{W}\right)} g_0^*\left(-\tau_k + \frac{n}{W}\right) g_0\left(-\tau_k + \frac{n}{W} - \frac{v}{f_0} \tau\right) \approx \frac{N_n}{T} \int g_0^*(x) g_0\left(x - \frac{v}{f_0} \tau\right) dx \quad (\text{B-44})$$

in which T is the duration of $g_0(t)$ and N_n ($\gg 1$ by hypothesis) is a random variable denoting the number of reflectors in an integration interval equal to T centered on tap delay n/W . Noting that $\beta\left(\frac{n}{W}\right) = E\left[\frac{N_n}{T}\right]$ we obtain the equation

$$R_{nn}(\tau) = \frac{1}{W} \beta\left(\frac{n}{W}\right) \iint a^2 D\left(v, a, \frac{n}{W}\right) e^{-j2\pi v \tau} C(-rv\tau) da dv \quad (\text{B-45})$$

Integrating over a , we may express (B-45) in the single integral form

$$R_{nn}(\tau) = \frac{1}{W} \hat{Q}\left(\frac{n}{W}\right) \int F\left(v, \frac{n}{W}\right) e^{-j2\pi v \tau} C(-rv\tau) dv \quad (\text{B-46})$$

where

$$F\left(v, \frac{n}{W}\right) \triangleq \frac{\int a^2 D\left(v, a, \frac{n}{W}\right) da}{\iint a^2 D\left(v, a, \frac{n}{W}\right) da dv} \quad (\text{B-47})$$

and

$$\hat{Q}\left(\frac{n}{W}\right) \triangleq \beta\left(\frac{n}{W}\right) \iint a^2 D\left(v, a, \frac{n}{W}\right) da dv \quad (\text{B-48})$$

Note that the area under $F(v, n/W)$ is unity. One may call $F(v, n/W)$ *the path loss weighted Doppler PDF* (for the n^{th} tap weight). $\hat{Q}\left(\frac{n}{W}\right)$ is proportional to the mean squared value of $h_n(t)$,

$$E\left[|h_n(t)|^2\right] = R_{nn}(0) = \frac{1}{W} \hat{Q}\left(\frac{n}{W}\right) \quad (\text{B-49})$$

In Appendix A, $\hat{Q}(\xi)$ has been defined as the *power delay profile*.

We consider now the more general calculation of the cross-correlation function of the weights for tap n and for tap m ,

$$\begin{aligned}
R_{nm}(\tau) &= E\left[h_n^*(t)h_m(t+\tau)\right] \\
&= \sum_{l=0}^K \sum_{k=0}^K E\left[a_k a_l e^{j(\phi_l - \phi_k)} e^{-j2\pi v_k \tau} g_0^*\left(-\frac{v_k}{f_0}t - \tau_k + \frac{n}{W}\right) g_0\left(-\frac{v_l}{f_0}t - \frac{v_l}{f_0}\tau - \tau_l + \frac{m}{W}\right)\right] \quad (B-50)
\end{aligned}$$

Due to the assumed independence of the phases, the cross-product terms vanish in the expectation, yielding

$$R_{nm}(\tau) = \sum_{k \in \left(\alpha\left(\frac{n+m}{2W}\right)\right)} E\left[a_k^2 e^{-j2\pi v_k \tau} g_0^*\left(-\frac{v_k}{f_0}t - \tau_k + \frac{n}{W}\right) g_0\left(-\frac{v_k}{f_0}t - \frac{v_k}{f_0}\tau - \tau_k + \frac{m}{W}\right)\right] \quad (B-51)$$

For the channel being analyzed, it will be seen that the cross-correlation function decreases rapidly with increasing $|m-n|$. It is assumed that for small values of $|m-n|$, $\alpha(n/W)$ and $\alpha(m/W)$ will not differ much. To simplify the analysis we have used α computed at the average of the tap weight delays, i.e., we will use $\alpha\left(\frac{m+n}{2W}\right)$. We also use this average approach in specifying the various density functions and parameters dependent on n/W . With this approximation, the analysis follows closely the previous analysis. The result is

$$R_{nm}(\tau) = \frac{1}{W} \beta\left(\frac{m+n}{2W}\right) \iint a^2 W\left(v, a, \frac{m+n}{2W}\right) e^{-j2\pi v \tau} C(-rv\tau + m - n) da dv \quad (B-52)$$

Integrating over a , we arrive at the single-integral expression

$$R_{nm}(\tau) = \frac{1}{W} \hat{Q}\left(\frac{m+n}{2W}\right) \int F\left(v, \frac{m+n}{2W}\right) e^{-j2\pi v \tau} C(-rv\tau + m - n) dv \quad (B-53)$$

The cross-power spectral density is the Fourier transform of the cross-correlation function,

$$\begin{aligned}
P_{nm}(f) &= \int R_{nm}(\tau) e^{-j2\pi f \tau} d\tau \\
&= \frac{1}{W} Q\left(\frac{m+n}{2W}\right) \int F\left(v, \frac{m+n}{2W}\right) \int C(-rv\tau + m - n) e^{-j2\pi(f+v)\tau} d\tau dv \quad (B-54)
\end{aligned}$$

The inner integral is simply related to $E(f)$, the energy density spectrum of the bandwidth-normalized reference impulse response,

$$E(f) = \int C(\tau) e^{-j2\pi f\tau} d\tau \quad (\text{B-55})$$

Using (B-55) to evaluate the inner integral in (B-54) we find that the cross-spectrum can be expressed as

$$P_{nm}(f) = \frac{1}{W} \hat{Q}\left(\frac{m+n}{2W}\right) \int F\left(v, \frac{m+n}{2W}\right) \frac{1}{|v|r} E\left(-\frac{f+v}{vr}\right) e^{-j2\pi(m-n)\left(\frac{f+v}{vr}\right)} dv \quad (\text{B-56})$$

The power spectrum of the n 'th tap weight is thus

$$P_{nn}(f) = \frac{1}{W} \hat{Q}\left(\frac{n}{W}\right) \int F\left(v, \frac{n}{W}\right) \frac{1}{|v|r} E\left(-\frac{f+v}{vr}\right) dv \quad (\text{B-57})$$

It is instructive to compare the tap gain correlation functions and spectra for the WB channel as derived above with corresponding ones for a channel consisting of a filter with the same band limited direct-path reference impulse response $g_0(t)$ in cascade with a hypothetical WSSUS⁵³ channel [5]. In this comparison, we make use of the smooth assumption, wherein the delay-Doppler scattering function $S(\xi, \nu)$ changes little over a delay (ξ) interval comparable to the duration of $g_0(\xi)$. This is consistent with the multipath assumptions we have made for the WB channel in this report.

Equations (C-8) and (C-10), respectively, repeated below, present the tap gain cross-correlation functions for the band limited WSSUS channel using the smooth assumption

$$R_{nm}(\tau) = C(m-n) \frac{1}{W} Q\left(\tau, \frac{m+n}{2W}\right) \quad (\text{B-58})$$

⁵³ The WSSUS channel can be represented as a continuum of fixed statistically independent scatterers which cause statistically stationary scintillation. The power spectrum and auto-correlation function for scatterers causing delays in the interval $(\xi, \xi + d\xi)$ is given by $S(\xi, f)d\xi$ and $Q(\tau, \xi)d\xi$, respectively, where $S(\xi, f)$ is called the scattering function [5]. We call $Q(\tau, \xi)$ the tap gain correlation function (an alternate terminology was used by the author in [5] but the present terminology has a more intuitive appeal).

$$P_{nm}(f) = C(m-n) \frac{1}{W} S\left(\frac{m+n}{2W}, f\right) \quad (\text{B-59})$$

Consider now the form that the tap weight cross-correlation function (B-53) takes as r approaches 0 for the WB channel,

$$\begin{aligned} \lim_{r \rightarrow 0} R_{nm}(\tau) &= C(m-n) \frac{\hat{Q}\left(\frac{m+n}{2W}\right)}{W} \int F\left(v, \frac{m+n}{2W}\right) e^{-j2\pi v\tau} dv \\ &= C(m-n) \frac{\hat{Q}\left(\frac{m+n}{2W}\right)}{W} K\left(-\tau, \frac{m+n}{2W}\right) \end{aligned} \quad (\text{B-60})$$

where

$$K\left(\tau, \frac{m+n}{2W}\right) = \int F\left(v, \frac{m+n}{2W}\right) e^{-j2\pi v\tau} dv \quad (\text{B-61})$$

is the characteristic function of the loss-weighted Doppler PDF. Fourier transforming the limit (B-60) we find that as r approaches 0, the tap weight cross-power spectrum approaches a limiting form

$$\lim_{r \rightarrow 0} P_{nm}(f) = C(m-n) \frac{1}{W} \hat{Q}\left(\frac{m+n}{2W}\right) F\left(-f, \frac{m+n}{2W}\right) \quad (\text{B-62})$$

Comparing the expressions for the WSSUS channel with those for the channel modeled here in the limit as r approaches 0, we can make the following identifications

$$Q(\tau, \xi) = \hat{Q}(\xi) K(-\tau, \xi) \quad (\text{B-63})$$

$$S(\xi, f) = \hat{Q}(\xi) F(-f, \xi) \quad (\text{B-64})$$

Thus, with the smooth assumption, we have shown that the NB channel (i.e., the WB channel for $r \rightarrow 0$) can be represented as the cascade of the direct path reference filter with a WSSUS channel having the scattering and tap gain correlation functions given by (B-64) and (B-63) respectively. Since $K(0, \xi) = 1$, $\hat{Q}(\xi) = Q(0, \xi) \equiv Q(\xi)$, which is identical to the delay power spectrum of the WSSUS model. It is worth reminding the reader that we have used the smooth assumption in arriving at these conclusions.

An interesting question is: how small does r have to be in order for the WB channel to be represented as a NB channel? To answer this question, we expand the tap weight correlation function, (B-45) in a Taylor series in r by expanding the correlation function $C(-rv\tau)$ in a Taylor series and integrating the individual terms in the summation. The result is

$$R_{nn}(\tau) = \hat{Q}\left(\frac{n}{W}\right) \sum_{k=0}^{\infty} \frac{\tau^k r^k \bar{f}^k}{k!} \frac{d^k K\left(-\tau, \frac{n}{W}\right)}{d\tau^k} \quad (\text{B-65})$$

where

$$\bar{f}^k = \int_{-1/2}^{1/2} f^k E(f) df \leq \left(\frac{1}{2}\right)^k \quad (\text{B-66})$$

is the n^{th} moment of the energy density spectrum of the normalized direct path reference impulse response. Note that this spectrum is normalized to unit bandwidth and unit area.

The magnitude of the derivative in (B-65) is upper-bounded as follows

$$\left| \frac{d^k K\left(-\tau, \frac{n}{W}\right)}{d\tau^k} \right| = (2\pi)^k \left| \int v^k F\left(v, \frac{n}{W}\right) e^{-j2\pi v\tau} dv \right| \leq (2\pi)^k \bar{|v|^k} \leq (2\pi v_{\max})^k \quad (\text{B-67})$$

where

$$\bar{|v|^k} = \int |v|^k F\left(v, \frac{n}{W}\right) dv \quad (\text{B-68})$$

is the k^{th} magnitude moment of $F(v, n/W)$ and v_{\max} is the magnitude of the maximum Doppler shift.

For r small we may use the first three terms in the series expansion (B-65) to approximate $R_{nn}(\tau)$,

$$R_{nn}(\tau) \approx \hat{Q}\left(\frac{n}{W}\right) \left(K\left(-\tau, \frac{n}{W}\right) + \tau r \bar{f} \frac{dK\left(-\tau, \frac{n}{W}\right)}{d\tau} + \frac{\tau^2 r^2 \bar{f}^2}{2} \frac{d^2 K\left(-\tau, \frac{n}{W}\right)}{d\tau^2} \right) \quad (\text{B-69})$$

We define the time constant τ_{\max} as the value of τ beyond which $|R(\tau)|$ is negligible. For small r , this is also the value of τ beyond which $\left|K\left(\tau, \frac{n}{W}\right)\right|$ is negligible. In order to approximate the left side of (B-69) by the first term on the right-hand side, it is sufficient to require that the sum of the second two terms in (B-69) be small compared to $Q(n/W)$ (the maximum of the first term) for all $\tau \leq \tau_{\max}$. From (B-66) and (B-67) an upper bound to the maximum of the sum of these two terms at the maximum value of $\tau = \tau_{\max}$ is given by

$$\begin{aligned} & \left| \hat{Q}\left(\frac{n}{W}\right) \left| \tau r f^{-1} \frac{dK\left(-\tau, \frac{n}{W}\right)}{d\tau} + \frac{\tau^2 r^2 f^2}{2} \frac{d^2K\left(-\tau, \frac{n}{W}\right)}{d\tau^2} \right| \right| \\ & \leq \hat{Q}\left(\frac{n}{W}\right) \left(\frac{\pi r \tau_{\max} v_{\max}}{2} + \frac{(\pi r \tau_{\max} v_{\max})^2}{8} \right) \end{aligned} \quad (\text{B-70})$$

Thus, it is sufficient to require that

$$\frac{\pi r \tau_{\max} v_{\max}}{2} \ll 1 \quad (\text{B-71})$$

in order for the WB channel to be approximated by a band limited WSSUS channel. This is a conservative requirement. Using the definition of r , this inequality can also be expressed as,

$$W \ll \frac{2}{\pi \xi_{\max}} \quad (\text{B-72})$$

where ξ_{\max} is the maximum change in delay over the correlation time τ_{\max} , assuming a linear change in delay with time. Aside from the factor of $2/\pi$, this is identical to the inequality derived by the author previously [6] for a collection of moving scatterers to produce tap gain correlations identical to those of fixed scintillating scatterers in a band-limited channel.

B.5 Numerical Examples

In this section, we evaluate tap weight correlation functions and spectra for two simplified but non-trivial UWB examples: outdoor base-station to urban mobile and indoor fixed terminal to mobile terminal. In both cases, we make four simplifying assumptions,

- (1) Hypothetical isotropic antenna patterns at transmitter and receiver.
- (2) The multipath path-loss $(a_k)^2$ and Doppler shift v_k are statistically independent for $k \in \alpha_n$.
- (3) The Doppler PDF is independent of tap weight delay.
- (4) The strength of the tap weight decreases exponentially as the tap weight delay increases.

These assumptions simplify the presentation greatly and yield a formulation that presents clearly the essential difference between narrowband and UWB channel tap gain correlation functions. Moreover, these simplifications do not compromise our conservative analysis of the suitability of DSSS/UWB modem operation. Two major factors degrade such modem operation at a given SNR: the rapidity of tap weight fading in relation to the time constants of the channel measurement process, and the multipath spread. The latter factor affects the number of taps R needed in the Rake to combine the significant multipath components. The importance of these factors arises from the fact that the more rapid the fading, the more degraded the channel measurement and the more degraded the predetection multipath diversity combining. In addition, the larger R needed, the larger the amount of noise contributed to the combiner output. The precise shapes of the fading power spectrum of the tap weights and the precise distribution of the multipath will normally be less important than the tap weight fading bandwidth and channel multipath spread per se (barring singular cases).

Our attention is confined here to the heavily shadowed urban channel, whether outdoor or indoors, where multiple reflections are the rule. Under such conditions, the coupling between path loss and azimuthal arrival angle that exists with single reflections is not likely to be significant. Equation (B-12) shows that the Doppler shift of the k^{th} path, assuming a stationary transmitter, is given by $\frac{v_R}{\lambda_0} \cos d_k$, where d_k is the angle between the mobile velocity vector and the direction vector of the incoming ray, and v_R, λ_0 are the velocity of the

receiver and the wavelength corresponding to the carrier frequency. Ignoring elevation angles, d_k can be equated to the difference between the azimuth angles of the mobile velocity vector and the direction vector. Thus a decoupling of dependence between path loss and azimuthal angle results in a decoupling between Doppler shift and path loss. The outdoor and indoor cases considered below differ only in the shape of the Doppler PDF and appropriate values for maximum Doppler shift and multipath spread.

Using assumptions (1) and (2) detailed above,

$$D\left(v, a, \frac{n}{W}\right) = D(v)A\left(a, \frac{n}{W}\right) \quad (\text{B-73})$$

where $D(v)$ is the assumed common path Doppler PDF and $A(a, n/W)$ is the PDF for path amplitude conditioned on the multipath components affecting the n^{th} tap weight. Using (B-73) in (B-47), (B-48), (B-53), and (B-57),

$$F\left(v, \frac{n}{W}\right) = D(v) \quad (\text{B-74})$$

$$\hat{Q}\left(\frac{n}{W}\right) = \beta\left(\frac{n}{W}\right) \int a^2 A\left(a, \frac{n}{W}\right) da \quad (\text{B-75})$$

$$R_{nm}(\tau) = \frac{1}{W} \hat{Q}\left(\frac{m+n}{2W}\right) \int D(v) e^{-j2\pi v\tau} C(-rv\tau + m - n) dv \quad (\text{B-76})$$

$$R_{nn}(\tau) = \frac{1}{W} \hat{Q}\left(\frac{n}{W}\right) \int D(v) e^{-j2\pi v\tau} C(-rv\tau) dv \quad (\text{B-77})$$

$$P_{nm}(f) = \frac{1}{W} \hat{Q}\left(\frac{m+n}{2W}\right) \int D(v) \frac{1}{|v|r} E\left(-\frac{f+v}{vr}\right) e^{-j2\pi(m-n)\left(\frac{f+v}{vr}\right)} dv \quad (\text{B-78})$$

$$P_{nn}(f) = \frac{1}{W} \hat{Q}\left(\frac{n}{W}\right) \int D(v) \frac{1}{|v|r} E\left(-\frac{f+v}{vr}\right) dv \quad (\text{B-79})$$

It is important to note that

$$Q\left(0, \frac{n}{W}\right) = \hat{Q}\left(\frac{n}{W}\right) \quad (\text{B-80})$$

where it will be recalled⁵⁴ that $Q(\tau, \xi)$ and $Q(0, \xi)$ are the *tap gain correlation function* and *delay power spectrum* of the WSSUS representation of the channel when $r \rightarrow 0$.

To complete the model we now specify $\widehat{Q}(\xi)$, $D(\nu)$, and $C(\tau)$. Using assumption (4) requires that $\widehat{Q}(\xi)$ decrease exponentially with ξ . This assumption can be justified heuristically by review of multipath measurements for the indoor and outdoor urban channels which show that the measured power vs. path delay for the unresolvable multipath portions of the impulse response of indoor and outdoor urban channels is frequently well-modeled by an exponentially decaying shape⁵⁵. We assume that the path delay starts at 0 delay⁵⁶ and the power delay profile has the exponential shape

$$\widehat{Q}(\xi) = \frac{1}{\sigma} e^{-\frac{\xi}{\sigma}}; \xi \geq 0 \quad (\text{B-81})$$

where σ is the delay constant, i.e., the delay at which the power delay profile decreases by the factor e . Note that $Q(\xi)$ has been normalized to unit area. It follows that

$$R_{nm}(0) = \frac{1}{W\sigma} e^{-\frac{m+n}{2W\sigma}}; n, m \geq 0, \sigma \gg \frac{1}{W} \quad (\text{B-82})$$

The second inequality states that the power vs. delay changes little in a delay interval of the order of the tap spacing, $1/W$, which is equivalent to the *smooth* assumption, defined in section B.4.1.

With regard to $D(\nu)$, consider first communications between a fixed elevated base station and an urban mobile, a channel which has been treated extensively in the literature (e.g., see [25, 26]). In these references, calculations are carried out of the power spectrum of a received carrier. For simplicity, we assume an isotropic receiving antenna and arrival angles uniformly distributed in azimuth with small elevation angles. The Doppler shift for the k^{th} reflector is given by (B-12) with $\nu_T = 0$

$$\nu_k = \nu_{\max} \cos d_k \quad (\text{B-83})$$

⁵⁴ See summary below equation (B-62).

⁵⁵ See [33] for a recent summary of measurements for the UWB channel. .

⁵⁶ We are modeling the excess delay channel.

where d_k is the angle between the mobile velocity vector and the direction vector of the incoming ray and

$$v_{\max} = \frac{v_R}{\lambda_0} \quad (\text{B-84})$$

is the maximum Doppler shift, λ_0 is the wavelength of light at the carrier frequency and v_R is the speed of the mobile. Ignoring elevation angles, d_k can be equated to the difference between the azimuth angles of the velocity vector and the direction vector. By hypothesis, then, d_k is uniformly distributed over the interval $(0, 2\pi)$. The PDF for

$$x = \cos d_k \quad (\text{B-85})$$

is then readily determined as

$$U(x) = \begin{cases} \frac{1}{\pi\sqrt{1-x^2}}; & |x| \leq 1 \\ 0 & ; |x| > 1 \end{cases} \quad (\text{B-86})$$

The PDF of the Doppler shift is just a scaled version of (B-86),

$$D(v) = \begin{cases} \frac{1}{\pi v_{\max} \sqrt{1 - \frac{v^2}{v_{\max}^2}}}; & |v| \leq v_{\max} \\ 0 & ; |v| > v_{\max} \end{cases} \quad (\text{B-87})$$

Using (B-74) in (B-62) it is seen that for the narrow band case, the power spectrum of the n^{th} tap weight, $P_{nn}(f)$, is proportional to $D(f)$. This is consistent with the prior referenced narrow band calculations of the received power spectrum due to a carrier assuming isotropic antennas⁵⁷.

Consider now indoor UWB communications from a stationary transmitter to a mobile receiver. Here we assume that the multipath arrival angles at the receiver are uniformly distributed in solid angle. Let (α, θ) be the azimuth and zenith angle coordinates,

⁵⁷ These references carry out power spectrum calculations for non-isotropic receive antennas also.

respectively, for a spherical coordinate system centered at the receiving antenna. In [27, 28] it was shown that a uniform distribution in solid angle corresponds to a uniform PDF in α , i.e., $1/2\pi$ for $0 < \alpha < 2\pi$, and a non-uniform PDF in θ of $\frac{1}{2}\sin\theta$ for $0 < \theta < \pi$. (B-81) expresses the Doppler shift of the k^{th} received multipath component as $v_{\max} \cos d_k$, where d_k is the angle between the mobile velocity vector and the direction vector of the incoming ray. As pointed out in [27, 28], due to the assumed uniform PDF of arrival in solid angle, we can choose the orientation of the z axis at will without changing the statistics of (α, θ) . If we choose the z axis in the direction of the mobile velocity vector, then $d_k = \theta_k$ and the PDF of the Doppler shift becomes equal to a scaled version of the random variable $y = \cos\theta$ where now θ has the PDF, $\frac{1}{2}\sin\theta$ for $0 < \theta < \pi$. It is readily determined that this PDF is uniform over the interval $(-1 \leq y \leq 1)$, i.e.

$$U(x) = \begin{cases} \frac{1}{2}; & |x| \leq 1 \\ 0; & |x| > 1 \end{cases} \quad (\text{B-88})$$

Thus for the indoor channel example

$$D(v) = \begin{cases} \frac{1}{2v_{\max}}; & |v| \leq v_{\max} \\ 0; & |v| > v_{\max} \end{cases} \quad (\text{B-89})$$

For illustrative purposes, we assume that the energy density spectrum of the reference direct path impulse response equals the energy density spectrum of a Gaussian shaped pulse truncated to a bandwidth which encompasses 99.9 percent of the energy. This leads to the following expressions for the normalized energy density spectrum, $E(f)$, and aperiodic auto-correlation function, $C(\tau)$ ⁵⁸,

$$E(f) = 2.628e^{-21.655f^2}; |f| \leq \frac{1}{2} \quad (\text{B-90})$$

$$C(\tau) \approx e^{-4558\tau^2} \quad (\text{B-91})$$

⁵⁸ We are neglecting the small perturbation caused by the truncation of the Gaussian shaped energy density spectrum.

With the above definitions and assumptions the common normalized tap weight

cross-correlation function as a function of the normalized delay $t = \tau v_{\max}$ is given by the

integral

$$c(t, r, m - n) = \frac{R_{nm}(t/v_{\max})}{\tilde{Q}\left(\frac{m+n}{2W}\right)/W} = \int_{-1}^1 U(x) e^{-j2\pi xt} e^{-.4558(-rxt+m-n)^2} dx \quad (\text{B-92})$$

and the normalized auto-correlation function by

$$c(t, r) = \int_{-1}^1 U(x) e^{-j2\pi xt} e^{-.4558(rxt)^2} dx \quad (\text{B-93})$$

Note that the normalized tap weight cross-correlation function depends on $m-n$ only. In terms of the normalized frequency variable, $g = f/v_{\max}$, the normalized cross-power spectra as a function of the normalized frequency is given by

$$p(g, r, m - n) = \frac{v_{\max} P_{nm}(gv_{\max})}{\tilde{Q}\left(\frac{m+n}{2W}\right)/W} = \int U(y) \frac{1}{|y|r} E\left(-\frac{g+y}{yr}\right) e^{-j2\pi(m-n)\left(\frac{g+y}{yr}\right)} dy \quad (\text{B-94})$$

and the power spectrum of the n^{th} tap weight by

$$p(g, r) = \int U(y) \frac{1}{|y|r} E\left(-\frac{g+y}{yr}\right) dy \quad (\text{B-95})$$

Since, by hypothesis, $E(f)$ is zero outside the band $-1/2 < f < 1/2$, and $U(y)$ is zero outside the interval $-1 < f < 1$, the limits on the integrals in (B-94) and (B-95) are given by $\{\text{Max}[-1, -g/(1-r/2)], -g/(1+r/2)\}$ for $g > 0$ and by $\{-g/(1+r/2), \text{Min}[1, -g/(1-r/2)]\}$ for $g < 0$. When $|g| > (1+r/2)$ the integration intervals vanish and the integral is zero.

Appendix C Tap Gain Correlation Functions for the Band Limited WSSUS Channel

A model that has proved useful for representing narrow band channels ($r \ll 1$) is the complex low-pass WSSUS model [5] in which the channel is represented as a continuum of independent *non-moving* scintillating scatterers. In this section, we will derive the tap weight correlation functions for the tapped delay line model of a band limited WSSUS channel. The same direct path reference impulse response $g_0(\xi)$ is assumed as for the WB channel model.

Like white noise, the WSSUS channel cannot be measured exactly because infinite bandwidth is required. Thus, it is necessary to view both through the distortion introduced by a “probing” linear filter and infer the characteristics of these processes from the measurements. To simplify the inference we make the *smooth* assumption as was discussed for the WB channel. One consequence of this assumption is that the path delay profile changes little in a delay interval equal to the duration of the probing filter impulse response ($g_0(\xi)$ in the present case).

By hypothesis we assume that the channel we are analyzing is the cascade of a filter having impulse response $g_0(\xi)$ with a WSSUS channel having impulse response $k(t, \eta)$. It is readily determined that the time variant impulse response of this cascade is given by the convolution integral

$$h(t, \xi) = \int g_0(\xi - \eta) k(t, \eta) d\eta \quad (C-1)$$

The frequency domain equivalent of (C-1) is given by

$$H(f, t) = G_0(f) K(f, t) \quad (C-2)$$

where the spectra in (C-2) are Fourier Transforms of corresponding functions of delay

variables in (C-1),

$$\begin{aligned} H(f, t) &= \int h(t, \xi) e^{-j2\pi f\xi} d\xi \\ G_0(f) &= \int g_0(\xi) e^{-j2\pi f\xi} d\xi \\ K(f, t) &= \int k(t, \xi) e^{-j2\pi f\xi} d\xi \end{aligned} \quad (C-3)$$

By hypothesis, $G_0(f)$ is band-limited to $(-W/2, W/2)$ Hz. As a result, we see from (C-2) that $H(f, t)$ is also band-limited to this frequency band. Thus (B-3) applies and the n 'th tap weight of the tapped delay line model is given by

$$h_n(t) = \frac{1}{W} h\left(t, \frac{n}{W}\right) = \frac{1}{W} \int g_0\left(\frac{n}{W} - \xi\right) k(t, \xi) d\xi \quad (C-4)$$

To determine the correlation properties of these tap weights, we need to review the correlation properties of $k(t, \xi)$ for the WSSUS channel. The WSS (wide-sense-stationary) property applies to variation of $k(t, \xi)$ along the time axis t . The US (uncorrelated scattering) property applies to variation of $k(t, \xi)$ along the delay axis, ξ , which has the character of non-stationary white noise. As a consequence, the cross-correlation function of the impulse response takes the form [5],

$$E\left[k^*(t, \xi) k(t + \tau, \xi + \rho)\right] = Q(\tau, \xi) \delta(\rho) \quad (C-5)$$

where $\delta(\cdot)$ is the unit impulse function. It is shown in [5] that $Q(\tau, \xi)$ is actually the cross-power spectral density between $K(f, t)$ and $K(f, t + \tau)$. However $Q(\tau, \xi)$ also has the phenomenological interpretation as the auto-correlation function of differential scatterers providing path delays in the interval $(\xi, \xi + d\xi)$. For this reason, it is also called the *tap gain auto-correlation function*. $Q(0, \xi) \equiv Q(\xi)$ is the power spectral density of fluctuations in $K(f, t)$ as a function of the frequency variable. $Q(\xi)$ has been called the *delay power spectrum* [5].

The cross-correlation function between tap weights n and m is given by the integral

$$E\left[h_n^*(t) h_m(t + \tau)\right] = \frac{1}{W^2} \int \int g_0^*\left(\frac{n}{W} - \xi\right) g_0\left(\frac{m}{W} - \eta\right) E\left[k^*(t, \xi) k(t + \tau, \eta)\right] d\xi d\eta \quad (C-6)$$

Using (C-5) in (C-6)

$$R_{nm}(\tau) = E[h_n^*(t)h_m(t+\tau)] = \frac{1}{W^2} \int g_0^*\left(\frac{n}{W} - \xi\right) g_0\left(\frac{m}{W} - \xi\right) Q(\tau, \xi) d\xi \quad (C-7)$$

We note the symmetry properties

$$\begin{aligned} R_{nm}(\tau) &= R_{mn}^*(-\tau) \\ Q(\tau, \xi) &= Q^*(-\tau, \xi) \end{aligned} \quad (C-8)$$

In keeping with the smooth assumption, $Q(\tau, \xi)$ changes little for variations in ξ of the order of the duration of the impulse response $\bar{g}(\xi)$. With the smooth assumption and use of the normalized aperiodic correlation function of the direct path reference impulse response, (see (B-33) through (B-39)), it is readily seen that

$$R_{nm}(\tau) \approx C(m-n) \frac{1}{W} Q\left(\tau, \frac{n+m}{2W}\right) \quad (C-9)$$

Note that with the smooth assumption for the complex low-pass WSSUS channel, the cross-correlation function between tap weight n and tap weight m factors into the product of a function of $(m-n)$ and a function of $(m+n)$ and τ .

The cross-spectrum between the tap weights m and n is given by the Fourier Transform of the tap weight cross-correlation function (C-7). This may be carried out with the aid of the following transform

$$S(\xi, \nu) = \int Q(\tau, \xi) e^{-j2\pi\nu\tau} d\tau \quad (C-10)$$

$S(\xi, \nu)$ has been called the scattering function or the delay-Doppler scattering function in [5], as it describes the intensity of power received for differential delay elements in the range $(\xi, \xi+d\xi)$ and Doppler shifting elements in the range $(\nu, \nu+d\nu)$. Fourier transforming (C-7), we find

$$\begin{aligned}
P_{nm}(f) &= \int R_{nm}(\tau) e^{-j2\pi f\tau} d\tau \\
&= \frac{1}{W^2} \int g_0^*\left(\frac{n}{W} - \xi\right) g_0\left(\frac{m}{W} - \xi\right) S(\xi, f) d\xi \\
&\approx C(m-n) \frac{1}{W} S\left(\frac{m+n}{2W}, f\right)
\end{aligned} \tag{C-11}$$

For the special case $m=n$ we obtain the auto-correlation function and power spectrum of tap weight n as

$$R_{nn}(\tau) = \frac{1}{W^2} \int \left| g_0\left(\frac{m}{W} - \xi\right) \right|^2 Q(\tau, \xi) d\xi \approx \frac{1}{W} Q\left(\tau, \frac{n}{W}\right) \tag{C-12}$$

$$P_{nn}(f) = \frac{1}{W^2} \int \left| g_0\left(\frac{m}{W} - \xi\right) \right|^2 S(\xi, f) d\xi \approx \frac{1}{W} S\left(\frac{n}{W}, f\right) \tag{C-13}$$

Appendix D Performance Evaluation of Delay-Compensated Decision-Directed, Parallel-Probe, and Serial-Probe Rake Modems

D.1 Introduction

This section summarizes the performance evaluation of delay-compensated decision-directed, parallel-probe, and serial-probe Rake modems by modifying the evaluation of the non-delay-compensated decision-directed Rake modem presented in Appendix A. For simplicity we assume that the tap weight measurement filters are “boxcar” discrete filters. The results are readily generalized to any measurement filter impulse response. Delay compensation attempts to match the processing group delay in the data transmission path to that in the tap weight formation path. This matching improves modem performance by reducing the decorrelation between tap weight fluctuations and correlator output fluctuations due to time-selectivity.

D.2 Delay-Compensated Decision-Directed Modem Performance

A block diagram of the Rake combiner for the decision-directed Rake modem with delay compensation is shown in Figure 2-5. The effect of delay compensation can be simply analyzed by noting that from a stochastic point of view we will obtain the same results if, instead of inserting a compensating delay in the data path equal to the group delay of the tap weight filter path, we replace the tap weight filter with a hypothetical filter boxcar filter in which the group delay is zero. Either way matches the group delay of the two paths and yields the same results. However, changing the group delay of the tap weight filter path is simply a change in the tap weight filter. So the three methods of performance analysis apply, but numerical results must be

obtained with a changed value for the tap weight filter impulse response. Use of the boxcar filter which integrates over an odd number N_f of I&D outputs results in a particularly simple change.

The general expression for the discrete impulse response of the tap weight path including the delay of T used to line up the decision-directed data cancellation is

$$g_w(t) = \sum_{m=1}^{\infty} b_{m-1} \delta(t - mT) \quad (D-1)$$

where $g_w(t)$ is the impulse response of the tap weight filter including the delay of T used in the decision directed data cancellation. Using the procedure described above and assuming N_f odd, the impulse weights for $g_w(t)$ change from

$$b_m = \begin{cases} \frac{1}{N_f}; & 0 \leq m \leq N_f - 1 \\ 0; & \text{elsewhere} \end{cases} \quad (D-2)$$

to

$$b_m = \begin{cases} \frac{1}{N_f}; & -\frac{N_f-1}{2} \leq m \leq \frac{N_f-1}{2} \\ 0; & \text{elsewhere} \end{cases} \quad (D-3)$$

D.3 Parallel Probe Modem Performance

In the case of the parallel probe DSSS/Rake modem the transmitted power is apportioned to a data DSSS signal and a probe DSSS signal each having statistically independent random chip sequences occupying the same bandwidth. Ideally, each of these signals “sees” the same channel and has the same terminal equipment impulse response. Separate correlation processing of the received signals is applied with the data and probe chip sequences. Because the probe and data chip sequences are independent, there is little interference at the correlator outputs, assuming sufficient processing gain. Then the received probe signal, having no data modulation, can be

used without decision-directed processing to estimate the tap weights for the data signal path correlators. Delay compensation is inserted in the data path prior to weighting.

We now formulate an expression for the received sampled signal fed to the Rake demodulator. With the definition of the composite channel filter incorporating the chip pulse forming filter and successive band limiting filtering operations in the transmitter, the transmitted signal, $z(t)$, can be represented as the sum of hypothetical impulse trains

(cf. (A-2))

$$z(t) = \frac{1}{\sqrt{1+g}} \sum a_q m_q \delta\left(t - \frac{q}{W}\right) + \sqrt{\frac{g}{1+g}} \sum p_q \delta\left(t - \frac{q}{W}\right) \quad (\text{D-4})$$

a_q is the q -th DSPN data-path chip modulation, m_q is the data modulation superimposed on the q -th data-path DSPN chip, and p_q is the q -th DSPN probe-path chip modulation. As will be seen, the ratio of the power in the received probe signal to the power in the received data signal is g .

To obtain $s(t)$, the signal component of the received process prior to receiver sampling, we pass the impulse trains (D-4) through the composite filter, with the result

(cf. (A-6))

$$s(t) = \frac{1}{\sqrt{1+g}} \sum a_q m_q h\left(t, t - \frac{q}{W}\right) + \sqrt{\frac{g}{1+g}} \sum p_q h\left(t, t - \frac{q}{W}\right) \quad (\text{D-5})$$

Thus the received signal including noise is given by

$$w(t) = s(t) + \eta(t) \quad (\text{D-6})$$

where $\eta(t)$ is a complex white noise at the input to the Rake demodulator. The mean absolute squared value of the input signal conditioned on the channel fluctuations is given by

$$\overline{|s(t)|^2} = \frac{1}{1+g} \sum_p \left| h^2\left(t, t - \frac{p}{W}\right) \right| + \frac{g}{1+g} \sum_p \left| h^2\left(t, t - \frac{p}{W}\right) \right| \quad (\text{D-7})$$

Thus, by construction, the received signal-to-noise ratio for the parallel probe modem is the same as for the decision-directed modem with the ratio of the received power in the probe signal to the received power in the data signal equal to g . It is clear, a priori, that there is an optimum value of g , since if g is too large the output SNR will decrease due to the decreasing power allocated to the data signal and if g is too small the channel measurement will get so noisy as to increasingly degrade performance. While optimal adjustment of measurement filter time constant and number of Rake taps is possible at the receiving end with the aid of the channel measurement function of the system, optimal adjustment of the parameter g requires a two way link.

Carrying through a performance analysis using the SNR method, paralleling that for the decision-directed modem, the channel raw bit error probability is estimated as

$$p_{rb} = \phi\left(\sqrt{\rho_{out}}\right) \quad (D-8)$$

where $\phi(\cdot)$ is given by (3-49), ρ_{out} is the (decision variable) SNR given by

$$\rho_{out} = \frac{2A^2\rho^2}{R\gamma + B\rho} \quad (D-9)$$

and ρ is the input SNR in a bandwidth equal to the symbol rate (i.e. E_S/N_0), γ is the two sided noise bandwidth of the tap weight filter ($=1/N_f$ for the boxcar filter) and A , B are coefficients dependent on channel parameters. In the parallel probe case, the coefficients A and B have modified expressions. We present results here only for the specialization of the tap weight cross-correlation functions and cross-power spectra to two scenarios: outdoor base-station to urban mobile and indoor fixed terminal to mobile terminal assuming a dense multipath model. Section 3.1.4 summarizes these models and associated parameters and functions. Then, assuming delay

compensation and parallel probing, the coefficients A and B are given by

$$A = \left(1 - e^{-\frac{R}{\tau}}\right) \frac{\sqrt{g}}{1+g} \operatorname{Re} \left\{ \int_{-1-\frac{r}{2}}^{1+\frac{r}{2}} p(f,r) \operatorname{sinc}^2(fx) G_1(fx) df \right\} \quad (\text{D-10})$$

$$B = \left(1 - e^{-\frac{R}{\tau}}\right) \frac{1}{1+g} \left\{ g \int_{-1-\frac{r}{2}}^{1+\frac{r}{2}} p(f,r) \operatorname{sinc}^2(fx) |G_1(fx)|^2 df + \gamma \int_{-1-\frac{r}{2}}^{1+\frac{r}{2}} p(f,r) \operatorname{sinc}^2(fx) df \right\} \quad (\text{D-11})$$

The function $G_1(f)$ is the Fourier transform of a normalized version of $g_w(t-T)$ wherein $T=1$. For the discrete tap weight boxcar filter with N_f odd, the transfer function $G_1(f)$ with delay compensation is given by,

$$G_1(f) = \frac{1}{N_f} \sum_{p=-\frac{N_f-1}{2}}^{\frac{N_f-1}{2}} e^{-j2\pi pf} = \frac{\operatorname{Sin}(N_f \pi f)}{N_f \operatorname{Sin}(\pi f)} \quad (\text{D-12})$$

Consider now application of the Gaussian noise method to parallel probing raw bit error rate estimation. As for the decision-directed modem, the estimation of raw bit error for the Gaussian noise method is given by (cf. (3-58))

$$p_{rb} = P_R \left(\sqrt{\frac{\rho}{\gamma}} [B - 2A\sqrt{\gamma}], \sqrt{\frac{\rho}{\gamma}} [B + 2A\sqrt{\gamma}] \right) \quad (\text{D-13})$$

for parallel probing. To obtain the raw bit error rate estimate for parallel probing we need to merely substitute in (D-14) the proper expressions for A and B given by (D-11) and (D-12), respectively, for the indoor and outdoor dense multipath models.

We consider now the exact method of raw bit error probability evaluation for parallel probing. This method has been summarized in section 3.2.3 and discussed in detail in section

A.4.2. It applies to the special case in which both the tap weights and the noises at the correlator outputs may be approximated by zero mean complex Gaussian statistics. Then the combiner output decision variable assuming a fixed data bit, may be expressed as a Hermitian quadratic form q in zero mean complex Gaussian variables (see (2-5)). The raw bit error probability is given by

$$p_{rb} = \Pr[q < 0] = \int_{-\infty}^0 W(q) dq = -\frac{1}{2\pi j} \int_{-j\infty}^{j\infty} \frac{1}{z \text{Det}[\mathbf{I} - z\mathbf{M}\mathbf{Q}]} dz \quad (\text{D-14})$$

where \mathbf{Q} is the matrix defining the quadratic form and \mathbf{M} is the covariance matrix for the quadratic form variables. In this study, the variables are the outputs of the R tap weight filters and the R correlators requiring a $2R \times 2R$ matrix for \mathbf{M} and \mathbf{Q} . The derivations in sections 3.2.3 and A.4.2 use tap weight and correlator output variables in which the corresponding noise components have been normalized to unity average magnitude squared values, as detailed in (A-102) to (A-107). For parallel probing, Equations (A-106) and (A-107) defining the normalized tap weight and correlator outputs, respectively, are changed to

$$\mu_{pk} = \sqrt{\frac{g}{1+g}} \sqrt{\frac{WN}{2N_0\gamma}} \hat{h}_p \left(kT + \frac{T}{2} + \frac{p}{W} \right) \quad (\text{D-15})$$

$$v_{pk} = \frac{1}{\sqrt{1+g}} \sqrt{\frac{WN}{2N_0}} \tilde{h}_p \left(kT + \frac{T}{2} + \frac{p}{W} \right) \quad (\text{D-16})$$

These normalizations, which do not change the raw bit error probability, allow the covariance matrix \mathbf{M} to be expressed as the sum of the identity matrix \mathbf{I} and the covariance matrix of the normalized variables. The elements of this latter matrix for the parallel probe modem, replacing (3-76) to (3-78) for the decision-directed modem, are given by

$$\overline{\mu_n^* v_m} = \frac{\sqrt{g}}{1+g} \frac{\rho}{\sqrt{\gamma}} \frac{e^{-\frac{n+m}{2\tau}}}{\tau} \int_{-1-\frac{r}{2}}^{1+\frac{r}{2}} p(f, r, m-n) \text{sinc}^2(fx) G_1(fx) e^{j2\pi fx \left(\frac{m-n}{N}\right)} df \quad (\text{D-17})$$

$$\overline{\mu_n^* \mu_m} = \frac{g}{1+g} \frac{\rho}{\gamma} \frac{e^{-\frac{n+m}{2\tau}}}{\tau} \int_{-1-\frac{r}{2}}^{1+\frac{r}{2}} p(f, r, m-n) \text{sinc}^2(fx) |G_1(fx)|^2 e^{j2\pi fx \frac{m-n}{N}} df \quad (\text{D-18})$$

$$\overline{v_n^* v_m} = \frac{1}{1+g} \rho \frac{e^{-\frac{n+m}{2\tau}}}{\tau} \int_{-1-\frac{r}{2}}^{1+\frac{r}{2}} p(f, r, m-n) \text{sinc}^2(fx) e^{j2\pi fx \frac{m-n}{N}} df \quad (\text{D-19})$$

where $G_1(f)$ is given by (D-13) in keeping with the assumption of delay compensation and boxcar tap weight filtering.

D.4 Serial Probe Modem Performance

In the case of the serial probe modem, a known periodic data subsequence of period P is inserted in the data sequence. The corresponding portion of the transmitted signal serves as the channel probe. Tap weight measurement is conducted only with this probing subsequence, thus avoiding the use of decision-directed operation. Note that the tap weight filter receives a correlator I&D output every PT seconds instead of every T seconds as in the decision-directed and parallel probe tap weight filters. One may construct an interpolating digital filter (e.g. see [29]) clocked every T seconds which simultaneously averages the received probe sequence and up-samples to rate $1/T$. However, this filter would no longer be a boxcar filter. Alternatively, one may implement a boxcar filter clocked at the rate $1/PT$, and use the same weight for $P-1$ successive correlator outputs. This procedure will retain most of the advantages of delay compensation without the complexity of interpolation when, as will usually be the case, the group delay is much larger than $(P-1)T$. Another approach is to provide $P-1$ separate delay

compensation circuits; one for each of the $P-1$ data bit positions. Time multiplexing is then used to provide the correct delay compensation for each data bit. In our analysis, we assume perfect delay compensation for each data bit.

We now outline the changes in Appendix A to derive the raw error rate for the serial probe modem. Note first that, in comparing modems, it is necessary to keep the data rate and total transmitted power the same (thus keeping E_S/N_0 the same). Thus, if the symbol duration is T for the decision-directed system, it is necessary to reduce the symbol duration for the serial probe system to

$$T' = T \frac{P-1}{P} \quad (\text{D-20})$$

to maintain the same data rate. This reduces the number of chips in a data symbol from N to⁵⁹

$$N' = N \frac{P-1}{P} \quad (\text{D-21})$$

which gives the following expression for the combiner complex output

$$C_k' = \sum_{p=0}^{R-1} \left(W \hat{h}_p^* \left(kT' + \frac{T'}{2} + \frac{p}{W} \right) + \hat{n}'_{pk} \right) \left(d_k W \tilde{h}'_p \left(kT' + \frac{T'}{2} + \frac{p}{W} \right) + n'_{pk} \right) \quad (\text{D-22})$$

where

$$\tilde{h}'_p(t) = h_p(t) \otimes \frac{1}{T'} \text{Rect} \left[\frac{t}{T'} \right] \quad (\text{D-23})$$

$$\hat{h}'_p(t) = \tilde{h}'_p(t) \otimes g'_w(t) = h_p(t) \otimes \frac{1}{T'} \text{Rect} \left[\frac{t}{T'} \right] \otimes g'_w(t) \quad (\text{D-24})$$

in which

⁵⁹ To simplify the presentation, we ignore the discrete nature of the variables T , T' , N , and N' .

$$g'_w(t) = \frac{1}{N_f'} \sum_{m=-\frac{N_f'-1}{2}}^{\frac{N_f'-1}{2}} \delta(t - mPT') \quad (\text{D-25})$$

is a hypothetical boxcar tap weight filter of duration N_f' samples with group delay subtracted to simply model the effect of delay compensation. We note that (D-26) represents ideal delay compensation.

Modifying (A-102) for the serial probe case, the average strengths of the correlator and tap weight filter noise outputs become

$$\overline{|n'_{pk}|^2} = \frac{2WN_0}{N_f'}; \quad \overline{|\hat{n}'_{pk}|^2} = \frac{2WN_0}{N_f'} \frac{1}{N_f'} \quad (\text{D-26})$$

With the aid of (D-21)-(D-27) the output SNR used in the SNR method can be shown to be given by

$$\rho_{\text{out}} = \frac{2(A')^2 \left(\frac{P-1}{P}\right)^2 \rho^2}{\frac{R}{N_f'} + B' \frac{P-1}{P} \rho} \quad (\text{D-27})$$

where ρ is E_s/N_0 and A' , B' are given by the following expressions for the indoor and outdoor dense multipath channels

$$A' = \left(1 - e^{-\frac{R}{\tau}}\right) \int_{-1-\frac{r}{2}}^{1+\frac{r}{2}} p(f, r) \text{sinc}^2(fx') \frac{\sin(N_f' \pi P x' f)}{N_f' \sin(\pi x P' f)} df \quad (\text{D-28})$$

$$B = \left(1 - e^{-\frac{R}{\tau}} \right) \left\{ \begin{array}{l} \int_{-1-\frac{r}{2}}^{1+\frac{r}{2}} p(f, r) \operatorname{sinc}^2(fx') \left(\frac{\sin(N_f' \pi P x' f)}{N_f' \sin(\pi P x' f)} \right)^2 df \\ + \frac{1}{N_f'} \int_{-1-\frac{r}{2}}^{1+\frac{r}{2}} p(f, r) \operatorname{sinc}^2(fx') df \end{array} \right\} \quad (D-29)$$

where

$$x' = v_{\max} T' \quad (D-30)$$

For the Gaussian noise method and use of the serial probe modem, the raw bit error probability estimate becomes changed to

$$P_{rb} = P_R \left(\sqrt{\rho \frac{P-1}{P} N_f' \left[B' - \frac{2A'}{\sqrt{N_f'}} \right]}, \sqrt{\rho \frac{P-1}{P} N_f' \left[B + \frac{2A'}{\sqrt{N_f'}} \right]} \right) \quad (D-31)$$

As discussed above, the covariance matrix of the normalized tap weights and correlator outputs is sufficient to allow calculation of the raw bit error rate for the exact method. For the serial probe case, the elements of this covariance matrix are given by

$$\overline{\mu_n^* \nu_m} = \rho \frac{P-1}{P} \sqrt{N_f'} \frac{e^{-\frac{n+m}{2\tau}}}{\tau} \int_{-1-\frac{r}{2}}^{1+\frac{r}{2}} p(f, r, m-n) \operatorname{sinc}^2(fx') \frac{\sin(N_f' \pi P x' f)}{N_f' \sin(\pi P x' f)} e^{j2\pi f x' \frac{m-n}{N_f'}} df \quad (D-32)$$

$$\overline{\mu_n^* \mu_m} = \rho \frac{P-1}{P} N_f' \frac{e^{-\frac{n+m}{2\tau}}}{\tau} \int_{-1-\frac{r}{2}}^{1+\frac{r}{2}} p(f, r, m-n) \operatorname{sinc}^2(fx') \left(\frac{\sin(N_f' \pi P x' f)}{N_f' \sin(\pi P x' f)} \right)^2 e^{j2\pi f x' \frac{m-n}{N_f'}} df \quad (D-33)$$

$$\overline{v_n^* v_m} = \rho \frac{P-1}{P} \frac{e^{-\frac{n+m}{2\tau}}}{\tau} \int_{-1-\frac{r}{2}}^{1+\frac{r}{2}} p(f, r, m-n) \text{sinc}^2(fx') e^{j2\pi fx' \frac{m-n}{N'}} df \quad (\text{D-34})$$

D.5 Composite Modems

It is possible to conceive composite modems in which the methods described for channel measurement are combined. For example, one may carry out decision directed channel measurement on the purely data portions of the parallel and serial probe modems and combine these measurements with those for the non data portions of the modems. Such composite modems have not been evaluated in this report.